HIGH-SILICA, LARGE PORE MOLECULAR SIEVES: SYNTHESIS, MODIFICATION AND CATALYSIS

A THESIS

SUBMITTED TO THE

UNIVERSITY OF PUNE

FOR THE DEGREE OF

DOCTOR OF PHILOSOPHY

(IN CHEMISTRY)

BY

M. SASIDHARAN

TH-1042

CATALYSIS DIVISION

NATIONAL CHEMICAL LABORATORY

PUNE-411008, INDIA

JUNE (1996)

...TO MY BELOVED PARENTS AND TEACHERS

CERTIFICATE

Certified that the work incorporated in the thesis **"High-Silica, Large Pore Molecular Sieves: Synthesis, Modification and Catalysis"** submitted by Mr. M. Sasidharan, for the degree of Doctor of philosophy, was carried out by the candidate under my supervision in the National Chemical Laboratory, Pune, India. Such material as has been obtained from other sources has been duly acknowledged in the thesis.

(RAJIV KUMAR)

(Research Guide)

ACKNOWLEDGMENTS

M. SASIDHARAN

Contents...

CHAPTER 1

GENERAL INTRODUCTION

1.1 DEFINITION OF ZEOLITES

Zeolites, the most widely studied class of molecular sieves, are crystalline, microporous, hydrated aluminosilicates. Structurally, they are comprised of a framework based on an infinitely extending three-dimensional network of SiO_4 and AlO_4 tetrahedra linked together through common oxygen atoms. The isomorphic substitution of Si^{4+} by Al^{3+} gives rise to a net negative charge balanced by non-framework cations. The general formula of zeolites can be represented as:

$$M_{2/n} [(AlO_2)_x (SiO_2)_y]. \ Z \ H_2O$$
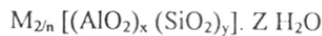
where "M" is the charge compensating cation with valency n, generally from group I or II. Both inorganic (mono or divalent metal ions) as well as organic cations may be used to compensate the framework charge. "Z" represents the moles of water molecules which are reversibly adsorbed and the values of y/x can be from one to infinity since according to Loewenstein's rule when two tetrahedra are linked by one oxygen bridge, the center of only one of them can be occupied by aluminum.

1.2 CLASSIFICATION

The zeolite structure is mainly comprised of a tetrahedral primary unit, TO_4, where T can be either Si or Al. Zeolites can be classified on the basis of morphological characteristics [1-4], crystal structure [1,5], chemical composition [6], and effective pore diameter [1,7]. Based on morphology, zeolites are classified as fibrous, lamellar or materials with an open framework structure. Structural classification of the zeolites has been proposed depending on differences in secondary building units and they are grouped as: Analcime, Natrolite, Chabazite, Philipsite, Heulandite, Mordenite, Faujasite, Laumontite, Pentasil and Clathrate. The classification under chemical composition is exclusively based on the Si/Al ratio (SAR) [6] as follows: (a) low silica

1

(SAR = 1-1.5), (b) medium silica (SAR = >1.5 - 5), (C) high silica (SAR = > 5- several thousand) and (d) Al-free, pure silica zeolites. Zeolites are also classified with respect to their pore openings, defined as the number of T (or TO_4 T = Si or Al) units that shape the channels. There are four types of pore openings known to date in the microporous zeolites referred to as the 8-, 10-, 12 and 14-ring openings called small-, medium-, large and extralarge-pore zeolites, respectively. A list of some common zeolites, classified according to their pore openings, is presented in Table 1.1.

1.3 ORGANIC STRUCTURE- DIRECTING AGENTS

The use of organic amines and quarternary ammonium ions in zeolite synthesis has resulted in a number of new zeolite structures as well as a high silicon to aluminum ratio for a given structure. The organic additive can act as a structure-directing, gel modifying, charge compensating cation and/or void filler. The formation of different structures with the same organic additives and the synthesis of a particular zeolite structure using a variety of organic additives have been reported. In order to explain the structure-directing effect of these organic species, a template theory was proposed [8]. Although, the exact mechanism of the templating effect is not fully understood, Lok et.al. [8] suggested that the templating effect is influenced by the charge distribution, size and geometric shape of the template.

The presence of TMA has a structure directing effect and results in many structures. In Table 1.2, a comprehensive list of various organic quaternary ammonium salts and amine templates along with the corresponding zeolite structure formed using such templates is given.

Table 1.1 Classification of zeolite according to the pore opening

8-membered ring (small pore):(IZA code)		10-membered ring (medium pore):(IZA code)		12-membered ring (large pore): (IZA code)		14-membered ring[a]
Linde A	(LTA)	ZSM-5	(MFI)	X	(FAU)	UTD-1 [Ref.9]
Bikitaite	(BIK)	ZSM-11	(MEL)	Y	(FAU)	
Chabazite	(CHA)	ZSM-22	(TON)	EMC-2	(EMT)	
Edingtonite	(EDI)	ZSM-23	(MTT)	LTL		
Erionite	(ERI)	ZSM-35	(FER)	Beta	(BEA)	
Gismondine	(GIS)	ZSM-50/EU-1	(EUO)	ZSM-12	(MTW)	
ZK-5	(KFI)	ZSM-57	(MFS)	ZSM-18	(MEI)	
ZSM-39	(MTN)	NU-10	(TON)	NU-13	(MTW)	
ZSM-51	(NON	NU-87	(NES)	SSZ-24	(AFI)	
Levynite	(LEV)	Theta-1	(TON)	Mordenite (MOR)		
Melinoite	(MER)			Omega (MAZ)		
Natrolite	(NAT)			Mazzite (MAZ)		
Paulingite	(PAU)			ZSM-20 (EMT/FAU)		
Phillipsite	(PHI)					
Rho	(RHO)					

a: UTD-1 (University of Texas at Dallas number-1) is the only 14-membered ring synthetic zeolite published recently. The zeolite was synthesized using bis(pentamethyl cyclopenta dienyl)- Cobalt (III) hydroxide.

Table 1.2 Organic additive and zeolite-structure relationship

Organic additive	Structure type	References
Tetramethylammonium (TMA)⁺	Gismondine, sodalite, zeolite P, gmelinite, faujasite, zeolite E, zeolite A, ZSM-4, Nu-1, Fu-1, zeolite O, Offretite, ZSM-47, ZSM-6, ZSM-39	10-25
Tetraethylammonium (TEA)⁺	ZSM-8, ZSM-12, ZSM-20, ZSM-25, ZSM-5, Beta, Mordenite	26, 27, 28
Tetrapropylammonium (TPA)⁺	ZSM-5	29
Tetrabutylammonium (TBA)⁺	ZSM-11	30
1,2-Diaminoethane	ZSM-5, ZSM-21, ZSM-35	31-33
1,3-Diaminopropane	ZSM-35, ZSM-5	31,32, 34
1,4-Diaminobutane	ZSM-35, ZSM-5	31,32, 34
1,5-Diaminopentane	ZSM-5	31,32, 35
1,6-Diaminohexane	ZSM-5, ZSM-22	31, 32,35
1,7-Diaminoheptane	ZSM-11	36
1,8-Diaminooctane	ZSM-11, ZSM-48	36
1,9-Diaminononane	ZSM-11	36
1,10-Diaminodecane	ZSM-11	36

Further, in addition to mono-quaternary ammonium salts, di-quaternary ammonium salts have also been used in the synthesis of high-silica molecular sieves (Table 1.3). The di-quaternary salts may be represented by the general formula $[R_3-N^+-(CH_2)_x-N^+-R_3]$ Br_2^-, where R may be methyl, ethyl, propyl, butyl, benzyl or a mixture thereof, and 'x' = 3-10. In the case of bis-quaternary ammonium cations, both the chain length and terminal alkyl groups determine the particular structure. By systematically increasing the value of 'x' in bis-quaternary salts and keeping their terminal alkyl groups as methyl, a number of zeolites are formed (Table -1.3). Further, the synthesis of high-silica, large-pore zeolite ZSM-12, has been reported by using mixed alkyl bis-quaternary salt of the formula: $[(C_2H_5)(CH_3)_2-N^+-(CH_2)_6-N^+-(CH_3)_2(C_2H_5)]2Br^-$ [43], and $[(CH_3)_2(C_6H_5CH_2)-N^+-(CH_2)_6-N^+-(CH_2C_6H_5)(CH_3)_2]2Br^-$ [44].

Recently, using a new di-quaternary ammonium salt, *viz* $[(C_2H_5)_3-N^+-(CH_2)_6-N^+-(C_2H_5)_3]2Br^-$, a novel, high-silica zeolite, designated as NCL-1 was synthesized by Kumar et.al. [47,48]. The zeolite NCL-1 can be synthesized in the range of $Si/Al \geq 20$ including, an Al-free all silica analogue [48]. Based on adsorption and catalytic test reactions [49] such as m-xylene conversion, constraint index (CI), [50] spaciousness index [51] and n-decane hydroisomerization/hydrocracking [52], it was concluded that the zeolite NCL-1 belongs to large-pore category, the effective void space being comparable to that of zeolite mordenite.

Table 1.3. Di-quaternary ammonium salts and zeolite structure relationship

No	Diquaternary ammonium salt	R-group	-$(CH_2)_x$-	Zeolite	Ref.
1	Trimethylene bis(trimethyl ammonium bromide)	-CH_3	3	ZSM-39, Eu-4	28, 37
2	Tetramethylene bis(trimethyl ammonium bromide)	-CH_3	4	Eu-1	28
3	Pentamethylene bis(trimethyl ammonium bromide)	-CH_3	5	Eu-1	38
4	Hexamethylene bis(trimethyl ammonium bromide)	-CH_3	6	ZSM-48, Eu-1	39, 40
5	Heptamethylene bis(trimethyl ammonium bromide)	-CH_3	7	ZSM-23, MCM-10	41, 42
6	Octametylene bis(trimethyl ammonium bromide)	-CH_3	8	ZSM-23	41
7	Nonamethylene bis(trimethyl ammonium bromide)	-CH_3	9	Eu-2	39
8	Decamethylene bis(trimethyl ammonium bromide)	-CH_3	10	Nu-87	28
9	Tetramethylene bis(ethyl dimethylammonium bromide)	-CH_2CH_3, -CH_3	4	ZSM-12	43
10	Hexamethylene bis(ethyl dimethylammonium bromide)	-CH_2CH_3, -CH_3	6	ZSM-12	43
11	Hexamethylene bis(dimethyl benzylammonium bromide)	-CH_2CH_3, -CH_3	6	ZSM-12	44
12	Hexamethylene bis(tripropyl ammonium bromide)	-C_3H_7	6	ZSM-5	45
13	Hexamethylene bis(tributyl ammonium bromide)	-C_4H_9	6	ZSM-5	45
14	Pentamethylene bis(triethyl ammonium bromide)	-CH_2CH_3,	5	ZSM-57	38
15	Hexamethylene bis(triethyl ammonium bromide)	-CH_2CH_3,	6	NCL-1	47,48

1.4 ISOMORPHOUS SUBSTITUTION IN ZEOLITES

Modification of zeolites through isomorphous substitution can influence their Brönsted acidity, Lewis acidity, and their ability to oxidize organic molecules. Modification and subsequent improvement of the above mentioned properties, have led to significant development in the areas of adsorption and catalysis. The first isomorphous replacement of Si by Ge was reported by Goldsmith [53] in 1952. The framework T-sites in zeolites can be replaced mainly by tri and tetra valent metal ions. However, recently Bhaumik and Kumar have reported the incorporation of a small amount of pentavalent As^{5+} in MFI structure (As(V)-silicate) [54]. The metal can occupy one or more of the following positions in the zeolites.

- Framework positions

- Defect sites (Si-O-M)

- Cation exchange sites

- Inside the pores or on the external sites as finely dispersed metaloxides

- Bulk oxides on the external surface.

Framework isomorphous substitution in zeolites has been reviewed by various authors [2, 55-58]. The possibility of isomorphous substitution and the stability of a particular metal ion in the zeolite tetrahedral framework is supposed to be governed by Pauling's theory [59]. According to this theory, the metal ion will be stable in the tetrahedral framework when ρ ($\rho = r_c/r_o$, where r_o is the radius of the oxygen and r_c is the cation radius) is in the range of $0.414 > \rho > 0.225$. Values of Pauling criteria for selected metal ions have been given in Table 1.4. According to Pauling's

Table 1.4. Values of Pauling criterion for various elements[59] reported.

Critical values (ρ_{cr})	Preferred coordination number	Corresponding cations
$0.732 > \rho > 0.414$	6	Mn^{2+}, Zn^{2+}, Cu^{2+}; Fe^{3+}, Cr^{3+}, Ga^{3+}, As^{3+}; Ti^{4+}, V^{4+}, Sn^{4+}, Pt^{4+}; Sb^{5+}, Mo^{6+}
$0.414 > \rho > 0.225$	4	Be^{2+}, Al^{3+}, Mn^{4+}, Ge^{4+}, Si^{4+}; V^{5+}, As^{5+}, P^{5+}; Cr^{6+}, Se^{6+};
$0.225 > \rho > 0.147$	3	B^{3+}

theory, for the cations whose ρ is out of this range, the substitution is either impossible or should take place to a lesser extent. However, metal ions such as Fe^{3+}, Ti^{4+}, Ga^{3+}, Sn^{4+} and V^{5+}, whose ρ values are out of this range, have been successfully incorporated into the framework probably due to their stability in tetrahedral environments.

The modification of zeolites through isomorphous substitution can be performed through various methods such as direct hydrothermal synthesis and liquid- and vapor-phase post-synthesis treatments. Generally, direct hydrothermal synthesis vis-a-vis post synthesis method is favored because it leads to better incorporation of a wide variety of metal ions such as Al^{3+}, B^{3+}, Cr^{3+}, Fe^{3+}, Ga^{3+}, Ge^{4+}, Sn^{4+}, Ti^{4+}, V^{4+}, and As^{5+}. Liquid-phase, post-synthesis incorporation of Fe^{3+}, Si^{4+}, and Ti^{4+} into the framework of various zeolites has been reported using ammonium salts of the corresponding metal hexafluorides (NH_4MF_6) [61]. In vapor-phase methods, the zeolite is dealuminated and then annealed with the vapor of a volatile compound of the metal to be incorporated [62]. Complete replacement of Al by these post-synthesis methods has not been reported.

1.5 CHARACTERIZATION

Various characterization techniques, commonly employed in the study of the physico-chemical properties of zeolites, are outlined below along with brief description.

1.5.1 Powder X-ray Diffraction

X-ray diffraction (XRD) indicates uniqueness in structure, as the powder diffraction pattern is a fingerprint of individual structures. The powder pattern provides information on (i) the degree of crystallinity, (ii) the identification of structure type (iii) the phase purity, and (iv) the

unit cell parameters [63-67]. The XRD technique is widely used for structure determination, especially by single crystal methods [68]. Modern methods including *ab initio* structure determination and Rietveld refinements have also been used to refine the structure of number of zeolites [69]. The XRD results presented in this thesis, mainly provide information about phase purity, degree of crystallinity and unit cell parameters of zeolite NCL-1.

1.5.2 Infrared Spectroscopy

Infrared spectroscopy (IR) is an useful technique for the elucidation of broad structural features, modification through isomorphous substitution as well as to determine the nature, number and strength of acid sites. The framework vibrations of the zeolites are observed in the range of 300-1300 cm^{-1} and can be classified into two groups. (i) internal vibrations of TO$_4$ units or structure insensitive vibrations and (ii) vibrations due to external linkages of the TO$_4$ units or structure sensitive vibrations [70,71]. The characteristic infrared bands are given below.

Internal tetrahedra

Asymmetric stretching	1250 - 590 cm^{-1}
Symmetric stretching	720-650 cm^{-1}
T-O bend	420 - 500 cm^{-1}

External linkages

Asymmetric stretching	1050 - 1150 cm^{-1}
Symmetric stretching	750 - 820 cm^{-1}

| Double ring | 650 - 500 cm^{-1} |
| Pore opening | 300 - 420 cm^{-1} |

The pentasil family of materials (ZSM-5 and ZSM-11) are identified by their absorption bands near 550 cm^{-1} characteristic of 5 membered rings in the structure [72-74]. In the case of the mordenite family, the absorption band is observed near 560 cm^{-1} [73,74]. IR spectroscopy has also been extensively used to study both the acidity and basicity using probe molecules such as ammonia, pyridine, benzene, carbon monoxide, pyrrole, CO_2 etc [75-77]. The framework IR studies as well as their acidity measurements through TPD of zeolite NCL-1 are discussed in chapter III.

1.5.3 Nuclear Magnetic Resonance (NMR) Spectroscopy

NMR spectroscopy is an important tool to characterize and distinguish between framework and non-framework atoms [78-91]. In view of the present work, ^{29}Si, ^{27}Al, and ^{71}Ga were of the main interest in characterizing zeolite NCL-1 and its Ga-substituted analogues. In zeolite systems, the ^{29}Si NMR spectrum may contain one to five peaks corresponding to the five different chemical environments, viz Si(0Al, 4Si), Si(1Al, 3Si), Si(2Al, 2Si), Si(3Al, 1Si), and Si(4Al, 0Si). As the silicon atom is replaced by Al atoms, the δ value is shifted down field with each aluminum substitution resulting in a chemical shift of about 5 ppm [80].

The chemical shift (δ,ppm) values for ^{27}Al vary with respect to the coordination number of the aluminum atom. The shifts in δ values (with respect to a $Al(NO_3).6H_2O$ standard) observed are about +50 to +80 ppm for AlO_4 (Td), about -10 to +20 ppm for AlO_6 (O$_h$) and about +30 to

+40 ppm for relatively rare AlO_5 (penta) unit [78,80]. In the case of ^{71}Ga in Td environment, the chemical shift ranges from +145 to +155 ppm with respect to a $Ga(NO_3)$ standard [91-93].

1.5.4 Electron Spin Resonance (ESR) Spectroscopy

ESR spectroscopy is a sensitive tool for characterizing metal ions containing unpaired electrons. Placing these metal ions in magnetic field causes a split in spin states of the unpaired electrons according to symmetry. The electron undergoes a transition to an excited state by the absorption of microwave energy when it satisfies the resonance condition. The splitting of the magnetic levels can give information regarding the symmetry around the metal (M^{n+}) ion [94].

ESR spectroscopy has been routinely used to identify coordination number and oxidation state around the metal ions such as Fe^{3+}, V^{4+}, Cr^{3+}, Cu^{2+} and Co^{3+}. In the case of iron , if Fe^{3+} ions are present in perfect tetrahedral or octahedral coordination, only one signal is observed at g = 2.0. However, as the distortion increases the signal moves towards the down field region and can have values between 2 to 6. In the case of ferri-silicates, a signal at about g = 4.3 (perfect orthorhombic g = 4.27) can be attributed to orthorhombic symmetry. Apart from the g = 4.3 for framework Fe, Ratnasamy et al.[95,96] observed peaks at 2.0, 2.3, and 5.3. The 5.3 signal was assigned to extra lattice iron species. The signal at g = 2.3 is assigned to the iron oxide/hydroxide phase [94-96]. The ESR technique was employed to characterize the zeolite Fe-NCL-1 and the detailed descriptions are given in chapter III.

1.5.5 Ultraviolet-Visible Spectroscopy (UV-Vis)

UV-Vis spectroscopy is also an important technique which provides information about the coordination of metal ions. This technique has been extensively used in the case of titanium silicates in order to distinguish the framework titanium from bulk TiO_2. Titanium silicates exhibit strong band at around 212 nm in the UV-Vis spectrum [96-98] whereas crystalline TiO_2 (anatase phase) exhibits an absorption band around 330 nm. The absorption around 212 nm is attributed to an electronic transition from ligand to metal involving isolated framework Ti(IV) in a tetrahedral coordination [99]. An absorption due to isolated Ti(IV) in octahedral coordination is expected at about 240 nm. This technique has also been used for quantitative determination of extrafrmework titanium in titanium silicates [100].

1.5.6 Sorption and Diffusion Properties

Sorption analysis is used to characterize the void space, pore openings, shape-selective properties, and relative hydrophobic and hydrophilic nature of zeolites as well as other porous solids. Molecules that fill the pores of the zeolite and have minimal diffusional constraints, such as oxygen, nitrogen, water and n-hexane, have been used to determine the pore volume as well as degree of crystallinity. Barrer et al. have thoroughly studied sorption of various gases and vapors in natural as well as in synthetic zeolites [101-103].

The ability of molecular sieves to discriminate between molecules with different sizes and shapes, is used to determine the pore systems, that is whether the pore openings are comprised of 8-, 10-, or 12-member rings. The void volume of micro porous solids is often determined by

nitrogen sorption. Analysis of such sorption isotherm is also useful in determining the micropore

volume and pore size distribution of molecular sieves [104,105].

1.6 ACIDITY IN ZEOLITES

As discussed above in section 1.4, acidity in zeolites arises when Si^{4+} ion in silicate

framework is replaced by trivalent metal ions such as Al^{3+}, Fe^{3+}, and Ga^{3+}. This anionic framework

is neutralized by cations such as Li^+, Na^+, K^+, Rb^+, Cs^+, Ca^{2+}, Mg^{2+}, and quaternary ammonium

cation (as synthesized form). When these charge compensating cations are substituted by protons

through ammonium-ion exchange, followed by calcination at 500°C, the zeolite exhibits Brönsted

acidity. The number of Brönsted acid sites is equal to the number of framework AlO_4-tetrahedra

in zeolites. However, the strength of these acid sites depends on (i) the structure of zeolite (ii) the

silicon to aluminum ratio, and (iii) nature of trivalent metal ions in the zeolite framework

[106,107]. Zeolites also exhibit Lewis acidity. For example, a trigonally coordinated aluminum

atom in a zeolite is electron-deficient and can accept an electron pair and thus behave as a Lewis

acid [106]. The Lewis acidity can also be formed by high temperature (> 500°C) dehydroxylation

of the Si(OH)Al (i.e. Brönsted) sites. When extraframework Al^{3+} ions are associated with acidic

aluminum sites, they may produce "super acid sites" which are responsible for the higher cracking

activities. The 'super acid sites' are mainly observed in dealuminated zeolites [108].

When Si atoms are replaced by other tetravalent metal ions such as Ti^{4+}, V^{4+}, Zr^{4+}, and

Sn^{4+} in a neutral silicate framework, the resulting metallosilicates are charge neutral and they do

not possess any charge compensating cations. Figure 1 (species I) depicts the model proposed to

explain the reactivity of Ti^{4+} in oxidation reactions [109]. However, Kaliaguine et al. have

proposed a highly constrained sites for the titanium (Figure 1.1, species II and III) based on the ·
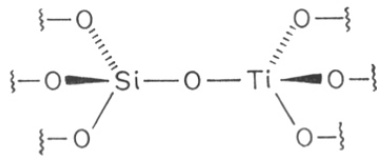
I
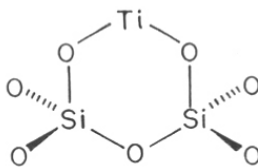
II
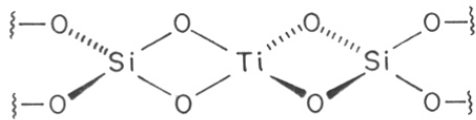
III

FIGURE 1: POSSIBLE STRUCTURE FOR TITANIUM SILICATES

bond distances obtained from the extended x-ray absorption fine-structure (EXAFS) data [110]. These Ti^{4+} ion in titanium-silicates behave as Lewis acid in the absence of H_2O_2 and H_2O [99].

1.7 CATALYSIS

1.7.1 Brönsted-Acid Catalyzed Vapor-Phase Reactions

The important features of zeolites and molecular sieves, which make them very attractive as catalysts and adsorbents are (i) their high activity and shape selectivity, (ii) ease of separation from a reaction mixture, (iii) ease of regeneration to their initial activity, (iv) higher thermal stability, and (v) eco-friendly nature. Catalytic transformations over zeolites may be broadly categorized as follows.

A: Isomerization and Rearrangements

During early stages of acid catalyzed reactions, zeolites were extensively used for the dewaxing of heavy petroleum fractions, selectoforming and catalytic reforming. Later, the zeolite were used to catalyze various petrochemical processes like, the Mobil-Badger ethylbenzene process, the disproportionation of toluene, the isomerization of xylenes and the manufacture of gasoline from methanol [111-113]. In recent years, the use of zeolites in catalyzing various reactions involving fine chemicals such as isomerization of cresols, chlorotoluenes, toluenitriles, toluidines and aniline have also been explored [114-120]. Recently, an excellent review of zeolite catalyzed reactions is reported by Venuto [121].

B. Aromatic Electrophilic Substitution Reactions

Aromatic electrophilic reactions such as alkylation of benzene, benzene derivatives and naphthalene have been extensively studied under vapor-phase fixed bed conditions. The alkylating reagents in these reactions can be either alcohols or alkenes. Alkylation with longer chain alcohols or alkenes needs to be carried out in the liquid-phase to avoid the cracking of alkylating reagents at high temperatures [122]. Shape-selective zeolites [123] play an important role in the preparation of selective p-isomer of benzene derivatives.

Aromatic acylation (Fridel-Crafts) reactions have also been carried out using zeolite catalyst [124]. Aromatic compounds with heteroatom can also be alkylated/acylated with very high selectivity [125]. The common feature in most of the above mentioned reactions is the formation of carbonium ion or electrophile.

1.7.2 Carbon-Carbon Bond Formation Reactions under liquid phase

Zeolite catalyzed liquid-phase carbon-carbon bond formation reactions are less common. The condensation of aldehydes and ketones over zeolites [126-132] has been studied extensively under vapor-phase, fixed-bed conditions. Formaldehyde and isobutylene can be condensed to isoprene [128]. Iron-containing ZSM-5 converts acetone selectively into 2,4- dimethylphenol [130]. Recently Kawai et.al. reported the liquid-phase, carbon-carbon bond formation between Silylenol ethers and various carbonyl compounds over CaY, SiO_2-Al_2O_3 [133]. Here in the present dissertation, the liquid-phase carbon-carbon bond formation reactions such as Mukaiyama aldol condensation, Michael addition, nucleophilic alkylation and acylation of silylenol ethers of

ketones over titanium-silicates like TS-1 are studied for the first time. The results are compared with those obtained over other zeolites and metallo-silicate analogues.

1.8 SCOPE OF THE THESIS

Chapter 1 provides a brief introduction about zeolites, their classification, modification, characterization and catalysis. The addition of an organic additive (template) can lead to the synthesis of high-silica zeolites. Template-zeolite structure relationships are reviewed, including the recently synthesized novel, high-silica, large-pore zeolite designated as NCL-1 using a new diquaternary salt hexamethylene bis (triethyl ammonium bromide).

Chapter II describes the synthesis of zeolite NCL-1. The role of various inorganic cations such as Li^+, Na^+, K^+, and Cs^+ in the synthesis of the silicon-end member zeolite NCL-1 (Si-NCL-1) will be discussed. The influence of various silica sources on the synthesis has also been studied and these results are presented. Synthesis of Al-, Ga-, and Fe-silicate analogues of novel, high-silica zeolite NCL-1 is given. Further, the synthesis procedure of titanium-silicate, used as catalyst for carbon-carbon bond formation reactions under liquid-phase conditions, is also given.

Chapter III describes the characterization of Al-, Ga-, and Fe-silicate analogues of zeolite NCL-1 and the Si-NCL-1 prepared in presence of various inorganic cations by various techniques including XRD, IR, ESR, MAS NMR, Scanning Electron Microscopy (SEM), and ion exchange capacity, sorption and surface area measurements.

Chapter IV describes acid-catalyzed reactions over zeolite NCL-1 under vapor-phase fixed bed conditions. The isopropylation of benzene to cumene, isomerization of 1,3,5-trimethylbenzene to 1,2,4-trimethylbenzene, the Fries rearrangement of phenylacetate to hydroxy acetophenone, and .

the selective decomposition of cumenehydroperoxide into phenol and acetone have been studied in detail.

Chapter V discusses liquid-phase carbon-carbon bond formation reactions using aluminum-free, titanium-silicate molecular sieves as a Lewis acid catalysts, for the first time. Mukaiyama aldol condensation between silylenol ethers (enolic form of ketones) and various aldehydes, Michael addition reaction between silylenol ether and various α,β-unsaturated carbonyl compounds, α-tert.butylation of cyclohexanone via silylenol ether with tertiary butylchloride, and the preparation of 1,3-diketones using silylenol ethers and acid chlorides have been studied. All the reactions have been carried out at low temperature (less than 60°C), under dry conditions, and the mechanism of the reactions are explained on the basis of the "oxophilic" Lewis acidity of titanium silicates. This is the first report of the use of TS-1 in non-oxidative, C-C bond formation reactions.

Chapter VI summarizes the salient features of the work carried at and discussed in the thesis. o

1.9 REFERENCES

1. D.W. Breck, *"Zeolite Molecular sieves: Structure, Chemistry and Use"* London, Wiley (1974).

2. R.M. Barrer, *"Hydrothermal Chemistry of Zeolites"* London, Academic Press (1982).

3. W.M. Meier, D.H. Olson, *"Atlas of Zeolite Structure Types"*, London, Butterworths, (1987).

4. W.L. Bragg, *"The atomic Structure of Minerals"*, Cornell University Press, Ithaca, New York (1937).

5. W.M. Meier, *"Molecular Sieves, Soc. of Chem. Ind.,* London, p10 (1968).

6. E.M. Flanigen, *"in Proceedings of the 5th International Conference on Zeolites"*, (L.V.C. Rees, Eds.), Naples, Italy, June 2-6, p760 (1980).

7. LB Sand, *Econ. Geol.,* p191 (1967).

8. B.M. Lok, T.R. Cannan and C.A. Messina, *Zeolites,* **3**, 282 (1983).

9. C.C. Freyhardt, M. Tsapatsis, R.F. Lobo, K.J. Balkus Jr and M.E. Davis, *Nature,* **381**, 295 (1996).

10. C. Baerlocher and WM. Meier, *Helv. Chem. Acta,* **52**, 1853 (1969).

11. C. Baerlocher and WM. Meier, *Helv. Chem. Acta,* **53**, 1285 (1970).

12. R. Allello and R.M. Barrer, *J. Chem. Soc., A*, 1470 (1972).

13. N.A. Acara, US Pat. 3 414 602 (1968).

14. E.M. Flanigen and E.B. Kellberg US Pat 4 241 036 (1968).

15. T.V. Whittam, US Pat. 4 060 590 (1977).

16. T.V. Whittam, EP Pat. Appl. 55 046 (1982).

17. T.V. Whittam, US Pat. 4 209 498 (1980).

18. D. Seddon and T.V. Whittam, EP Appl. 55 529 (1982).

19. M.K. Rubin, Ger. Offen. 1 806 154 (1969).

20. Union Carbide Corporation, B.P. Pat. 909 624 (1962).

21. G.T. Kokotailo and S. Sawruk, US Pat. 4 187 283 (1980).

22. F.G. Dwyer and E.E. Jenkins, US Pat. 4 287 166 (1981).

23. B.G. Pelrine, US Pat 4 259 306 (1981).

24. P. Chu, EP. Appl. 0 023 089 (1981).

25. Chu, Chinu-Chiun, US Pat. 4 206 843 (1981).

26. R.L. Wadlinger, G.T. Kerr and E.J. Rosinski, US Pat. 3 308 069 (1967).

27. Mobil Oil Corp. Neth. Pat. 7 014 807 (1971).

28. J.L. Casci, Stud. Surf. Sci. Catal., **28**, 215 (1986).

29. R.J. Argauer and G.R. Landolt, US Pat. 3 702 886 (1972).

30. P. Chu, US Pat. 3 709 979 (1973).

31. D.A. Hichkson, BE Pat. 8 886 833 (1981).

32. L.D. Rollmann, US Pat. 4 296 083 (1981).

33. C.J. Plank, E.J. rosinski and M.K. Rubin, US Pat. 4 016 245 (1977).

34. L. Marosi, M. Schwarzmann and J. Stabenow, EP. Appl. 49 386 (1982).

35. L.D. Rollmann and E.W. Valyocsik, US Pat. 4 139 600

36. L.D. Rollmann and E.W. Valyocsik, US Pat. 4 108 881.

37. E.W. Valyocsik, US Pat. 4 585 786 (1986).

38. T.V. Whittam, EP Appl. 54 363 (1982).

39. L.D. Rollmann and E.W. Valyocsik, EP Appl. 15 132 (1980).

40. J.L. Casci, B.M. Lowe and T.V. Whittam UK Pat.Appl. 2 077 709 (1982).

41. E.W. Valyocsik, US Pat. 4 481 177 (1984).

42. US Pat. 4 623 527.

43. R. Szostak, US Pat. 4 585 639 (1986).

44. A. Bhaumik and R. Kumar, *Microporous Materials*, 5, 173 (1995).

45. EP 174 121 (1986).

46. J.L. Casci, *Stud. Surf. Sci. Catal.* 28, 215 (1986).

47. R. Kumar, K.R. Reddy and P. Ratnasamy, US Pat. 5 219 813 (1993).

48. K. Ramesh Reddy, R. Kumar, V. Ramaswamy and A.V. Ramaswamy, *Zeolites*, 4, 326 (1994).

49. R. Kumar and K. Ramesh Reddy, *Microporous Materials*, 3, 195 (1994).

50. V.J. Frilette, W.O. Haag and R.M. Lago, *J. Catal.*, 67, 218 (1981).

51. J. Weitkamp and S. Ernst, *Stud. Surf. Sci. Catal.*, 38, 367 (1988).

52. J.A. Martens, M. Tielen, P.A. Jacobs and J. Weitkamp, *Zeolites*, 4, 98 (1984).

53. J.R. Goldsmith, *Min. Mag.*, 29, 952 (1952).

54. Asim Bhaumik and R. Kumar, *Catal. Lett.*, 35, 327 (1995).

55. M. Tielen, M. Geelen and P.A. Jacobs, *Acta. Phys. Chem.*, **31**, 1 (1985).

56. R. Szostak, Molecular Sieves: *Principles of Synthesis and Identification*, Van Nostrand Reinhold, New York, p79 (1989).

57. P. Ratnasamy and R. Kumar, *Catal. Lett.*, **22**, 229 (1993).

58. G. Bellussi and V. Fattore, *Stud. Surf. Sci. Catal.*, **69**, 79 (1991).

59. L. Pauling, in *"The Nature of Chemical Bond"*, Goskhimizdat, Hoscow, 1947.

60. A. Dyer, in *"An Introduction to Zeolite Molecular Sieves"*, John Wiley & Sons Ltd., p113 (1988).

61. G.W. Skeels and E.M. Flanigen, ACS Symposium Ser. 398, Washington D.C. p420 (1989).

62. A. Carati, S. Contarini, R. Millini and G. Bellussi, *Pro. Mat. Res. Soc.*, Extended Abstract (EA 24), 1990.

63. D.W. Breck and G.W. Skeels, US Pat. 4 503 023 (1985).

64. D.W. Breck, US Pat. 3 130 007 (1964).

65. A. Culfaz and L.B. Sand, *Adv. Chem. Ser.*, **121**, 140 (1973).

66. A. Erdem, M.S. Thesis, Worcester polytechnique Institute USA (1978).

67. K.J. Chao, T.C. Tasi, M.S. Chen and I.J. Wang, *Chem. Soc. Faradays Trans. 1*,**77**, 547 (1981).

68. J.J. Pluth, J.V. Smith and J.M. Bennett, *Acta. Crystallog.*, **C42**, 283 (1986).

69. P.R. Rudolf, C. Saldarriaga-Molina and A. Clearfield, *J. Phy. Chem.*, **90**, 6122 (1986).

70. E.M. Flanigen, H. Khatami and H.A. Szymanski, *ACS Symposium Ser.* **101**, Washington D.C., P201 (1971).

71. E.M. Flanigen, *ACS Symposium Ser.* **171**, Washington D.C., P80 (1976).

72. J.C. Jansen, F.J. Van der Gaag and H. Van Bekkum, *Zeolites,* **4**, 369 (1984).

73. P.A. Jacobs, H.K. Beyer and J. Valyan, *Zeolites,* **1**, 161 (1981).

74. G. Coudurier, C. Naccache and J.C. Vedrine, *J. Chem. Soc. Chem. Commun.,* 1413 (1982).

75. M.R. Boccuti, K.M. Rao, A. Zecchina, G. Leofanti, G. Petrini, *Stud. Surf. Sci. Catal.,* **48**, 133 (1989).

76. H.G. Karge, *Stud. Surf. Sci. Catal.,* **65**, 133 (1992).

77. V.A. Maroni, K.A. Martin and S.A. Johnson, *ACS Symposium Ser.,* **368**, 125 (1987).

78. G. Englhardt, and D. Michel, *High-resolution solid-state NMR of silicates and zeolites,* Wiley, London, p111 (1987).

79. E. Lippmaa, M. Magi, A. Samoson, G. Englhardt and A.R. Grimmer, *J. Am. Chem. Soc.,* **102**, 4889 (1980).

80. G. Englhardt, U. Loose, E. Lips, M. Tarmac and M. Magi, *Z. Anorak. All. Chem.,* **482**, 49 (1981).

81. M. Magi, A. Samoson, M. Tarmak, G. Englhardt and E. Lippmaa, *Dok. Akad. Nauk., USSR,* **261**, 1169 (1981).

82. G. Englhardt, E. Lippmaa and M. Magi, *J. Chem. Soc., Chem. Commun.,* 712 (1981).

83. S. Ramdas, J.M. Thomas, J. Klinowski, C.A. Fyfe and J.S. Hartman, *Nature,* **292**, 228 (1981).

84. J.M. Thomas, J. Klinowski, *Adv. Catal.,* **33**, 199 (1985).

85. J.M. Thomas, J. Klinowski, C.A. Fyfe, J.S. Hartman and L.A. Bursil, *J. Chem. Soc., Chem. Commun.,* 678 (1981).

86. J. Klinowski, J.M. Thomas, M. Audier, S. Vasudevan, C.A. Fyfe and J.S. Hartman, *J. Chem. Soc., Chem. Commun.,* 570 (1981).

87. J.B. Nagy, J.P. Gilson and E.G. Derouane, *J. Chem. Soc., Chem. Commun.,* 1129 (1981).

88. D. Greude and H.J. Behrens, *Cryst. Res. Technol.,* **16**, 1236 (1981).

89. C.A. Fyfe, J.M. Thomas, J. Klinowski and G.C. Gobbi, *Angew. Chem., Int. Ed. Engl.,* **22**, 259 (1983).

90. J. Klinowski, *Prog. Nucl. Magn. Reson. Spectrosc.,* **16**, 237 (1984).

91. J.B. Nagy, G. Englhardt and D. Michael, *Adv. Colloid Interface Sci.,* **23**, 67 (1985).

92. A.P.M. Kentgens, C.R. Bayense, J.H.C. van Hoof, J.W. de Haan and L.J.M. Van de Ven, *Chem. Phys. Lett.,* **176 (3,4)**, 399 (1991).

93. C.R. Bayense, P.M. Kentgens, J.W. de Haan, L.J.M. Van de van and J.H.C. van Hoof, *J. Phys. Chem.* **96**, 775 (1992).

94. N.P. Evmiridis, *Inorg. Chem.* **25**, 4362 (1986).

95. P. Ratnasamy, R.B. Borade, S. Sivasanker, V.P. Shiralkar and S.G. Hegde, *Acta. Phys. Chem.* **31**, 137 91985).

96. P. Ratnasamy and R. Kumar, *Catal. Today.,* **9**, 329 (1991).

97. G. Bellussi, A. Carati, M.G. Clerici, G. Maddinelli and R. Mellini, *J. Catal.,* **133**, 220 (1992).

98. J.S. Reddy and R. Kumar, *J. Catal.,* **130**, 440 (1991).

99. G. Bellussi, M.S. Rigutto, *Stud. Surf. Sci. Catal.,* **85**, 177 (1994).

100. A. Zecchina, G. Spoto, S. Bordiga, A. Ferrero, G. Petrini, G. Leofanti and M. Padovan, *Stud. Surf. Sci. Catal.,* **69**, 251 (1991).

101. R.M. Barrer and D.W. Riley, *Trans. Faraday Sdoc.*, **46**, 853 (1950).

102. R.M. Barrer and W.I. Stuart, *Proc. Roy. Soc.*, London, **A249**, 464, 484 (1959).

103. R.M. Barrer and R.M. Gibbsons, *Trans. Faraday Soc.*, **59**, 2569, 2875 (1963).

104. Hong-Xin. Li, J.A. Martins, P.A. Jacobs. et al., *"Innovation in Zeolite mater. Sci."* P.J. Groet, (ed.), p75 (1987).

105. N.J. Tapp, N.B. Milestone, D.M. Bibby, *"Innovation in Zeolite Mater. Sci."* P.J. Groet (ed.), p393 (1987).

106. D. Barthomeuf, *Stud. Surf. Sci. Catal*, **37**, 157 (1992).

107. J.W. Ward, *J. Catal.*, **16**, 173 (1970).

108. C. Mirodatos and D. Barthomeuf, *J. Chem. Soc. Chem. Commun.*, 39 (1981).

109. G. Bellusi, A. Carati, M. Clerici, G. Maddinelli, R. Millini, *J. Catal.*, **133**, 220 (1992).

110. D. Trong on, A. Bittar, S. Kaliaguine and L. Bonnevoit, *Catal. Lett.*, **16**, 85 (1992).

111. P.B. Weisz, *Pure Appl. Chem.*, **52**, 2091 / 2103 (1980).

112. C.D. Chang, C.T. Chu and R.F. Socha, *J. Catal.*, **86**, 289 (1984).

113. C.D. Chang, *Catal. Rev. Sci. Eng.*, **25**, 1 (1983), and reference therein.

114. F.J. Weigert, *J. Org. Chem.*, **52**, 3296 (1987).

115. C.D. Chang and P.D. Perkins, *Zeolites*, **3**, 298 (1983).

116. H. Le Blanc and L. Puppe, Ger. Offen. D.E. 3 332 687 (1985).

117. K. Honna, M. Sugimoto, N. Shimizu and K. Kurisaki., *Chem. Lett.*, 315 (1986).

118. W.F. Holderich, M. Hesse and F. Naumann, *Angew. Chem, Int. Ed. Engl.*, **27**, 226 (1988).

119. C. Neri and F. Buonomo, EP 100 117 (1983), Enichem Anic, S.P.A.

120. P.S. Lands and P.B. Venuto., *J. Catal.*, **6**, 245 (1966).

121. P.B. Venuto, *Microporous Materials*, **2**, 297 (1994).

122. G.T. Burress., EP 12 514 (1980).

123. M.M. Wu, US Pat., 4 391 998 (1983).

124. C. Gauthier, B. Chiche, A. Finiels and P. Geneste, *J. Mol. Catal.*, **50**, 219 (1989).

125. Y.I. Isakov and U.M. Minachev, *Russ. Chem. Rev.*, **51**, 1188 (1982).

126. T.J. Huang and W.O. Haag, US Pat. 4 339 606 (1982); EP 112 821 (1986).

127. K. Weissermel and H.J. Arpe, *Industrielle Organishe Chemie*, Verlag Chemie, Weinheim (1978) p108.

128. C.D. Chang, W.H. Lang and N. Morgan, EP 13 600 (1980).

129. Y. Servotte, J. Jacobs and P.A. Jacobs, in *"Proc. Zeocat Symp."*, Siofok (Hungary) 1985, *Acta. Phys. Chem.*, (Szeged) 1985, p1.

130. J. Shabati, R. Lazar and E. Biron, *J. Mol. Catal.*, **27**, 35 (1984).

131. H. Van Bekkum and H.W. Kouwenhoven, *Recl. Trav. Chim. Phy. Bas*, **108**, 283 (1989).

132. C.D. Chang and W.H. Lang, US Pat. 4 220 783 (1979).

133. M. Kawai, M. Onaka and Y. Izumi, *Bull. Chem. Soc. Jpn*, **61**, 1237 (1988).

CHAPTER 2

EXPERIMENTAL AND SYNTHESIS

2.1 INTRODUCTION

In this chapter, the hydrothermal synthesis of zeolite NCL-1 and its Ga- and Fe-silicate analogues are discussed. The ferri-silicate analogue of NCL-1 (Fe-NCL-1) was synthesized according to a modified procedure using a complex method [1,2]. Further, an all silica analogue of NCL-1 (Si-NCL-1) was prepared in the presence of various inorganic cations such as Li^+, Na^+, K^+ and Cs^+. The effect of various inorganic cations on the crystallization time has been studied. The synthesis of Si-NCL-1 has also been standardized using various, commercially available, fumed silicas with varying surface areas.

2.2 SYNTHESIS OF ORGANIC ADDITIVE: HEXAMETHYLENE BIS (TRI ETHYL AMMONIUM BROMIDE)

The organic additive hexamethylene bis (triethylammonium bromide) was synthesized by quaternizing triethylamine with 1,6-dibromohexane using acetone as solvent. The molar ratio of triethylamine to 1,6-dibromohexane was kept at 2.2 (Equation 2.1).

$$2(C_2H_5)_3N \; + \; \underset{Br}{CH_2}\!\!-\!\!(CH_2)_4\!\!-\!\!\underset{Br}{CH_2} \xrightarrow[\text{Refluxing}]{\text{Acetone}} \left[(C_2H_5)_3\,N\!\!-\!\!(CH_2)_6\!\!-\!\!N(C_2H_5)_3\right]^{2+}_{\,2Br^-}$$

-------- 2.1
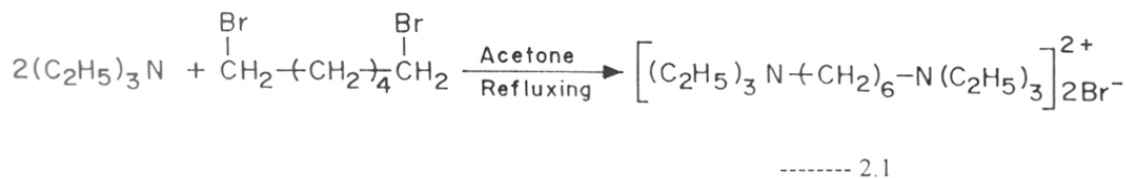
Procedure:

25g triethylamine (AR grade) and 20 g acetone (AR grade) were combined in a 250ml, round-bottom flask. 30g of 1,6-dibromohexane (Aldrich >99%) and 50g of acetone were added to this mixture. The reaction mixture was then refluxed for 12h, and after completion of the reaction, a white, diquaternary salt was formed with >90% yield. This salt was separated from the reaction mixture and dried under vacuum. The solid salt formed was characterized by chemical

analysis (C, H, and N), ^{1}H, and ^{13}C NMR, IR spectroscopy characterization and mass spectrometry. The data are presented below.

Chemical analysis:

Calculated $C_{18}H_{42}N_2Br_2$, wt.%	Found wt.%
C, 48.4	C, 48.7
H, 9.4	H, 9.5
N, 6.3	N, 6.2
Br, 35.6	Br, 35.9

The ^{1}H NMR spectrum of the sample is shown in Fig 2.1. The chemical shifts δ, are 10.1-1.37 (t, 6-C$\underline{H}_3$ 18H), 1.38-1.55 (m, 2-N-CH$_2$-CH$_2$-C$\underline{H}_2$- 4H), 1.58-1.80 (m, 2-N-CH$_2$-C$\underline{H}_2$- 4H) and 3.05- 3.44 (m, 8-N-C$\underline{H}_2$- 16H). The observed chemical shift positions and integration values (from the ^{1}H NMR spectrum) match the calculated values. Thus ^{1}H NMR data suggest that the resulting sample is hexamethylene bis(triethylammonium bromide).

The ^{13}C NMR (D$_2$O) spectrum of the sample is shown in Figure 2.2. The chemical shift (δ) values and corresponding assignments are: 7.9(6-CH$_3$), 22.0 (2 -N-CH$_2$-CH$_2$-$\underline{C}$H$_2$-), 26.3 (2-N-CH$_2$-$\underline{C}$H$_2$-), 53.7 (6-N-$\underline{C}$H$_2$-CH$_3$-) and 57.6 (2-N-$\underline{C}$H$_2$-CH$_2$-), respectively.

The mass spectrum of the sample is shown in Figure 2.3. The lines are assigned to: m/e 228 (4%, M$^+$-2C$_2$H$_5$Br), 199 (7%, 228-C$_2$H$_5$), 154 (7%), 142 (12%), 126 (8%), 108 (55%, C$_2$H$_5$Br), 101 (14%, N(C$_2$H$_5$)$_3$, 86 (100%, (C$_2$H$_5$)$_2$NCH$_2^+$ <----> (C$_2$H$_5$)$_2$N$^+$=CH$_2$)), 81 (11%), 72(9%, 86-CH$_2$) and 58 (19%, 86-C$_2$H$_5$).

The IR spectrum of the sample in chloroform shows absorption bands at 2926 cm^{-1} (strong), 1484 cm^{-1} (medium) and 1200-1240 cm^{-1}, which are due to C-H stretching, C-H bending
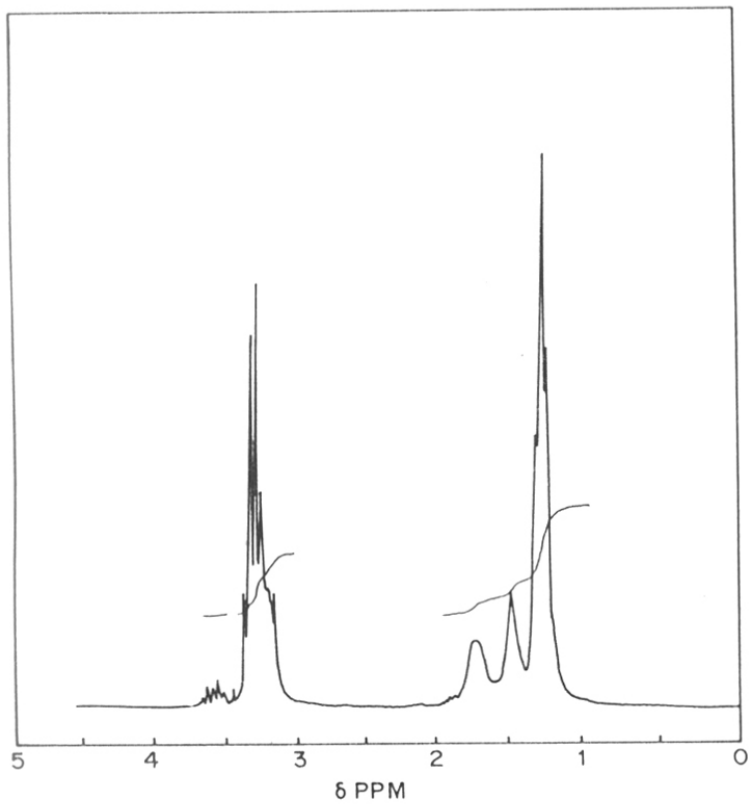
Fig.2.1 ^{1}H NMR spectrum of hexamethylene bis(triethylammonium bromide)
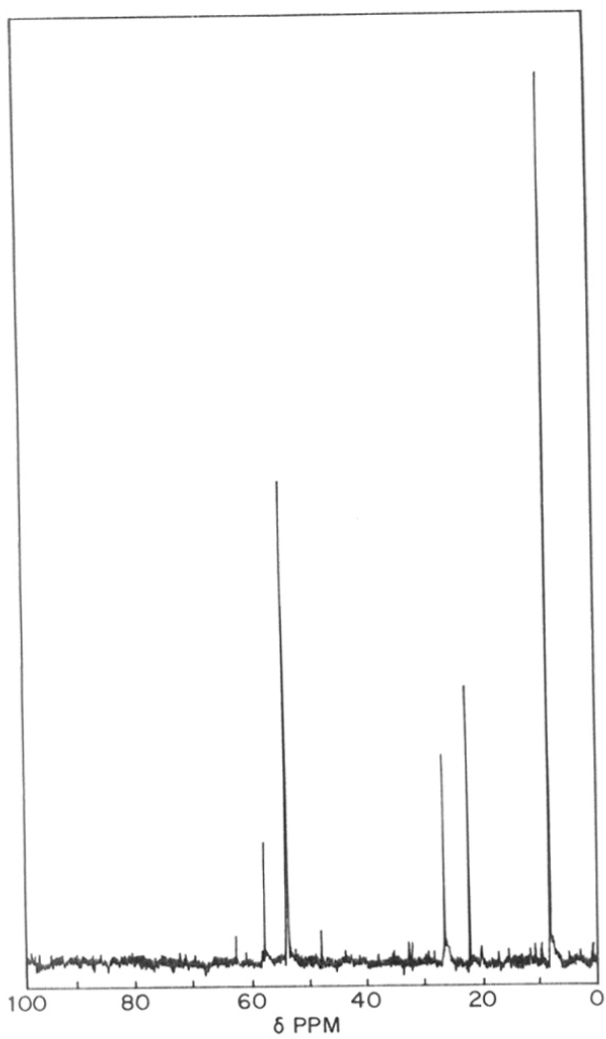
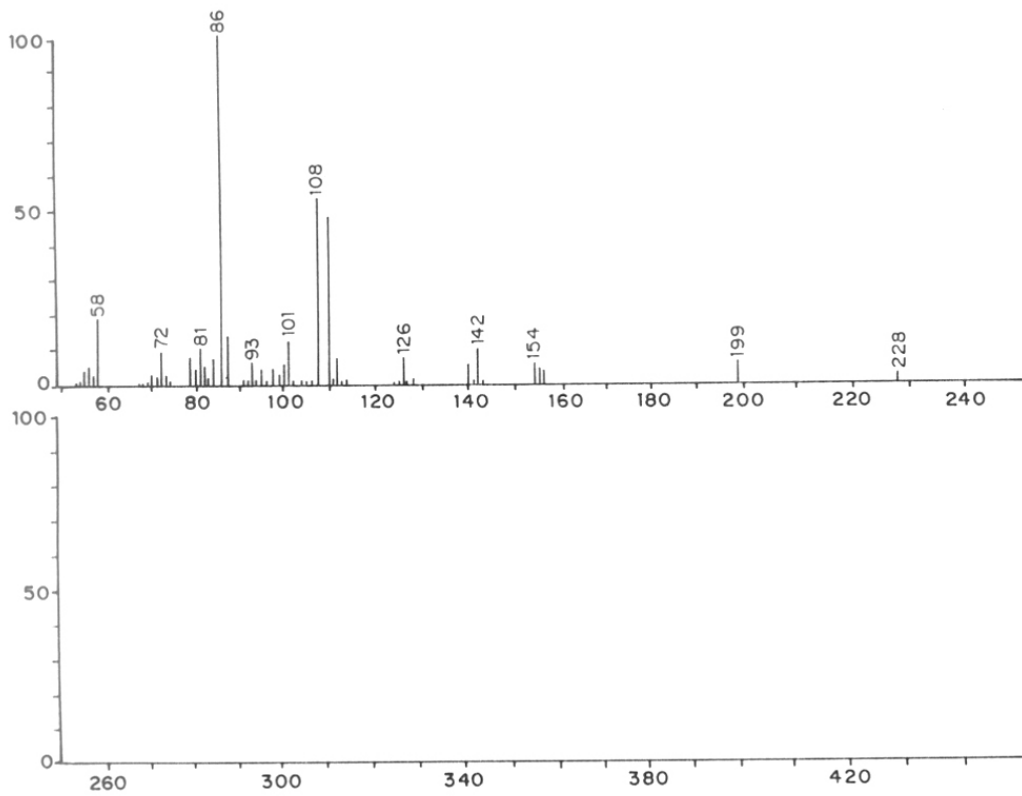Fig. 2.2 ^{13}C NMR spectrum of hexamethylene bis(triethylammonium bromide)

Fig.2.3   Mass spectroscopy of hexamethylene bis(triethylammonium bromide)

and C-N stretching vibrations, respectively. The absorption band due to C-Br vibration in the range of 500-600 cm^{-1} was not observed. This confirms the absence of reactant (1,6-dibromohexane) in the product. The above data confirm that the resulting salt is hexamethylene bis(triethylammonium bromide).

2.3 SYNTHESIS OF Al, Ga AND Fe-NCL-1 ZEOLITE

A typical stainless steel autoclave used in the hydrothermal zeolite synthesis is given in Figure 2.4. The raw materials used in the synthesis are presented in Table 2.2. The synthesis of NCL-1 samples with the Si/Al ratios 20, 80, 150, 250 and the aluminum-free polymorph were carried out using the following molar gel compositions.

OH$^-$/Si = 0.12, R$_2^+$/Si = 0.05, Na$^+$/Si = 0.25, H$_2$O/Si = 52

(where OH$^-$ = [Na$^+$] - 2[SO$_4^{2-}$])

The OH$^-$/Si ratio, 0.12, was adjusted by using appropriate amounts of sulfuric acid. The exact amount of reagents added for the preparation of each zeolite is listed in Table 2.3. In a typical preparation, the following procedure was used. A solution containing 1.5g NaOH in 10g H$_2$O was added to a slurry of 9.0g fumed silica in 60g H$_2$O. This mixture was stirred for 45min at 298K. To the above mixture, a solution containing the required amount of aluminum sulfate in water (0.60, 0.32, or 0.192g of Al$_2$(SO$_4$)$_3$.16H$_2$O in 10g of water for Si/Al ratios 80, 150, or 250, respectively) was added. The mixture was subsequently stirred for 20 min before a solution of 1.71g hexamethylene bis(triethylammonium bromide) in 15g H$_2$O was added. Finally, 0.72, 0.84, or 0.90g of H$_2$SO$_4$ in 10g water was added to the gels with Si/Al rations 80, 150 and 250, respectively. For the preparation of the NCL-1 sample with Si/Al = 20, aluminum isopropoxide (1.56g) was used as the aluminum source. The amount of sulfuric acid added to the final gel was

TEFLON GASKET
80 × 65 × 3

BOLT & NUT
Ø 10 × 30 mm Long

7 mm

150 mm

Ø 55 mm

Ø 65 mm
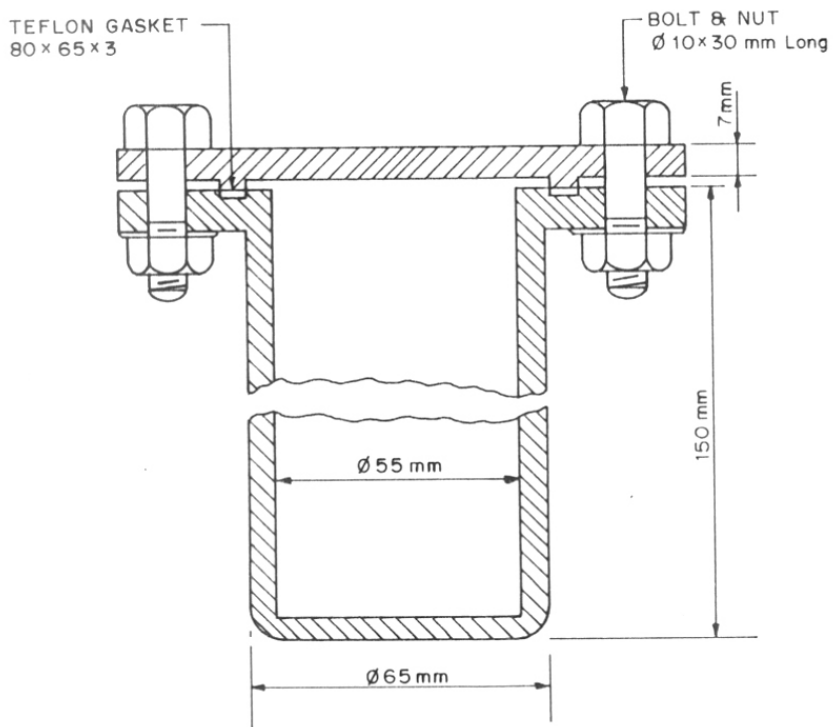
Fig.2.4   Stainless steel (316) autoclave with teflon gasket was used in the hydrothermal synthesis.

Table 2.2 Specifications of Reactants Used in the Synthesis of Metallosilicate Analogues of Zeolite NCL-1

	Reagent and source	Chemical formula	Purity, %
1	Fumed silica, S-5130, Sigma	SiO_2	99.5
2	Tetraethyl ortho silicate, TEOS, Aldrich	$Si(OEt)_4$	98.0
3	Silica sol (28 %) Lona industry, Bombay	SiO_2	28 % aqueous
4	Hexamethylene bis(triethylammonium bromide), Laboratory made	$[(C_2H_5)_3\text{-}N^+\text{-}(CH_2)_6\text{-}N^+\text{-}(C_2H_5)_3]^{2+}\ 2Br^-$	99.0
5	Ferric Sulfate, BDH	$Fe_2(SO_4)_3.\ 9H_2O$	98.0
6	Gallium nitrate, Aldrich	$Ga(NO_3)_3$	99.0
7	Aluminum sulfate, BDH	$Al_2(SO_4)_3.16H_2O$	98.0
8	Sodium hydroxide, Loba	$NaOH$	99.0
9	Lithium hydroxide, Loba	$LiOH$	98.0
10	Potassium hydroxide, Loba	KOH	99.0
11	Cesium chloride, Aldrich	$CsCl$	98.0
12	Hexamethylene bis(trietylammonium hydroxide), Laboratory made	$[(C_2H_5)_3\text{-}N^+\text{-}(CH_2)_6\text{-}N^+\text{-}(C_2H_5)_3]^{2+}\ 2OH^-$	20% aqueous solution

Table 2.3 Gel Composition in Synthesis of Various Metallosilicate Analogue of Zeolite NCL-1

Sample name	Si/M ratio	The amount of various reagents added, g					
		SiO_2	$M_2(SO_4)_3.xH_2O$	NaOH	Template	H_2O	H_2SO_4 (96%)
Si-NCL-1	∞	9 g	-	1.5 g	3.42 g	140 g	-
Al-NCL-1	250	9 g	0.192 g	1.5 g	3.42 g	140 g	0.90 g
Al-NCL-1	150	9 g	0.32 g	1.5 g	3.42 g	140 g	0.84 g
Al-NCL-1	80	9 g	0.60 g	1.5 g	3.42 g	140 g	0.72 g
Al-NCL-1	20	9 g	1.54 g	1.5 g	3.42 g	140 g	0.88 g
Ga-NCL-1	80	9 g	0.41 g	1.5 g	3.42 g	140 g	0.85 g
Ga-NCL-1	150	9 g	0.21 g	1.5 g	3.42 g	140 g	1.10 g
Fe-NCL-1	80	9 g	0.53 g	1.5 g	3.42 g	140 g	1.0 g
Fe-NCL-1	150	9 g	0.28 g	1.5 g	3.42 g	140 g	1.10 g

$M_2(SO_4)_3.xH_2O = Al_2(SO_4)_3.16H_2O$, $Fe_2(SO_4)_3.9H_2O$, $Ga_2(SO_4)_3$.

For Si/Al = 20, aluminum isopropoxide was used as aluminum source.

0.88g. The resultant reaction mixture was stirred for 1h and then autoclaved 5-12 days depending on the Si/Al ratio of the zeolite.

The synthesis of Ga- and Fe-NCL-1 samples [3] with Si/M ratio in the gel 80, and 150 were carried out using the following molar gel composition.

$OH^-/Si = 0.1 - 0.12$, $Na^+/Si = 0.25$, $R_2^+/Si = 0.05$, $H_2O/Si = 52$

(where $OH^- = [Na^+] - 2[SO_4^{2+}]$)

The OH⁻/Si ratio was adjusted by adding appropriate amounts of sulfuric acid to the gel. The Fe-NCL-1 samples were prepared according to our general and convenient method for preparing ferrisilicate molecular sieves using a complexing agent [1,2]. In a typical Fe-NCL-1 synthesis, an alkali solution containing 1.5g NaOH in 20g water was added to a slurry of 9g fumed silica (Sigma- 5130) in 60g water. This mixture was stirred for 45 min at 298K before adding it slowly, under vigorous stirring, to a solution containing the required amount of ferric sulfate and oxalic acid in water (0.53g or 0.28g of $Fe_2(SO_4)_3.9H_2O$ in 20g water to yield Si/Fe ratios of 80 or 150, respectively; oxalic acid/Fe = molar ratio 1.5). The mixture was stirred for 15 min before adding a solution containing 3.42g of hexamethylene bis(triethylammonium bromide) in 15g water. Finally, 1.0 or 1.1g sulfuric acid (96%) in 30g water was added to the gel having Si/Fe ratios 80 or 150, respectively. The resultant reaction mixture was stirred for 1h and then autoclaved for 7-10 days.

Similarly, gallo-silicate was prepared where, instead of ferric sulfate and oxalic acid, $Ga_2(SO_4)_3$ (0.41g or 0.21g for Si/Ga ratios of 80 or 150, respectively) was added. Further, the amount of sulfuric acid used was 0.85g or 1.1g for the ratios 80 or 150, respectively. In all cases the crystallization was conducted in a 200ml stainless steel autoclave at $443 \pm 2K$ under agitation (60 rpm). After crystallization, the solid was filtered, washed with water, dried at 393K, and

finally calcined in flowing dry air at 823K. The yield of crystalline solid (based on $SiO_2+M_2O_3$)
ranged between 85 - 90% for all samples.

2.4 SYNTHESIS OF Si-NCL-1: INFLUENCE OF INORGANIC CATIONS

The starting materials used were fumed silica, NaOH/NaCl (AR), CsCl (Aldrich, 98%),
KOH/KCl (AR), LiOH/LiCl (AR), and hexamethylene bis triethylammonium bromide,
HMBTEABr$_2$). In the presence of various cations, the following molar gel composition was used
to prepare Si-NCL-1.

SiO_2: 0.16 MOH: x MCl: 0.05 HMBTEABr$_2$: 52 H_2O

(where M = alkali metal)

In a typical synthesis of Si-NCL-1, a solution containing the required amount of alkali- metal
hydroxide in 10g water was added to a slurry of 4.5g of fumed silica (Sigma 5130, USA) in 30g
of water. Where necessary, the required amount of alkali salt was added. This mixture was stirred
for about 45 min at room temperature before adding a solution of 1.72g HMBTEABr$_2$
(Hexamethylene bis(triethylammonium bromide)) in 15g H_2O. No sulfuric acid was used. The
resultant reaction mixture was stirred for 1h and then autoclaved for 2-4 days. The crystallization
was conducted at 443K under agitation (60 rpm) using 100ml stainless steel autoclave. The
crystallization time for Si-NCL-1 in the presence of various inorganic cations ranges from 36 -
76h. The results are given in Table 2.4. After the crystallization, the solid was washed thoroughly
with distilled water, dried and calcined at 823K for 12h in flowing dry air. The yield of the
products ranges between 80 - 90% for all the samples.

2.5 INFLUENCE OF VARIOUS SILICA SOURCES

Fumed silica was found to be an ideal source (the formation of zeolite NCL-1 is more
favorable) of silica in the synthesis of Si-NCL-1 (Table 2.5). While, using fumed silica, pure and

Table 2.4 Effect of Various Alkali Cations on the Synthesis of Si-NCL-1.

Molar gel composition: 6.25 SiO_2: xM_1: yM_2: 0.325 HMBTEABr$_2$: 333H_2O

Sample no	x M_1	y M_2	Cryst.[a] time, h	pH initial	pH final	Product[b]	Crystallinity[c], %
1	1.0 NaOH	-	60	11.35	11.65	NCL-1	100
2	0.8 NaOH	0.2 LiOH	76	10.85	11.05	NCL-1	100
3	0.6 NaOH	0.4 LiOH	92	10.80	11.0	NCL-1 + Q	70.0
4	0.4 NaOH	0.6 LiOH	120	10.75	10.90	ZSM-5 + Q	-
5	0.2 NaOH	0.8 LiOH	120	10.70	10.90	Q	-
6	1.0 NaOH	0.2 LiCl	60	10.80	11.05	Q	-
7	0.5 NaOH	0.5 KOH	54	10.90	11.30	NCL-1	95
8	-	KOH	48	10.90	11.20	NCL-1	100
9	1.0 NaOH	0.2 KCl	60	10.85	11.20	NCL-1	95
10	1.0 NaOH	0.4 KCl	60	10.75	11.10	NCL-1	80
11	1.0 KOH	0.2 NaCl	60	10.75	11.10	NCL-1	90
12	1.0 KOH	0.4 NaCl	60	10.70	10.90	Q	-
13	1.0 NaOH	0.1 CsCl	36	11.20	11.55	NCL-1	100
14	1.0 NaOH	0.2 CsCl	36	11.20	11.60	NCL-1	95
15	1.0 NaOH	0.4 CsCl	60	11.05	11.35	NCL-1 + Ams	60
16	1.0 NaOH	0.8 CsCl	72	10.90	11.30	Ams	-
17[d]	-	-	72	12.30	11.85	Ams	-
18[e]	0.6 NaOH	0.4 LiOH	92	10.80	11.20	NCL-1 + Crist	20

a: crystallization time

b: Q = $\propto$-quartz; Ams = amorphous

c: crystallinity with respect to most crystallized product obtained in the present study.

d: No inorganic cations were used, instead hexamethylene bis(triethylammonium hydroxide) was used to maintain the pH.

e: H_2O/SiO_2 ratio = 33, Crist = Cristobalite

Table 2.5 Synthesis of Zeolite NCL-1 from Various Fumed Silica

No	Silica source	Surface area m²/g	OH⁻/Si mole ratio	Crystallization time, h	Phase	crystallinity %
1	Sigma S-5005	400 ± 20	0.18 - 0.25	48	NCL-1	100
2	Sigma S-5130	390 ± 40	0.14 - 0.16	60	NCL-1	100
3	CabO-Sil-M-5	200 ± 20	0.18 - 0.22	60	NCL-1	95
4	Bombay silica	150 ± 20	0.13 - 0.15	72	NCL-1	90
5	Aerosil silica	200 ± 20	0.14 - 0.16	72	NCL-1	95
6	Mettur chem	270 ± 20	0.18 - 0.22	60	NCL-1	95
7	TEOS	-	-	90	ZSM-5	-
8	Silica sol[a]	-	-	90	Ams	-
9	Sodium silicate[a]	-	-	90	Ams	-

Gel composition: Si/template = 20, H_2O/SiO_2 = 52, for silicas 1, 2, 3, 5 and 6, the particle size varies from 0.007 - 0.008 μm.
a: No NCL-1 phase is formed, only amorphous material was obtained.

fully crystalline NCL-1 phase was obtained in 60h, only amorphous material was obtained even after 4 days with other SiO_2 sources. Further, the synthesis of zeolite NCL-1 is also sensitive to the nature of fumed silica. An attempt has been made to optimize the synthesis of Si-NCL-1 using various commercially available fumed silicas by changing the synthesis parameters. The concentration of alkali hydroxide and pH of the synthesis gel greatly influence the synthesis of Si-NCL-1. Since the OH^-/Si ratio plays crucial role in the synthesis, the commercially available fumed silicas were standardized by changing OH^-/Si ratio and the results are given in Table 2.5. By optimizing the hydroxide ion concentration for various fumed silicas, pure Si-NCL-1 is obtained. The fumed silicas with particle size of 0.007 - 0.008 μm (Sigma 5005, Sigma 5130, CabO-Sil M-5 etc) were found to be an efficient source for the preparation of Si-NCL-1 molecular sieve.

2.6 SYNTHESIS OF TS-1

The reactants used for the synthesis of TS-1 were tetraethyl orthosilicate (Aldrich, 98%), tetrapropyl ammonium hydroxide (Aldrich, 99%, 20% aqueous solution) and titanium tetrabutoxide (Merck, 99.8%). In a typical synthesis procedure, 33g of tetrapropyl ammonium hydroxide was added to 22g of tetraethyl orthosilicate. To the resultant clear solution 0.85g of titanium tetrabutoxide in 5g of dry isopropanol was added. Finally, 45g of water was added to the above clear solution and stirred at 348K for about 3h to remove the alcohols. The mixture was then transferred to a stainless steel autoclave (100ml capacity) and was crystallized under static conditions and autogeneous pressure at 443K for 2 days. After the crystallization, the solid was washed thoroughly with distilled water and dried at 393K for 3h. The as-synthesized TS-1 was calcined at 773K for 8h under flow of air.

2.7 CHARACTERIZATION

2.7.1 X-Ray Diffraction (XRD)

Powder X-ray diffraction patterns were measured using a Rigaku X-ray diffractometter (model D/HAX III VC, Japan) with Ni-filtered, Cu-Kα radiation (λ = 1.5404 Å). The samples were scanned from 5 to 50 2θ° at a scan rate of 0.25° min^{-1}. The sample with the highest crystallinity (based on preliminary experiments) was taken as the reference sample to compare the phase purity and crystallinity of other samples. Peak areas were calculated from the collected data using semi-quantitative software program provided with the instrument. Silicon was used as the internal standard for calibrating the 2θ° values.

2.7.2 Infrared Spectroscopy

IR spectra was mainly used to study the framework vibration. The infrared spectra of the samples were scanned in NICOLET 60 SXB spectrometer in the wavenumber range of 300 - 1300 cm^{-1} using the KBr technique. FT IR spectra of samples in the region of OH stretching vibrations and of chemisorbed pyridine were recorded in transmittance mode by using self supported wafers (56mg/cm^2). The sample was activated in situ in a specially fabricated cell (Figure 2.5) under vacuum at 400°C for 4h and cooled down to 100°C before recording spectra. Then, pyridine (10mm pressure) was admitted in to the cell and equilibrated with the sample for 1h. Excess pyridine was then pumped out, and then the spectrum was recorded. In this manner, pyridine was pumped out at 100, 200, 300 and 400°C and cooled down to 100°C before recording spectrum.

2.7.3 ESR Spectroscopy

ESR spectra of ferrisilicate samples were recorded (Bruker ER 200D) at 9.7 MHz (X band) with a rectangular cavity (ST8424). Frequency modulation was carried out at 100 KHz .
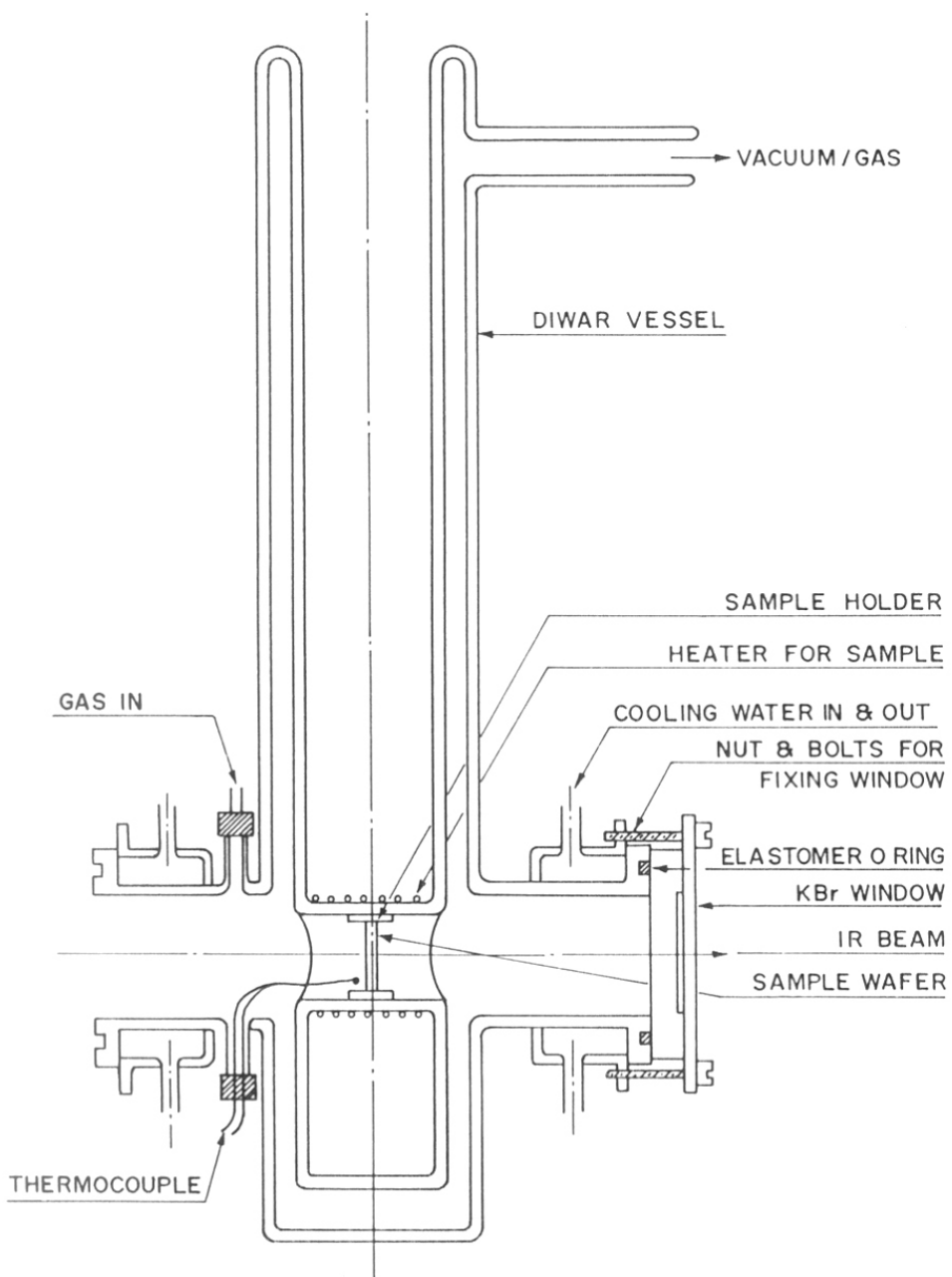
VACUUM / GAS

DIWAR VESSEL

SAMPLE HOLDER

HEATER FOR SAMPLE

COOLING WATER IN & OUT

NUT & BOLTS FOR FIXING WINDOW

GAS IN

ELASTOMER O RING

KBr WINDOW

IR BEAM

SAMPLE WAFER

THERMOCOUPLE

Fig.2.5   FT IR transmittance cell.

(intensity at 1.25 GPP) and a time constant of 10^3 msec was used. The hf power was chosen small enough to maximize the signal to noise (S/N) ratio.

2.7.4 MAS NMR Spectroscopy

The MAS NMR for ^{29}Si, ^{27}Al and ^{71}Ga were recorded at room temperature using BRUCKER MSL-300 spectrometer. The free induction decays were collected under MASS, and typically 2000 transients were accumulated to give an acceptable S/N ratio. Before Fourier-transformation, the FID was apodized with a 100 Hz exponential line broadening. ^{27}Al and ^{29}Si spectra were recorded using $Al(NO_3)_3.6H_2O$ and Tetramethylsilane as an internal standards.

2.7.5 Scanning Electron Microscopy

A scanning electron microscope (JEOL, JSM 5200) was used to investigate the morphology of the zeolite samples. In order to avoid surface charging and to protect the zeolite material from thermal damage by the electron beam, the sample was deposited on alumina and coated with a thin film of gold. In all the analyses a uniform film thickness of about 0.1 mm of sample was maintained. The scanning electron microscopy was mainly used to know the morphology of zeolite NCL-1.

2.7.6 UV-VIS Spectroscopy

The UV-VIS diffuse reflectance spectra for titanium-silicates were recorded using Pye Unichem SP-8-100 UV-Visible spectrometer. UV-VIS spectra was mainly used to find out the traces of anatase phase of titanium in titanium-silicates. The spectrum was recorded in the range of 200 to 800 nm.

2.7.7 Chemical Analysis

A known amount of sample (w_1) was placed in a platinum crucible with a lid and ignited to red hot. The sample was then cooled in desiccator and weighed again (w_2). The difference in weights ($w_1 - w_2$) gave the weight loss on ignition. The anhydrous weight of the sample was noted, and the sample was then treated with HF (40% electronic grade) and the silicon was removed in the form of H_2SiF_6 by evaporation on a hot plate. This procedure was repeated three times and the sample was again ignited, cooled in the deciccator and weighed. The loss in the weight of the sample indicated the content of silica. The residue was fused with potassium pyrosulfate and dissolved in distilled water. The final solution was analyzed for various metals such as Al, Fe, Ga, Na, K etc. by atomic absorption spectroscopy (Hitachi Z-800).

2.8 CATALYSIS

2.8.1 Vapor-Phase Reactions

The H-form of the zeolite NCL-1 was prepared by calcining the as-synthesized zeolites for 16h at 823K in flowing dry air to remove the organic additive. The sodium form of the zeolite was then subjected to repeated ion exchanges with 0.1M ammonium acetate solution at 353K for 6h. This exchange procedure was repeated thrice. The NH_4^+ form of the zeolite was calcined at 723K to get the H-form.

The catalytic vapor-phase reactions were performed at atmospheric pressure using a fixed-bed down-flow tubular silica reactor (Figure. 2.6). The reactor is made up of a fused-silica tube with 150 mm inner diameter and 350 mm length and provided with a thermowell. The thermowell is extended up to the catalyst bed. The H-form of catalyst powder was pressed at almost 10 tons of pressure, pelletized, crushed and sieved to obtain 20 - 30 mesh size. The catalyst was diluted with inert material (crushed porcelain beads). The catalyst was placed in the center of the reactor in such a way that the catalyst bed was sandwiched by inert porcelain beads. The reactants were passed into the reactor by a syringe pump (Sage Instruments, model 352) at a required feed rate, which varied from 2-15 ml/h. The catalytic reactor system shown in Figure 2.6 was attached to a heated sampling valve which was attached to GC. The reaction products were analyzed by using high-resolution capillary GC (HP-5890) equipped with a silicon gum column. The product stream from a sampling valve was collected after passing it through a condenser, cooled with ice-cold water.

2.8.2 Liquid-Phase Reactions

The liquid phase reactions were carried out in a glass, batch reactor. The catalyst was activated before the reaction at 473K for 3h and the reaction was performed under dry condition using dry solvents. The progress of the reactions was controlled by thin layer chromatography and isolated by column chromatography. The isolated products were confirmed by spectral techniques such as ^1H, ^{13}C, IR and mass spectral techniques.

Air/H_2/N_2

A - DRIER, 4A
B - FLOW METER
C - PREHEATER
D - FEED PUMP
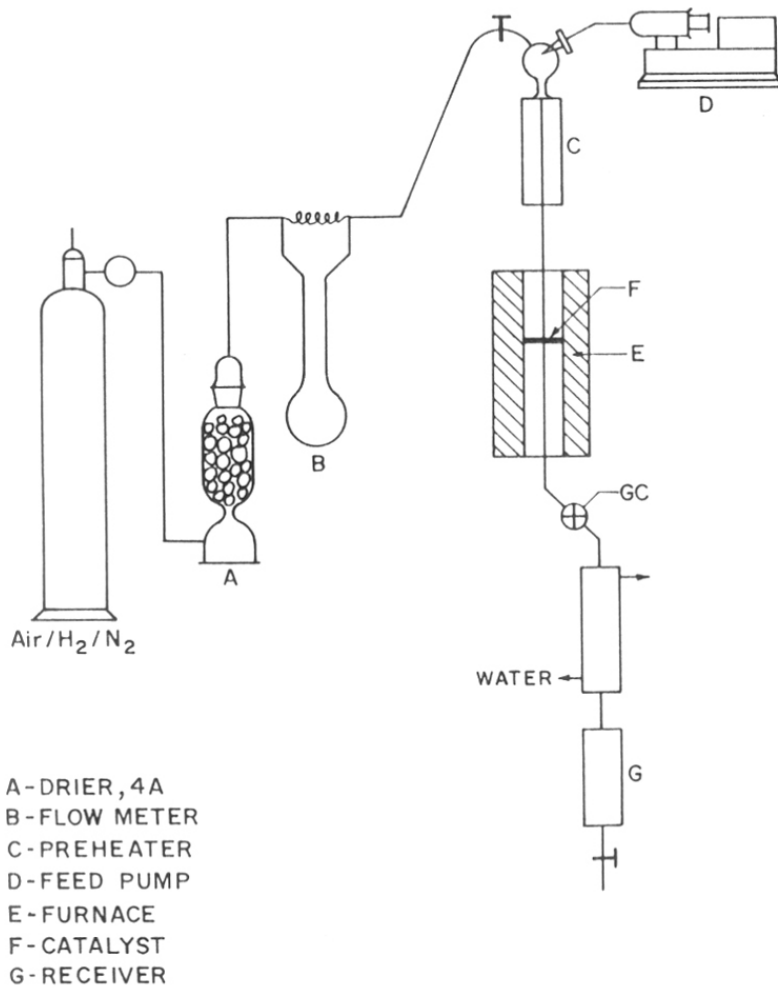E - FURNACE
F - CATALYST
G - RECEIVER

Fig.2.6   Fixed bed down-flow reactor.

2.9 SUMMARY

Hydrothermal synthesis of Al-, Ga- and Fe-silicate analogues of zeolite NCL-1 was carried out. The influence of various inorganic cations (Li$^+$, Na$^+$, K$^+$ and Cs$^+$) and fumed silicas (with different particle size) in the synthesis of Si-NCL-1 (an all silica analogue) was studied. The fumed silicas with particle size of 0.007 - 0.008 µm (Sigma 5005, Sigma 5130, CabO-Sil M-5 etc) were found to be an efficient source for the preparation of Si-NCL-1 molecular sieve.

2.10 REFERENCES

1.   P. Ratnasmy and R. Kumar, *Catal. Today,* 9, 329 (1991).

2.   A. Raj, K.R. Reddy and R. Kumar, in *Proc. 9th Intern. Zeolite Conf.* eds. R. Von. Ballmoos, J.B. Higgins and M.M.J. Treacy, (Butterworth-Heinemann, Toronto, 1993), Vol II, p 551.

3.   M. Sasidharan and R. Kumar, *Catalysis Letters,* (in press).
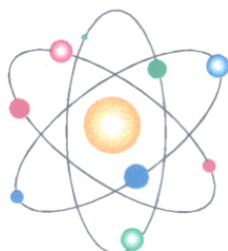
CHAPTER 3
CHARACTERIZATION

3.1 INTRODUCTION

In this chapter, the characterization of metallosilicates such as Al, Ga- and Fe-silicate analogues of zeolite NCL-1 as well as Si-NCL-1 prepared in the presence of various inorganic cations through various techniques is described.

3.2 CHARACTERIZATION OF Al, Ga, AND Fe-SILICATES

3.2.1 Powder X-Ray Diffraction (XRD)

The samples at each stage of the synthesis were analyzed by XRD for qualitative as well as quantitative phase identification. The X-ray powder pattern of NCL-1 samples with different metals (Al, Ga and Fe) are shown in Figure 3.1. The profiles 'a-d' refer to the calcined samples of Fe-, Ga-, Al-, and Si-NCL-1 (i.e. silicon polymorph of NCL-1) respectively. No extra impurity peaks were obtained. The integrated area of the XRD peaks in the 2θ range between 17-27 was used to determine the relative crystallinity of the metallosilicate analogues of zeolite NCL-1. During crystallization all the major lines grow simultaneously and the relative intensities of all the major peaks remain unchanged after complete crystallization. The sample exhibiting maximum area was taken as a reference (100% crystalline) sample and has been used to determine the relative intensity of other metallosilicates.

Table 3.1 shows the main peaks of the calcined Si-NCL-1 sample. The interplanar 'd' spacings (nm) were calculated using silicon as an internal standard. The relative intensities I/I_o of the lines were obtained after smoothing, background correction and $K\alpha_2$ stripping. The indexing of the peaks were performed by trial and error method using PDP11 software. After indexing the lines, the unit cell parameters and crystal symmetry were examined critically and was found to fit well into orthorhombic symmetry. From this it was found that NCL-1 possesses orthorhombic symmetry with a = 1.195 ± 0.03, b= 0.836 ± 0.003, c= 2.870 ± 0.004 nm. The 'd' values
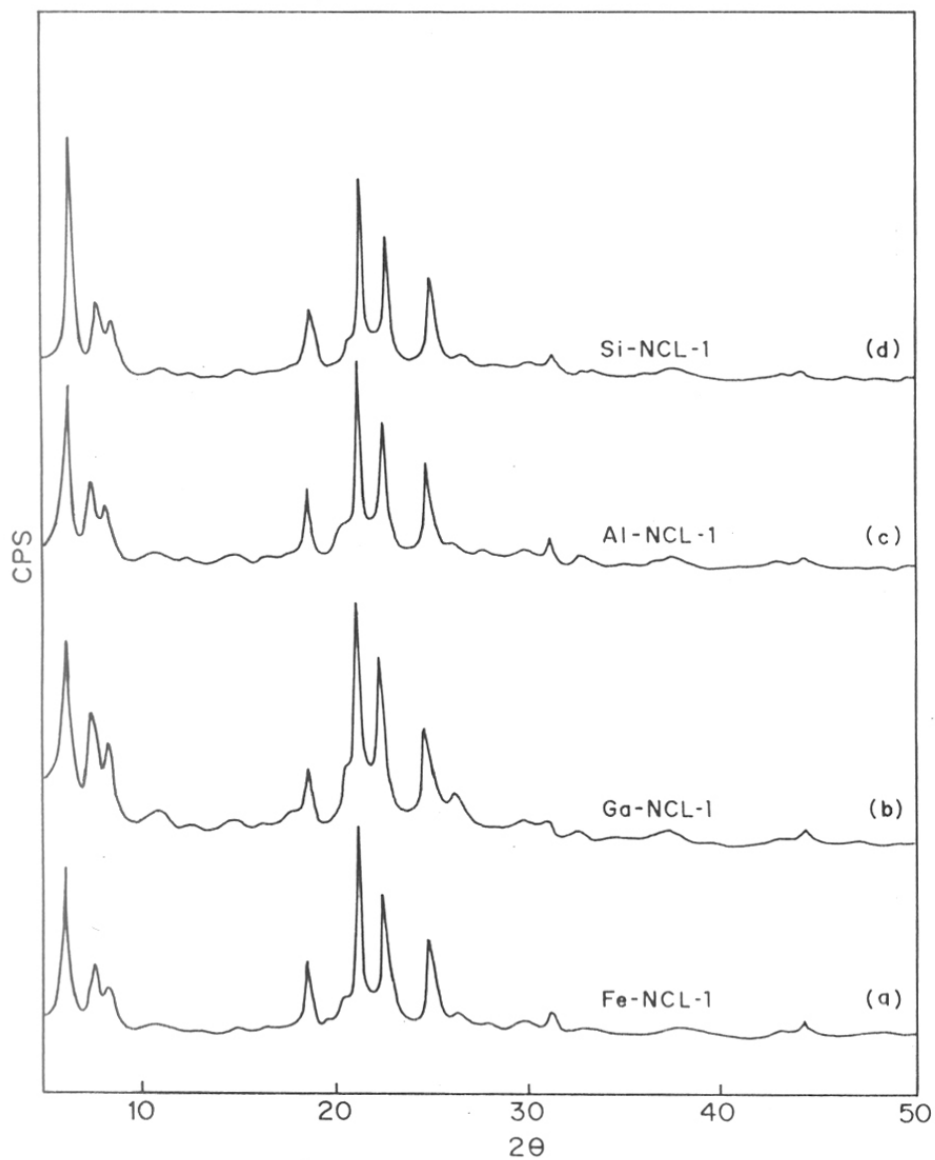
Fig.3.1   X-ray diffraction patterns of calcined NCL-1 samples, curves 'a' to 'd' refer
           to Fe-, Ga-, Al-NCL-1 samples with Si/M (molar ratio) of 88, 85, 83 and Si-
           NCL-1 (calcined form), respectively.

Table 3.1. XRD pattern of calcined Si-NCL-1[a].

d(expt.) nm	I/I$_o$	hkl	d(calc.) nm
1.435	100	002	1.435
1.195	25	100	1.195
1.098	22	101	1.102
0.802	2	110	0.808
0.711	1	004	0.712
0.607	2	-	--
0.599	5	014	0.599
0.556	1	113	0.556
0.502	4	203	0.501
0.479	32	006	0.478
0.430	12 (sh)	213	0.431
0.418	81	020	0.418
0.411	13 (sh)	205	0.411
0.401	17 (sh)	214	0.401
0.396	59	300	0.398
0.373	2	-	-
0.356	38	008	0.358
0.340	10	-	-
0.332	6	222	0.331
0.320	4	314	0.320
0.316	4	026	0.315
0.299	4	208	0.305
0.287	11	001	0.287

[a] Orthorhombic symmetry with a = 1.195±0.003, b = 0.836±0.003, c = 2.870±0.004 nm.

calculated on the basis of the above unit cell dimensions compare reasonably well with those observed experimentally (Table 3.1) [1].

3.2.2 Chemical Analysis

The chemical analyses of the samples A-F are given in Table 3.2. The zeolite sample with known weight was taken in a platinum crucible with lid and ignited for 1h till it becomes red hot. The anhydrous weight of the sample was noted after cooling in desiccator. To the residue a few drops of sulfuric acid was added followed by the addition of 15ml aqueous hydrofluoric acid (40%) and evaporated in hot plate. This procedure was repeated to ensure that all the SiO_2 was evaporated as H_2SiF_6. The difference in weight of the residue and the original weight gave the weight of SiO_2 in the sample. The residue was fused with potassium pyrosulphate till a clear liquid was formed. To the solid obtained after cooling, 2-3 drops of HCl were added and then dissolved in a known volume of water. This solution was analyzed in an atomic absorption spectrometer (model Hitachi Z-8000) for Na, K, Al, Ga and Fe.

3.2.3 Infrared Spectroscopy

The framework FT IR spectra (1300-400 cm^{-1} region) of calcined NCL-1 samples containing Al, Ga and Fe were recorded using Nicolet 60 SXB instrument by employing KBr pellet technique. Similar to aluminosilicates, the gallo and ferrisilicates also exhibit (Figure 3.2) distinct absorption bands at 1230, 1098, 793, 610, 548, 468, and 395cm^{-1}. Flanigen et.al. [2] assigned the frequencies 1230, 1098 and 793cm^{-1} to internal asymmetric stretching, external asymmetric stretching and external symmetric stretching, respectively. Further, the double rings and TO bending vibration of TO_4 tetrahedra (Ti = Si, Al, Ga and Fe) exhibit absorption band at 548 cm^{-1} and 468 cm^{-1} respectively. The presence of band around 610 cm^{-1} is probably due to

Table 3.2 Physico-chemical properties of Al-, Ga-, and Fe-NCL-1 zeolites

No	Sample Name	Si/M ratio Gel	Product	Na^+/M ratio	K^+/M ratio	surf.area m^2/g[a]	Sorption capacity, (wt%)[b] H_2O	n-hexane	mesitylene
A	Fe-NCL-1	80	88	0.72	0.70	320	5.0	6.6	4.6
B	Fe-NCL-1	150	175	0.75	0.73	328	4.9	6.5	4.8
C	Ga-NCL-1	80	85	0.82	0.82	318	5.0	6.4	4.7
D	Ga-NCL-1	150	153	0.89	0.87	313	4.9	6.6	4.5
E	Al-NCL-1	80	83	0.90	0.88	318	5.2	6.8	4.7
F	Al-NCL-1	150	157	0.92	0.91	323	4.6	6.9	4.8
G	Si-NCL-1	>3000	>3000	-	-	339	3.8	7.0	3.8

[a] From N_2 adsorption (p/p$_o$ = 0.005 -0.01)

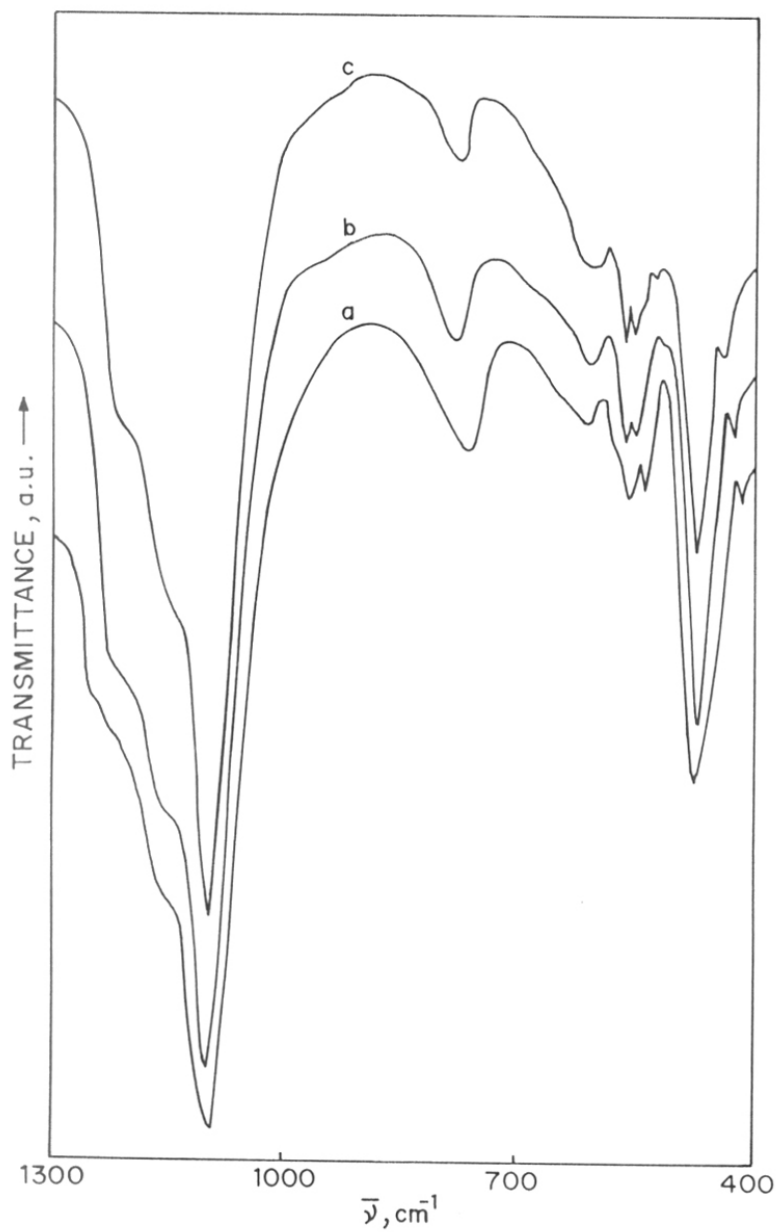[b] Gravimetric adsorption at 298K and p/p$_o$ = 0.5.

Fig.3.2   Framework IR spectra of NCL-1 calcined samples. Curves 'a' to 'c' refer to
Fe-, Ga-, Al-NCL-1 samples with Si/M (molar ratio) of 88, 85, and 83
respectively.

external links of 5-membered rings. ZSM-5 type zeolites exhibit bands around 590-620 cm^{-1} and are usually assigned to external links of complex 5-membered rings[3].

The infrared spectrum of the hydroxyl groups in the region of 3800-3300 cm^{-1} is shown in the Figure 3.3. The spectrum was recorded after degassing the zeolite wafer at 400°C under vacuum. The H-NCL-1 (Si/Al = 83) exhibits five bands at 3736, 3695, 3628, 3598, and 3520 (sh) cm^{-1} similar to what is observed in other zeolites. The band at 3736 and 3695 cm^{-1} are due to isolated silanol groups and hydroxyl groups attached to silica-alumina containing species, respectively. The structural acidic bridging Al-OH-Si groups (Brönsted acid sites) exhibit two peaks at 3628 and 3598 cm^{-1} as observed in the case of high-silica, large-pore zeolites ZSM-12 and mordenite [4,5]. These peaks are assigned to bridging hydroxyl groups vibrating in the main channels and the hydroxyl groups vibrating in small six or eight membered ring channels. In the case of NCL-1 also, eventhough exact structural morphology is not known yet, depending on some catalytic and adsorption properties [6] , it must be likely to have 12-ring unidimensional channels with associated 5- or 8-ring connecting channels. Therefore, the observed doublet peaks at 3628 and 3598 cm^{-1} are also likely to be due to OH groups located in 12-ring channel and 5- or 8-ring channels, respectively. In the case of Ga-, and Fe-NCL-1, the acidic bridging OH groups exhibit broad bands (no splitting) at 3640 cm^{-1} (a shoulder at 3605 cm^{-1}) and 3650 cm^{-1} respectively. However a strong signal at 3740 cm^{-1} with a shoulder at 3705 cm^{-1} corresponding to silanol group appears for both Ga-, and Fe-NCL-1 samples.

In Figure 5.4, 5.5, and 5.6, the FTIR spectra of chemisorbed pyridine are presented. All the samples show both Brönsted and Lewis acidity. The formation of pyridinium ions on Brönsted acid sites exhibit signals at 1630 and 1550 cm^{-1} and the pyridine coordinated to Lewis-centers exhibit signals at 1610 and 1446 cm^{-1}. Eventhough, Al-, Ga-, and Fe-NCL-1 samples
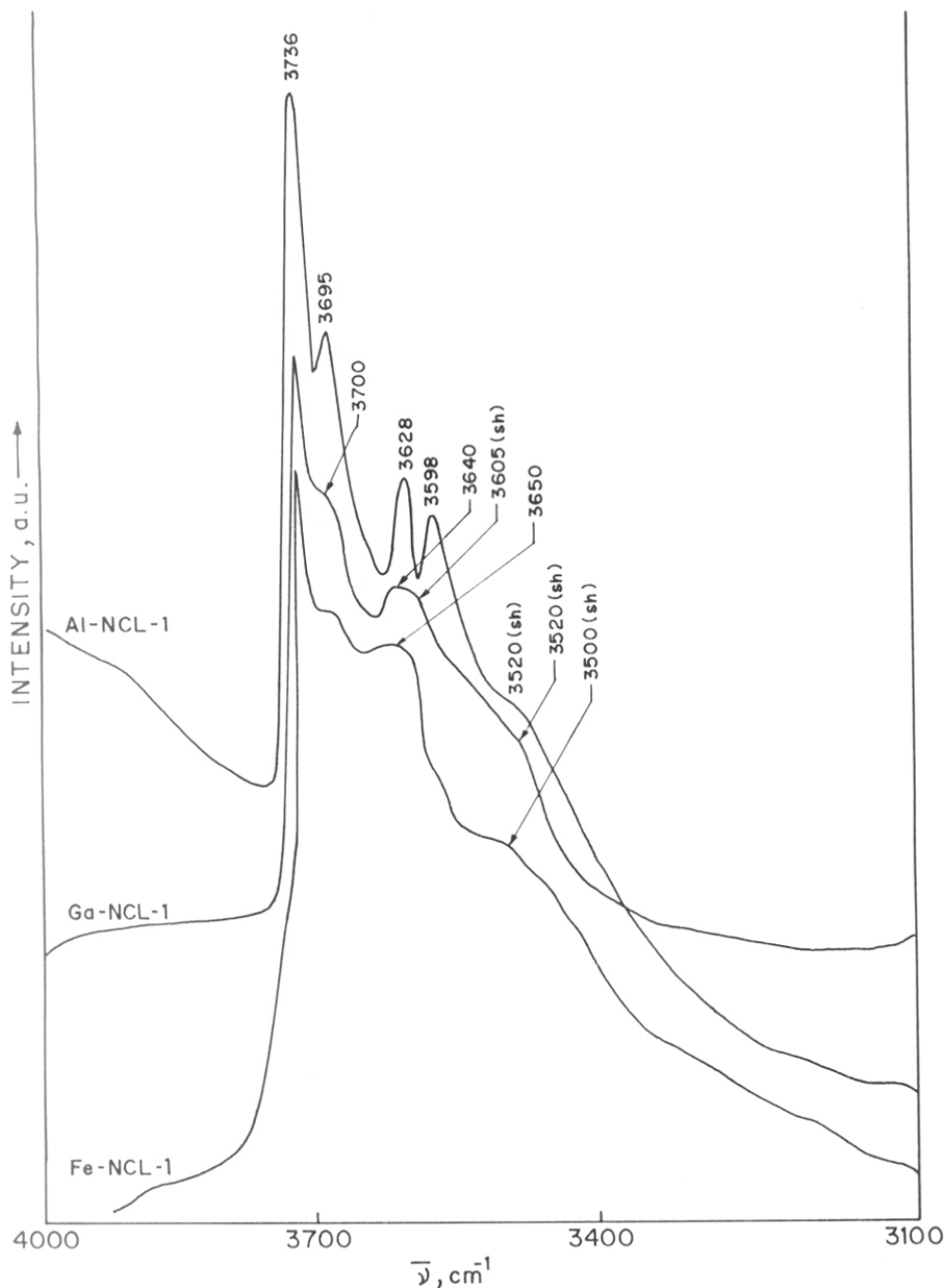
Fig.3.3   FT IR spectrum of the hydroxyl groups of NCL-1 samples in the region of 3800-3100 cm^{-1}.
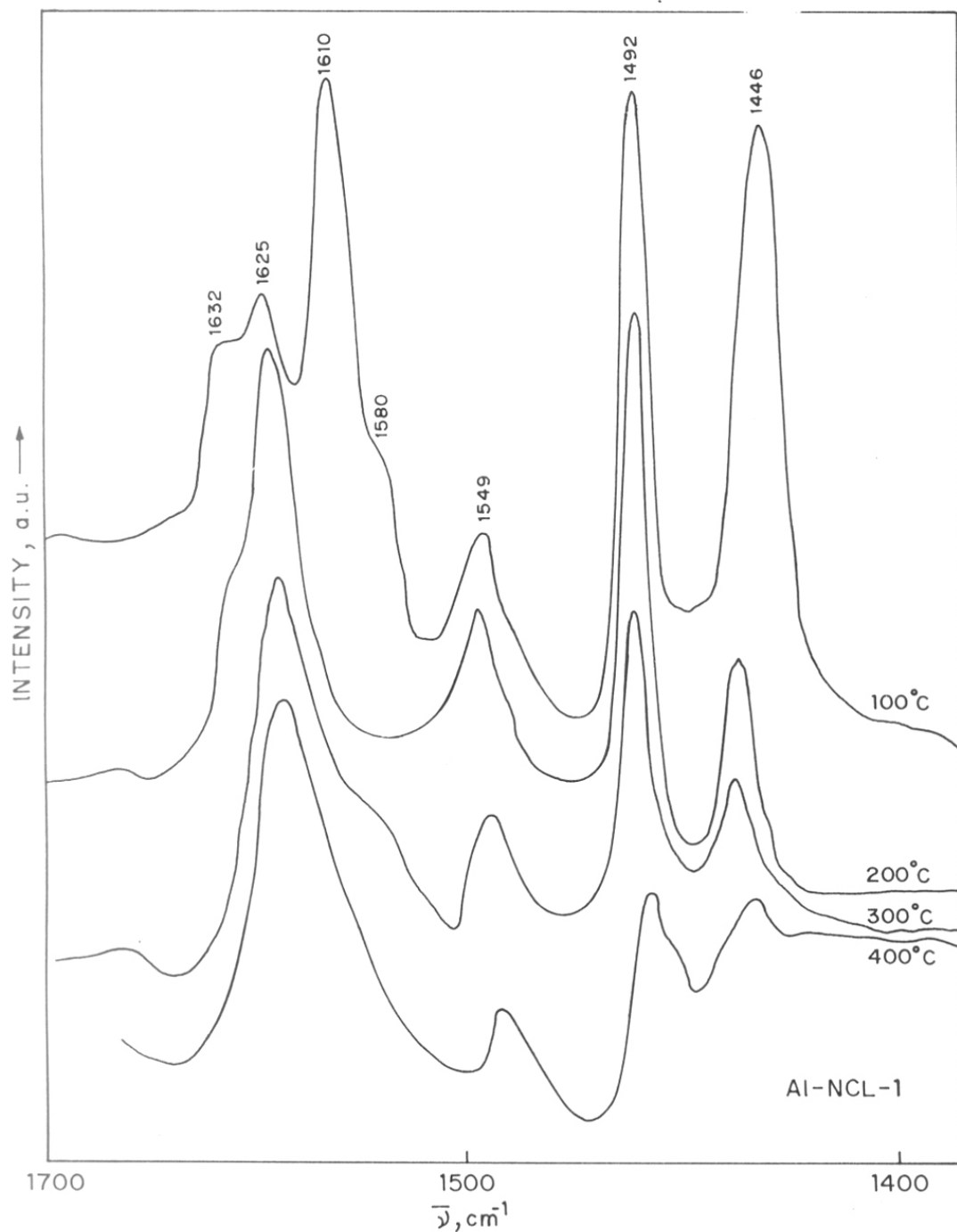
Fig.3.4   FT IR spectrum of chemisorbed pyridine of zeolite Al-NCL-1 (Si/Al = 83).
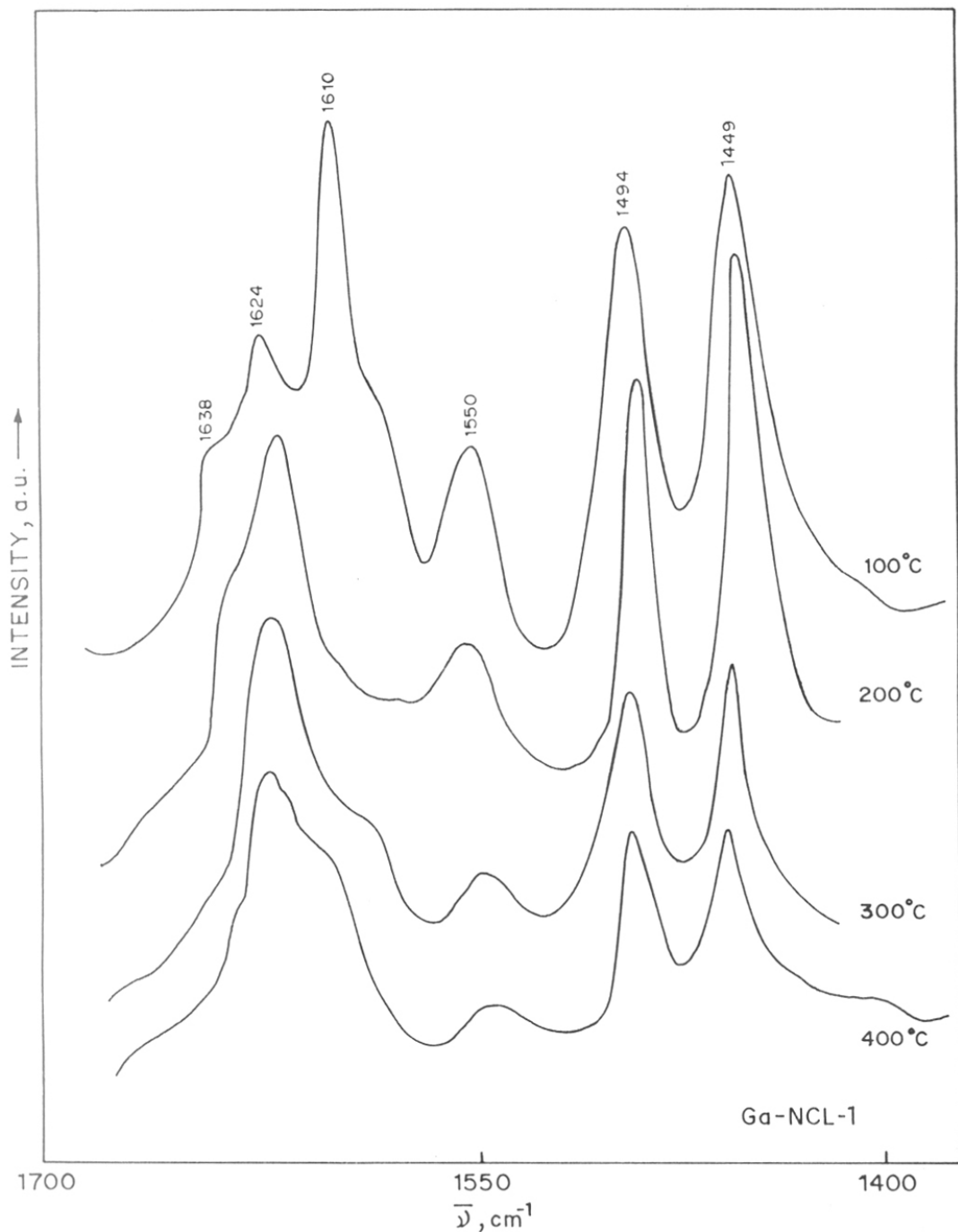
Fig.3.5   FT IR spectrum of chemisorbed pyridine of zeolite Ga-NCL-1 (Si/Ga = 85).
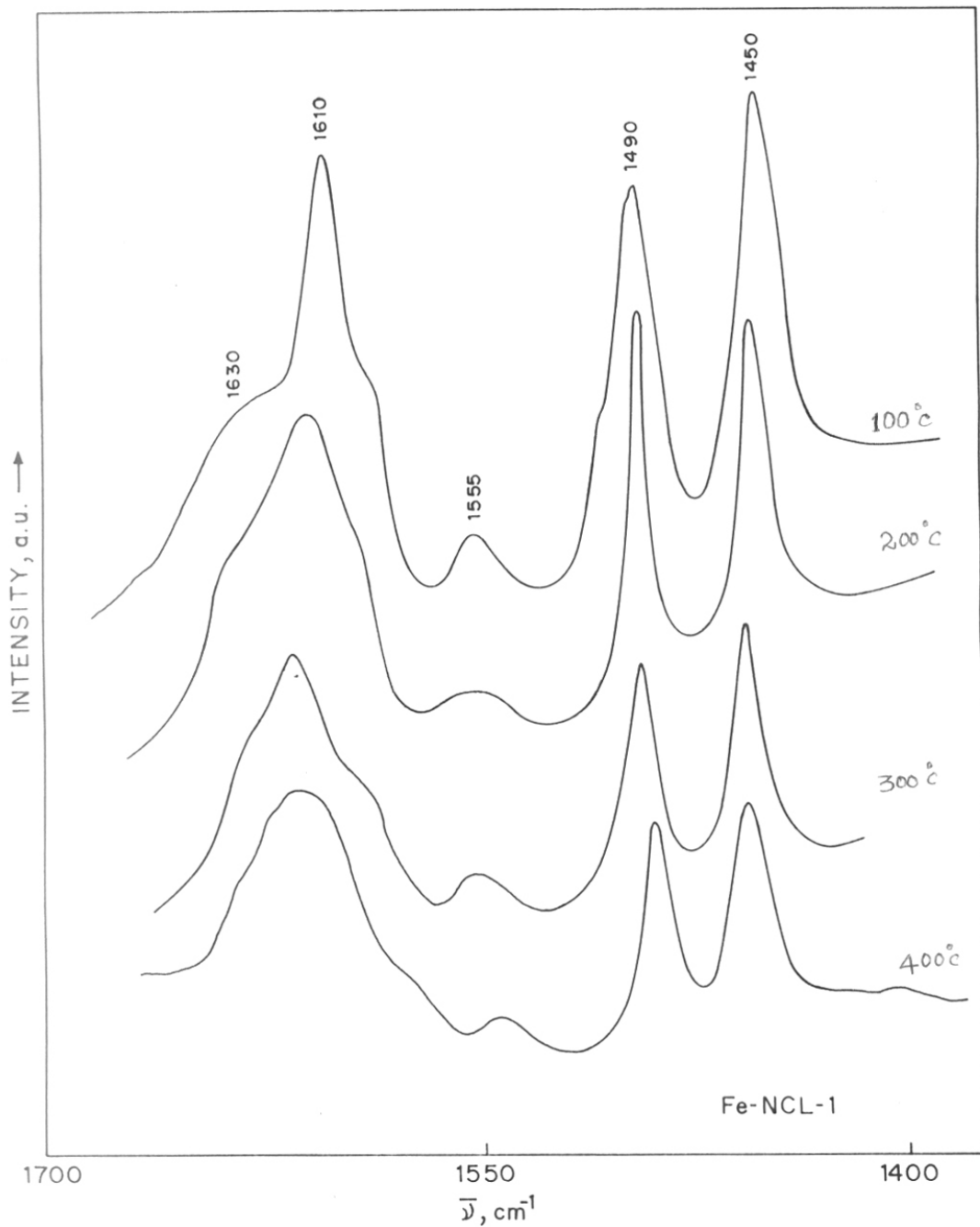
Fig. 3.6   FT IR spectrum of chemisorbed pyridine of zeolite Fe-NCL-1 (Si/Fe = 88).

show both Brönsted as well as Lewis acidity, the thermal stability of Al-, Ga-, and Fe-NCL-1 cations in NCL-1 framework differs significantly which is revealed by the variation of Brönsted and Lewis acidity as a function of chemisorption temperature. On increasing the desorption temperature of chemisorbed pyridine from 100°C to 400°C, a decrease in the Brönsted acidity in relation to the decrease in the Lewis acidity is more pronounced in Ga-, and Fe-NCL-1 compared to Al-NCL-1 sample. Thus, the thermal stability of Brönsted acidity varies in the order: Al- > Ga-, > Fe-NCL-1.

3.2.4 Temperature Programmed Desorption (TPD) of Ammonia

Figure 3.7 shows the temperature programmed desorption profiles of chemisorbed NH_3 from Al-, Ga-, and Fe-NCL-1 samples (curves "a-c" respectively). Similar to other high-silica zeolites [7], TPD profiles show three stages of NH_3 desorption giving rise to α, β, and γ peaks. These are in the temperature range RT-150°C, 150-250°C and 250-450°C, respectively. The α-peak is attributed to the desorption of strongly physisorbed and chemisorbed NH_3 on external silanol groups whereas β peak is due to NH_3 desorption from defect sites, cations and weak Brönsted sites. The third peak, i.e. γ peak, is considered to be due to NH_3 desorption from strong Brönsted and Lewis acid sites. This peak appears at 340, 325 and 300°C for Al-, Ga-, and Fe-NCL-1 samples respectively, indicating that the order of strength of Brönsted acid sites is: Al- > Ga- > Fe-NCL-1, similar results were obtained in the case of Al-, Ga- and Fe-ZSM-5 zeolites [7].
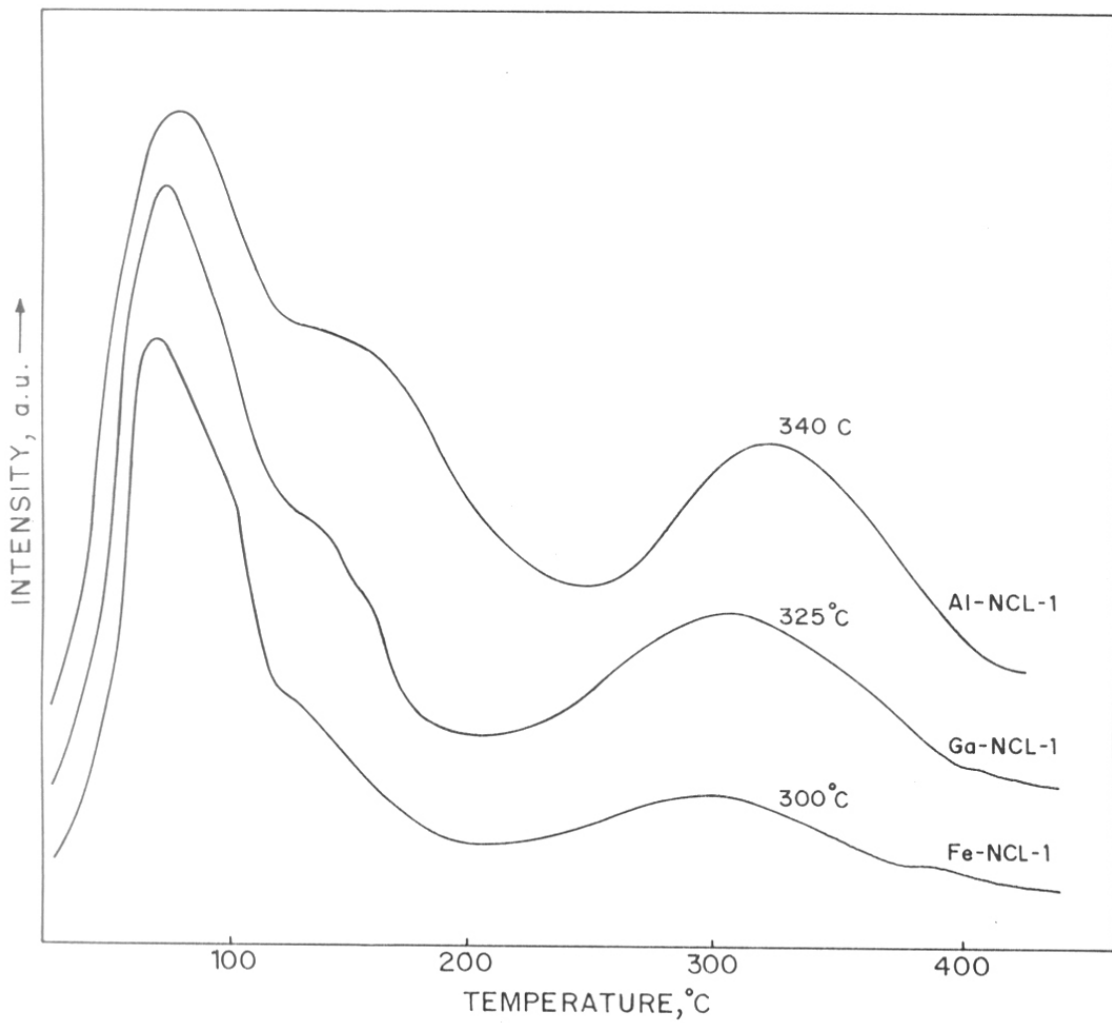
Fig.3.7   Temperature programmed desorption of chemisorbed NH_3 from Al-, Ga-, and Fe-NCL-1 samples.

3.2.5 Electron Spin Resonance Spectroscopy (ESR)

ESR spectra of ferrisilicate samples, recorded using Bruker ER200D at 9.7 MHz (X Band) with rectangular cavity (ST8424), are shown in Figure 3.8, exhibiting two signals, one around g = 4.3 and other at 2.0. These signals are characteristic of ferrisilicate molecular sieves and have been discussed in detail by many authors [8,9]. The presence of an ESR signal around g = 4.3 (vis-a-vis at g = 2) suggests the presence of Fe(III) as a matrix element intimately associated with the molecular sieve structure as expected for Fe(III) in distorted environment.

3.2.6 Solid State MAS NMR Spectroscopy

The solid state MAS NMR spectra of ^{29}Si, ^{27}Al, and ^{71}Ga samples of zeolite NCL-1 are depicted in Figure 3.9. Curves 'a' to 'c', refered to calcined samples of Si-NCL-1, Al-NCL-1 and Ga-NCL-1 respectively, exhibited only one signal at -112 ppm (with respect to TMS attributable to Si(0Al) tetrahedra). The samples containing aluminum exhibited only one signal at 52 ppm in the ^{27}Al spectrum characteristic of tetrahedral aluminum [11]. No signal due to octahedral Al^{3+} was observed. As expected, the Si-NCL-1 did not show any signal corresponding to ^{27}Al suggesting that the absence of aluminum in the Si-NCL-1 sample.

Figure 3.9(c) exhibit the solid state MAS NMR of Ga-NCL-1. The ^{71}Ga spectrum was recorded using $Ga(NO_3)_3.xH_2O$ as an external standard. The ^{71}Ga MAS NMR spectrographs exhibiting single peak at δ = 148 ppm (Ga^{3+} in tetrahedral environment) respectively, confirms the presence of Ga(III) in framework sites.

3.2.7 Ion Exchange Capacities

The calcined samples were treated with saturated NaCl solution for 10h at 293K (room temperature) to get the Na-form of the zeolites. The ion-exchange capacity measurements were performed by treating the Na-form of the zeolite (5g) with 50ml of 1M KNO_3 (a few drops of
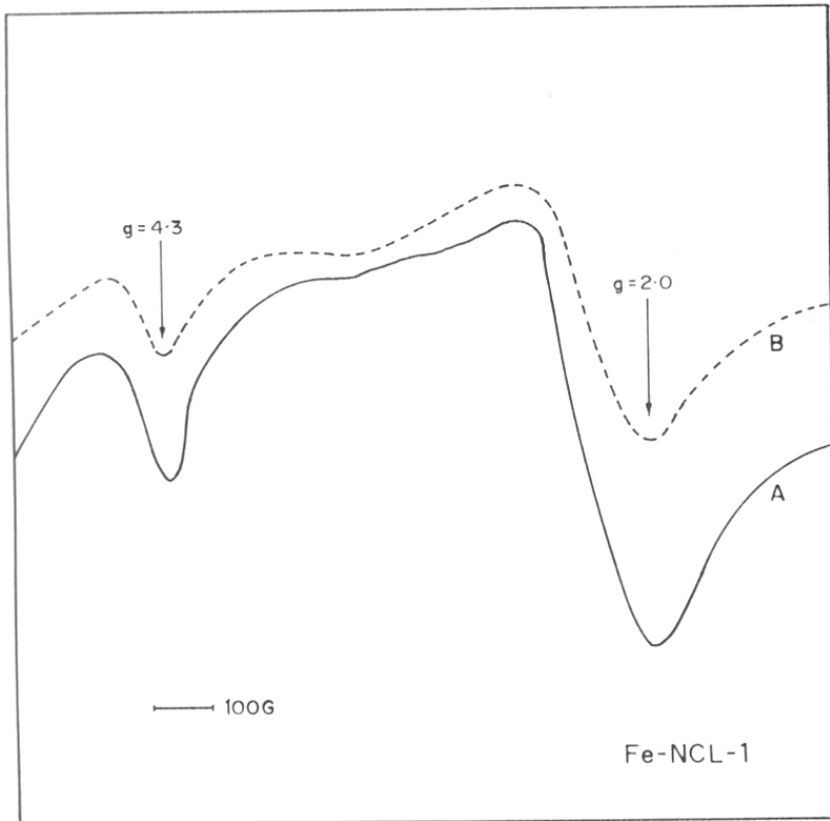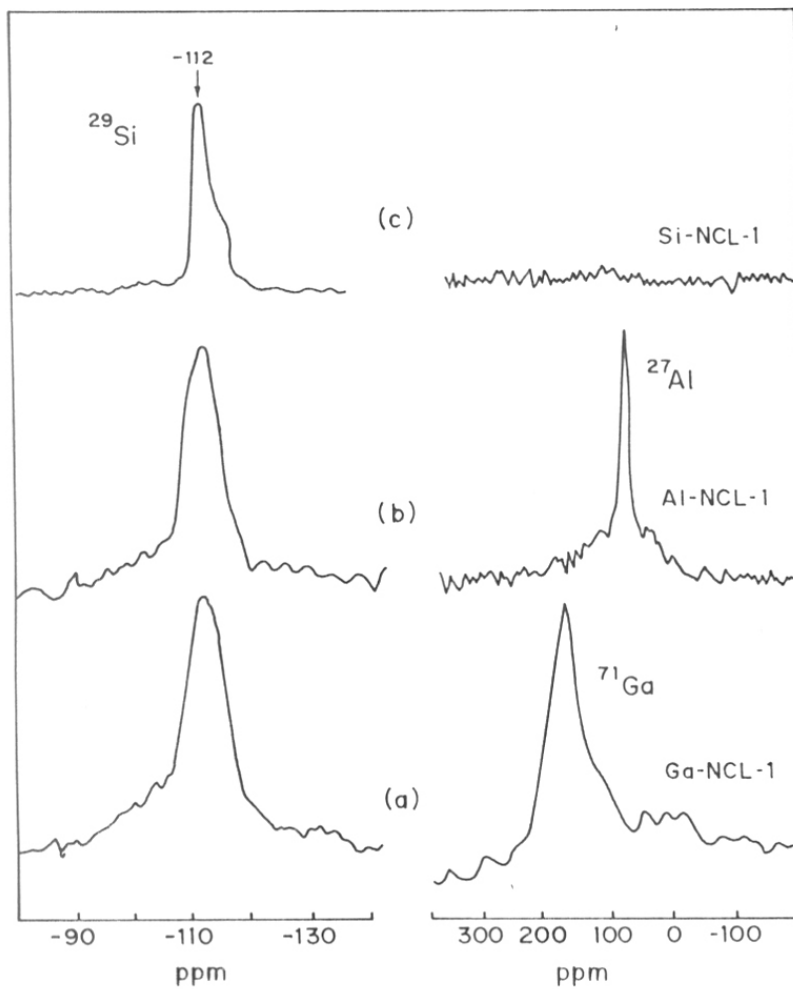
Fig.3.8   ESR spectra of Fe-NCL-1 (Si/Fe = 88).

Fig.3.9   MAS NMR spectra of NCL-1 samples. Spectra 'a' to 'c' refer to [71]Ga (Ga-NCL-1), [27]Al (Al-NCL-1) and [29]Si (Si-NCL-1) samples respectively.

dilute KOH to maintain the pH at $\approx$ 8) and then stirred for 3h at 353K, washed thoroughly with distilled water and dried at 393K to obtain the K-form of the zeolites. The ion exchange capacities for various metallosilicates were given in Table 3.2. The K-form of the zeolite was analyzed by chemical analysis procedure to obtain ion exchange capacity K^+/MO_2^+ molar ratio, M = Al, Ga or Fe according to the procedure given in the experimental section. The ion exchange capacities of zeolites can be taken as a convincing evidence for the presence of M^{3+} ions in the framework sites in the zeolite lattice [9,12]. The observed ion-exchange capacity (0.7–0.9) in the present study strongly support the presence of most of the Fe^{3+} and Ga^{3+} ions of the framework of zeolite NCL-1.

3.2.8 Adsorption Studies

Adsorption technique is routinely used to determine the extent of crystallinity and porosity of molecular sieves. One of the distinguishing properties of molecular sieves is their ability to discriminate molecules of different size. Those molecules whose critical diameter is smaller than the dimensions of the pore openings are easily adsorbed whereas larger molecules are either excluded or adsorbed with difficulty. The equilibrium sorption capacities of calcined H/Ga-NCL-1, H/Fe-NCL-1 and H/Al-NCL-1, for n-hexane, 1,3,5-trimethylbenzene and water, estimated at 298K and p/p_o = 0.5, are listed in Table 3.2. The comparable sorption values of Fe-, Ga- and Al-NCL-1 and those reported earlier for NCL-1 zeolite indicate the absence of occluded material inside the zeolite channels.

3.2.9 Surface Area Measurements

Surface area of NCL-1 samples containing different elements were measured at low pressure (p/p_o = 0.005-0.01) nitrogen adsorption isotherm at liquid nitrogen temperature and the values are listed in Table 3.2. From the adsorption isotherm, BET surface area was calculated [13]. The mesopore area was calculated from the t-plot [14]. The surface area of all the metallosilicates ranges between 315 to 340 m^2/g and t area (due to mesoporous impurities) of only 5-20 m^2/g, indicating the absence of any appreciable amount of amorphous material in the samples.
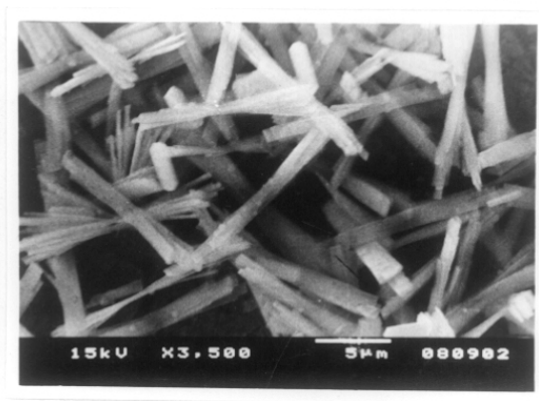
3.2.10 Scanning Electron Microscope

The scanning electron micrographs of metallosilicates analogues of zeolite NCL-1 are shown in Figure 3.10. Micrographs 'a' to 'c' refer to Al-, Ga-, and Fe-NCL-1 samples respectively. The particles of all the three samples consist of long bundle of needle shaped crystallites typical of NCL-1 morphology [1]. These micrographs clearly indicate the absence of amorphous material.

3.2.11 Catalytic Test Reaction

Like ion exchange capacity, the activity and selectivity in Brönsted acid catalysed reaction clearly suggest the presence of Al, Ga and Fe in the framework. Here, acid catalyzed isomerization and disproportionation of 1,3,5-trimethylbenzene, (1,3,5-TMB) was carried out over Fe-, Ga-, and Al-NCL-1 (samples A, C, and E respectively in Table 3.2). Figure 3.11 depicts the effect of reaction temperature on (i) TOF, moles of 1,3,5-TMB converted per mole of M^{3+} (M = Fe, GA and Al) per h (Figure 3.11A) and (ii) selectivity for 1,2,4-TMB among total products (Figure 3.11B, curves 'a-c' refer to Fe, Ga and Al-NCL-1 samples). As expected, with the increase in the reaction temperature the conversion increases, whereas the selectivity for 1,2,4-TMB
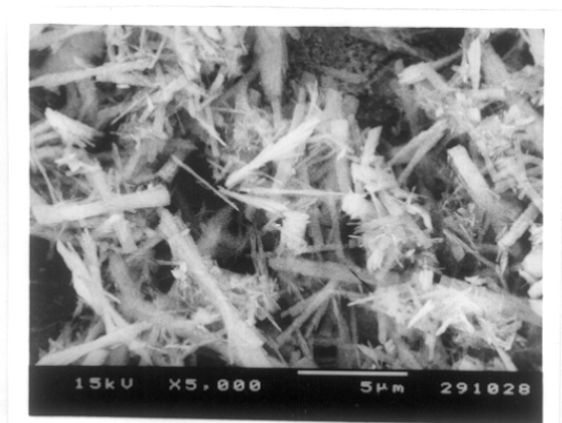
Fig.3.10   Scanning electron micrographs of NCL-1 samples. (a) Al-NCL-1 (Si/Al = 83), (b) Ga-NCL-1 (Si/Ga = 85), (c) Fe-NCL-1 (Si/Al = 88).
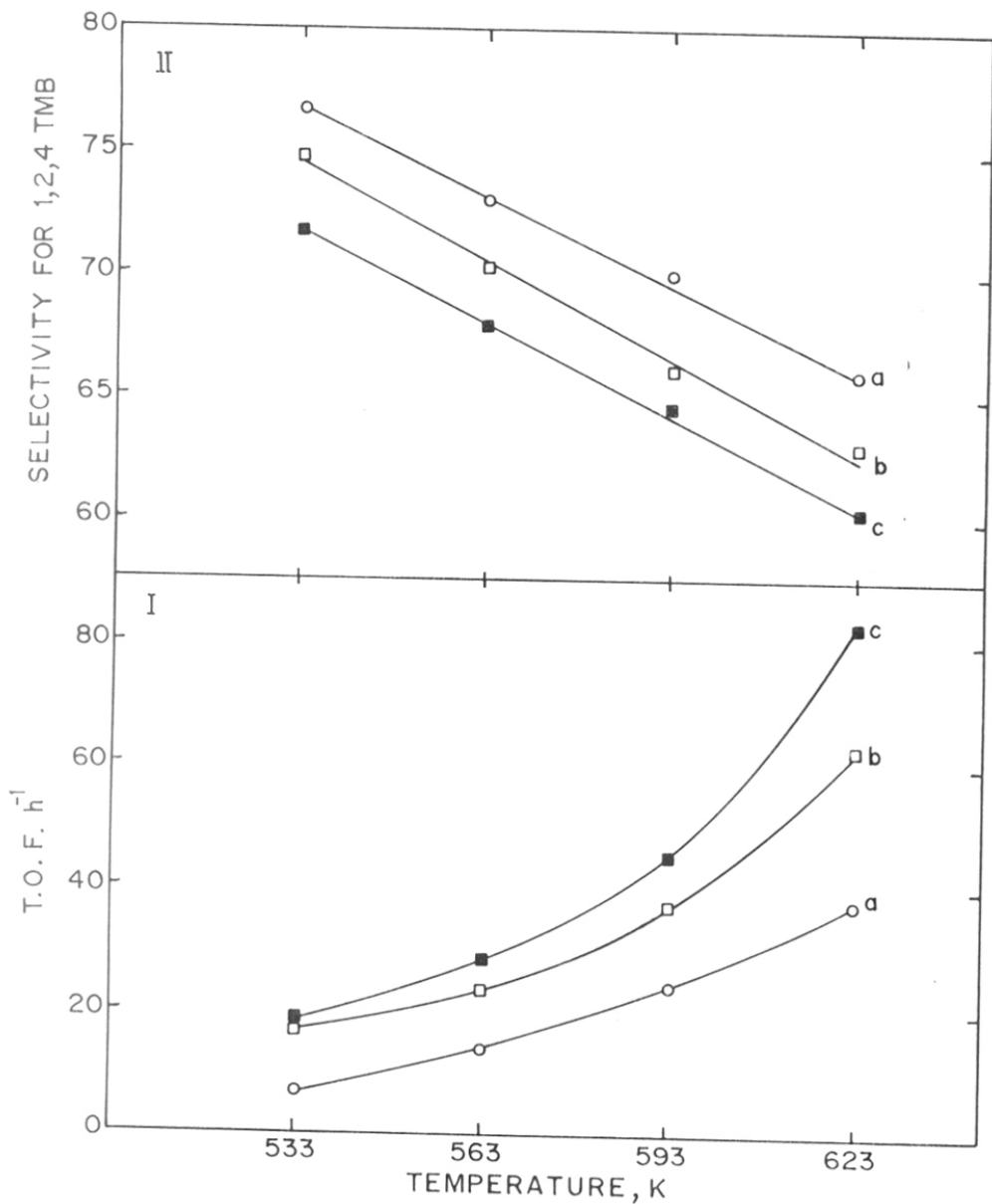
Fig.3.11   Isomerization of 1,3,5-trimethylbenzene to 1,2,4-trimethylbenzene over Al-, Ga-, and Fe-NCL-1. Effect of temperature on TOF (turn over frequency) (lower) and product selectivity (upper). WHSV = 3.4 h^{-1}, TOS, 30 min. Curves 'a-c' refer to Fe-NCL-1 (Si/Fe = 88), Ga- (Si/Ga = 85), and Al-NCL-1 (Si/Al = 83) respectively.

decreases slightly. The activity of the catalysts decreases as Al-> Ga > Fe-NCL-1, while the selectivity for 1,2,4-TMB among total products follows the reverse trend in accordance with the fact that the acid strength of isomorphously substituted zeolites decreases in the following order: Al-> Ga > Fe-silicate [8-10].

Figure 3.12 compares the selectivities for 1,2,4-TMB and isomerized (moles of 1,2,4-TMB + 1,2,3-TMB), vis-a-vis disproportionated (moles of tetramethylbenzenes), products exhibited by samples A, C and E (Fe, Ga and Al-NCL-1, respectively, Table 3.2) at same temperature and feed rate and at similar conversion level (obtained by varying the amount of the catalyst). At comparable conversion, the selectivity for both, 1,2,4-TMB and isomerization products decreases as: Fe- > Ga > Al-NCL-1 in accordance with the view that isomerization selectivity (vis-a-vis disproportionation) increases with the decrease in acid strength for a given zeolite structure [15].

3.3 EFFECT OF ALKALI METAL CATIONS ON Si-NCL-1 SYNTHESIS

3.3.1 Results and Discussion

Table 2.4 (chapter 2) summarizes the results obtained in the presence of various alkali metal cations. Sample 1 represents standard gel composition reported earlier [13]. Replacing part of the NaOH by LiOH increases the crystallization time (sample 2). Further, as the Li^+ ion concentration increases the mixture of NCL-1 + α-quartz (sample 3), ZSM-5 + α-quartz or pure α-quartz is formed (samples 4, 5). Since, the basicity of LiOH is less than that of NaOH (that is why pH decreases by increasingly replacing NaOH by LiOH, sample 2-5), LiCl was used along with NaOH (sample 6) to study the effect of Li^+. An addition of LiCl leads to the formation of α-quartz (sample 6).
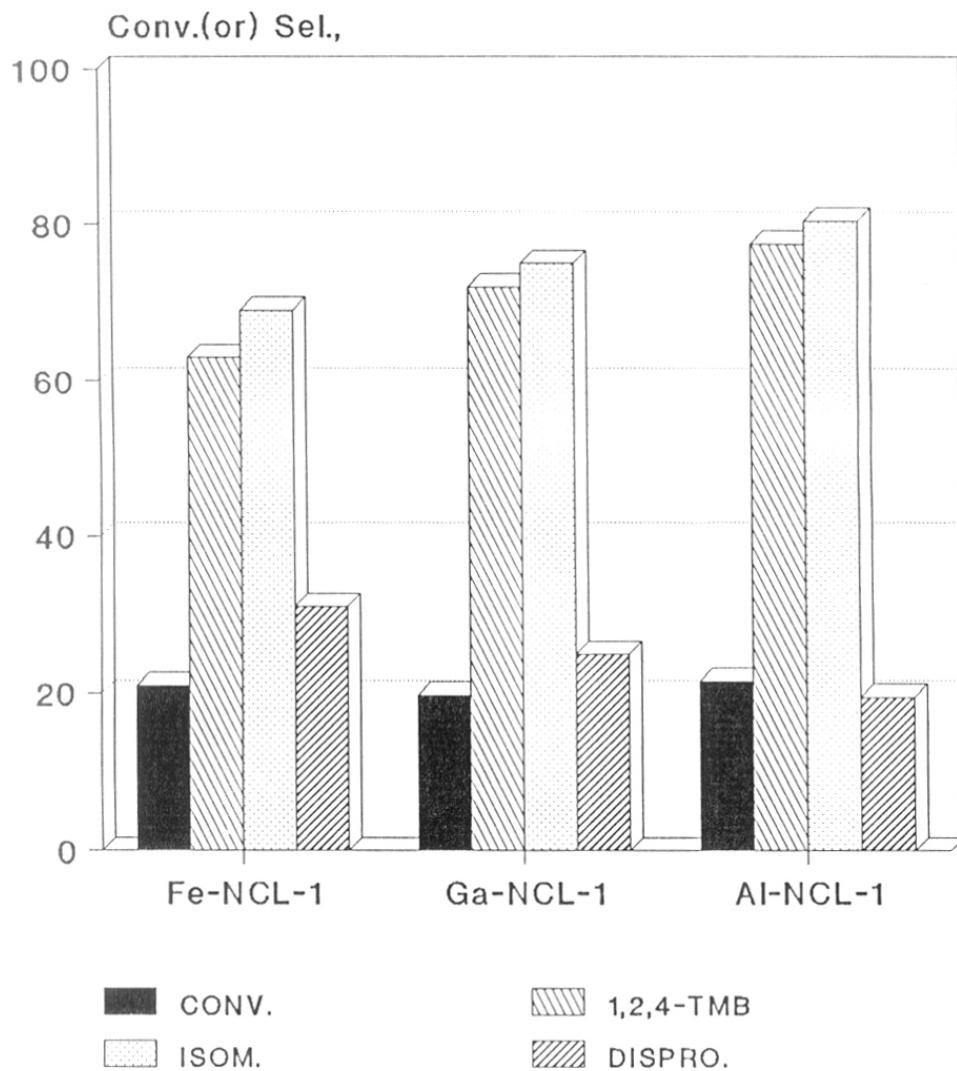
Fig.3.12 Comparison of selectivities for 1,2,4 TMB and isomerization (Vs disproportio nation) exhibited by Fe-, Ga- and Al-NCL-1 (Si/M = 88, 85 and 83 respectively) at comparable conversion level. Temperature = 563K, feed rate 3.4 h⁻¹, and TOS = 30 min., catalyst wt. on anhydrous basis (g) = 2.1, 1.3 or 1.0 respectively.

Both, partial and complete replacement of Na^+ by K^+ (sample **7&8**) favors the efficient formation of pure NCL-1 phase. When NaOH was partially (50%) replaced by KOH, a slight reduction in the crystallization time was observed (Sample **7**). The crystallization time was further reduced when NaOH was completely replaced by KOH (sample **8**). The addition of KCl to NaOH results in the formation of pure NCL-1 phase with slightly lower crystallinity (samples **9&10**). The addition of NaCl to KOH results in the formation of NCL-1 with slightly less crystallinity (sample **11**) or $\propto$-quartz (sample **12**). These results demonstrate that Si-NCL-1 phase can be efficiently synthesized using both NaOH or KOH, either independently or their mixture. However, the addition of salts like KCl or NaCl also affects the phase purity and crystallinity, indicating that not only alkalimetal hydroxide (pH) but alkalimetal chloride salts (metal ions) also influence the synthesis of NCL-1 zeolite.

However, it is quite interesting to note that an addition of small amount of CsCl ($Na^+ + Cs^+$) decreases the crystallization time significantly (sample **13&14**). But, further addition of CsCl to the synthesis gel results in either incomplete (sample **15**) or no crystallization (sample **16**) of Si-NCL-1. However, in the absence of any inorganic cations (sample **17**, where hexamethylene bis(triethylammonium) hydroxide was used to maintain the pH), no crystallization was observed. The overall crystallization rate of Si-NCL-1 using various inorganic cations follows the trend: $(Cs^+ + Na^+) > K^+ \geq Na^+ (Na^+ + Li^+)$. The basicity of these cations also follows the same trend. Figure 3.13 illustrates the crystallization kinetics for the systems using Na^+, $(Li^+ + Na^+)$, K^+ and $(Cs^+ + Na^+)$. It is clear from Figure 3.13 that these inorganic cations influence the synthesis of Si-NCL-1 at nucleation as well as crystallization stages. As the mineralisability of the inorganic base/cation increases the rate of overall crystallization also increases.
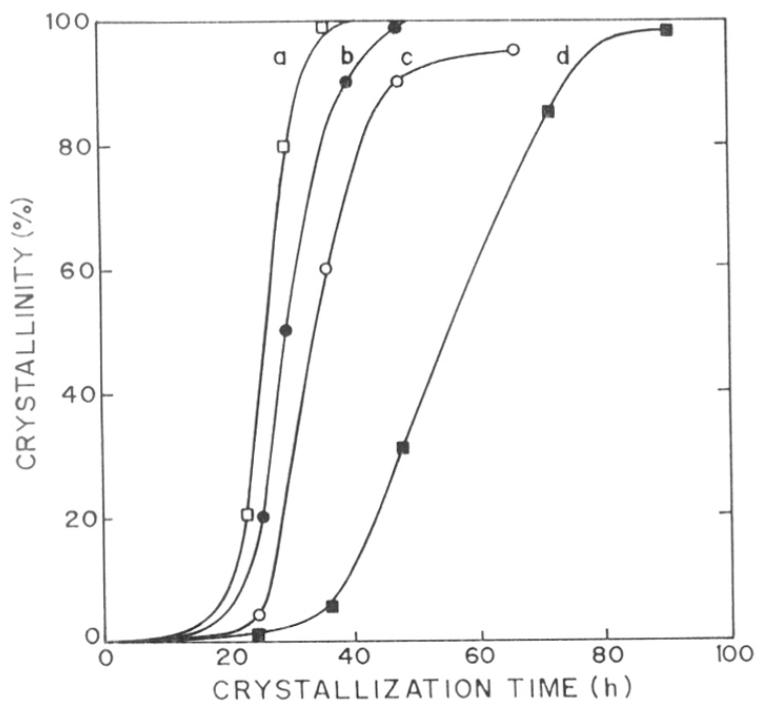
Fig.3.13   Crystallization kinetics for the synthesis of Si-NCL-1 in presence of various cations. Curves 'a' to 'd' refer to systems with $(Cs^+ + Na^+)$, Na^+, K^+ and $(Li^+ + Na^+)$ ions respectively.

3.3.2 Powder X-Ray Diffraction (XRD)

Figure 3.14 shows the powder X-ray diffraction pattern of NCL-1 samples with different alkali cations (the profiles 'a' to 'd' refer to sample with (Li^++Na^+), Na^+, K^+ and (Cs^++Na^+), respectively). The crystallinity of the samples was measured on the basis of integrated area of the peaks in the range of 2θ = 17-27 region. All the X-ray diffractograms match well with that reported earlier, and no impurity phases are observed.

3.3.3 Infrared Spectroscopy

The IR spectra of the samples were recorded in the PYE UNICAM SP3 300 spectrometer wavenumber range of 300-1400 cm^{-1} using nujol mull technique. The IR spectra of samples with Li^+, K^+ and Cs^+ exhibited distinct absorption bands at 1230, 1098, 793, 610, 548 and 468 cm^{-1} characteristic of NCL-1 zeolites similar to those observed in the case of Na^+. No extra bands were noticed due to the presence of other alkali cations.

3.3.4 Scanning Electron Microscope

The scanning electron micrographs of the samples with different alkali cations are shown in Figure 3.15 (micrographs 'a' to 'c' corresponds to samples with (Li^++Na^+), K^+ and Cs^+ respectively). All the samples show typical needle shaped crystals with crystal size ranging from 3-5 μm similar to that obtained using standard Si-NCL-1 synthesis with Na-cation. No larger crystal are formed due to the presence of Li^+, K^+ or Cs^+ ions. The micrographs clearly show that all the samples are fully crystalline and free from amorphous materials.
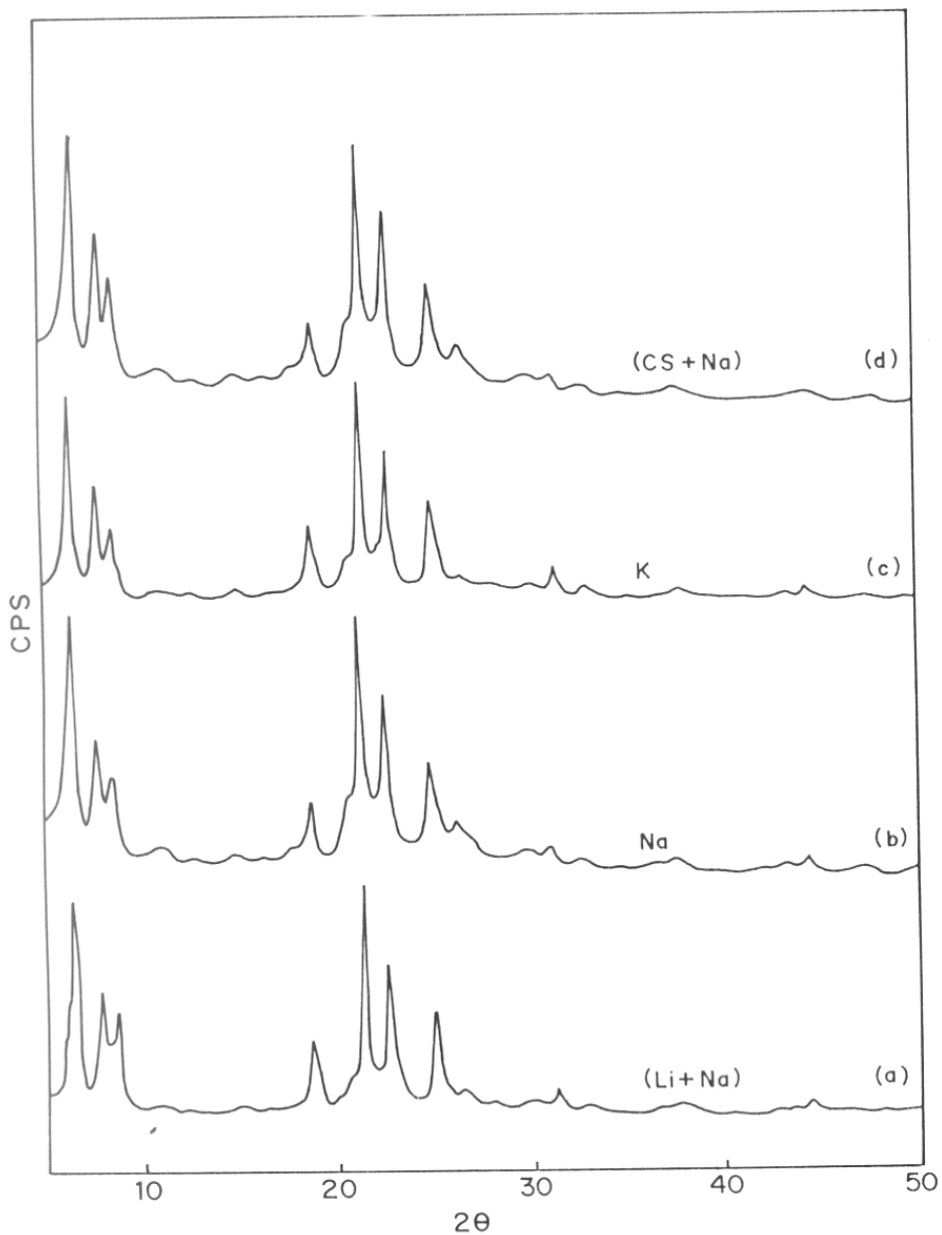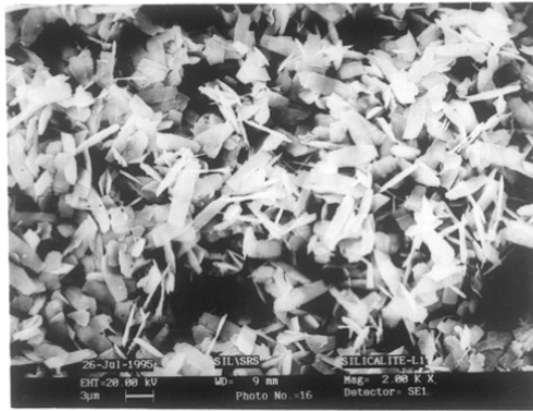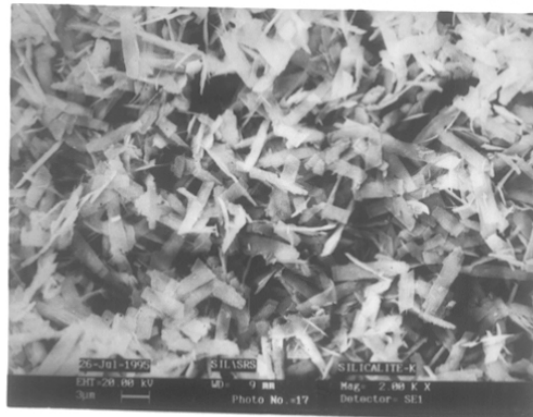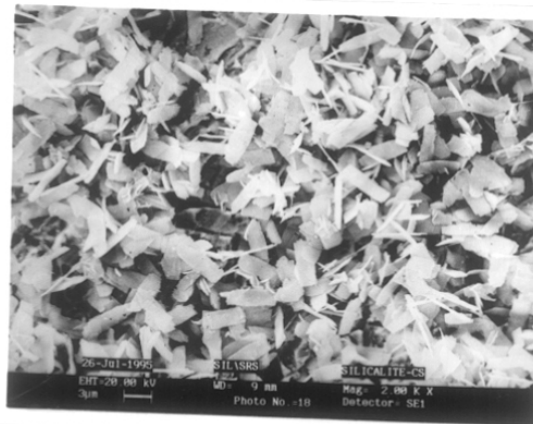
Fig.3.14   Powder X-ray diffraction pattern of NCL-1 samples with different alkali
cations. Curves 'a' to 'd' refer to samples with (Li⁺+Na⁺), Na⁺, K⁺, and
(Cs⁺+Na⁺) respectively.

Fig.3.15   Scanning electron micrographs of the samples with different alkali cations. Micrographs 'a' to 'c' corresponds to samples with $(Li^+ + Na^+)$, K^+ and $(Cs^+ + Na^+)$ respectively.

3.3.5 Sorption and Surface Area Measurements

The sorption measurements of water, n-hexane and mesitylene were carried out gravimetrically using a Cahn balance (Model: Cahn 2000G). The sorption capacity for samples with different alkali cations are listed in Table 3.3. The amount of adsorption of various sorbates was comparable with that reported for Si-NCL-1 earlier suggesting that all the samples are free from impurities. Omnisorb 100 CX unit (COULTER corporation, USA) was used for measurement of surface area through nitrogen adsorption and the values are listed in Table 3.3.

Table 3.3: Physico-chemical properties of zeolite NCL-1 containing various alkali metal ions.

Sample No.	System	Surface area m^2/g	H$_2$O	n-hexane	Mesitylene
			Amount adsorbed, wt%		
1	Na-NCL-1	339	3.77	6.96	4.72
2	(Li+Na)-NCL-1	330	3.86	7.09	4.84
3	K-NCL-1	334	3.71	6.78	4.67
4	(Cs+Na)-NCL-1	342	3.85	6.92	4.77

a: From nitrogen adsorption (p/p$_o$ = 0.005-0.01)

b: Gravimetric adsorption at 298K and at p/p$_o$ = 0.5.

3.4 SUMMARY

1. The XRD profiles of Al-, Ga-, and Fe-NCL-1 samples match well with that of Si-NCL-1 and no extra peaks were observed due the presence of iron and gallium.

2. FT IR spectra of hydroxyl groups for zeolite NCL-1 shows two peaks at 1632 and 1598 cm^{-1} corresponding to the hydroxyl groups located at the main channel and small rings respectively. The silanol groups appears at 1730 cm^{-1}.

3. FT IR spectra of chemisorbed pyridine shows both Brönsted and Lewis acidity.

4. ESR spectrum of Fe-NCL-1 sample shows two peaks with the value of g = 2.0 and 4.3 confirming the presence of iron in the Td environment.

5. MAS NMR spectra of Ga-NCL-1 sample exhibits a peak at 148 ppm suggesting the presence of gallium in the Td environment.

6. In the isomerization of 1,3,5-trimethylbenzene to 1,2,4-trimethylbenzene, the activity of the metallo-silicates follows the trend: Al-,> Ga-,> Fe-NCL-1. However, the selectivity for 1,2,4-trimethylbenzene follows the reverse order.

7. The XRD profiles of Si-NCL-1 prepared in presence of various inorganic cations match well with the reported values.

8. Scanning electron micrograph of Si-NCL-1 prepared in the presence of various inorganic cations shows needles or bundles of needles with crystal size 3-5 μm. No larger crystals are formed due to the presence of Li or K.

3.5 REFERENCES

1.   K.Ramesh Reddy, V. Ramasway, R. Kumar and A.V. Ramaswamy, *Zeolites,* **14,**   326
      (1994).

2.   E.M. Flanigen, H. Khatami and H.A. Szymanski, *Advances in Chemistry Series,*
      101, 201 (1971).

3.   J.L. Casci, V.T. Whittam and B.M. Lowe, *Proc. 6th Int. Conf. on Zeolites,* Reno,
      p 894 (1983).

4.   B.H. Chiche, R. Dutartre, F. Di Renzo, F. Fajula, A. Katovic, A. Regina and G.
      Giordano, *Cata. Lett.,* **31**, 359 (1995).

5.   M. Maache, A. Janin, J.C. Lavalley and E. Benazzi, *Zeolites,* **15**, 507 (1995).

6.   R. Kumar and K.R. Reddy, *Microporous Materials,* **3**, 195 (1994).

7.   N. Topsóe, K. Pedersen, and E.G. Derouane, *J. Catal.,* **70,** 41 (1981).

8.   R. Szostak, *"Principles of Synthesis and Identification",* Van Nostrand Reinhold,
      New york, p213 (1989).

9.   P. Ratnasamy and R. Kumar, *Catal. Today,* **9,** 329 (1991).

10.   C.T.W. Chu and C.D. Chang, *J. Phys. Chem.* **89**, 1569 (1989).

11.   C.A. Fyfe, G.T. Kokotailo, G.J. Kennedy and C.de Schutter, *J. Chem. Soc.,*
      Chem. commun., 306 (1985).

12.   R. Szostak and T.L. Thomas, *J. Catal.,* **100,** 555 (1986).

13.   S. Lowell and J.E. Sheilds, *"Powder Surface area and porosity".* 2nd Edition,
      Powder Technology Series, Chapman and Hall, London p14 (1984).

14.   S. Lowell and J.E. Sheilds, ibid p80 (1984).

15.   A. Raj, K.R. Reddy, J.S. Reddy and R. Kumar, *Stud. Surf. Sci. Catal.* **75B**, 1715   (1993).

CHAPTER 4

BRöNSTED ACID CATALYSED REACTIONS

4.1 INTRODUCTION

This chapter describes the catalytic performance of zeolite NCL-1 in Brönsted-acid catalyzed reactions such as: (i) isopropylation of benzene to cumene, (ii) isomerization of 1,3,5-trimethylbenzene to 1,2,4-trimethylbenzene, (iii) Fries rearrangement of phenylacetate to hydroxy acetophenones and (iv) decomposition of cumenehydroperoxide to phenol and acetone. The fixed-bed reactor system used for the vapor phase reactions is shown in the experimental section (Chapter 2, Figure 2.6).

4.2 ISOPROPYLATION OF BENZENE WITH 2-PROPANOL OVER Al-NCL-1.

Isopropylbenzene (cumene) is an important intermediate in the production of phenol. Diisopropyl benzenes (DIPBs) serve as intermediates for the production of resorcinol and hydroquinone. The m-DIPB is used as an intermediate for the production of cosmetics. The solid phosphoric acid (SPA) and other Friedel-Crafts catalysts are commonly used for the isopropylation of benzene to cumene [1,2]. The major drawback of these catalysts is their corrosive nature. Studies have also been made using various zeolite catalysts, such as H/ZSM-5, H/EU-1, H/ZSM-12, H/beta, H/mordenite and LaH/Y [3-8]. Large-pore, high-silica zeolites, e.g., ZSM-12 and beta, were found to be quite good catalysts for this reactions. Herein, the results of studies on the isopropylation of benzene with 2-propanol over zeolite NCL-1 are described. The influence of various reaction parameters on the activity and product selectivities are discussed. The isopropylation of benzene with 2-propanol is a multi-step, sequential reaction. The main reaction scheme can be represented as follows (scheme 4.1).
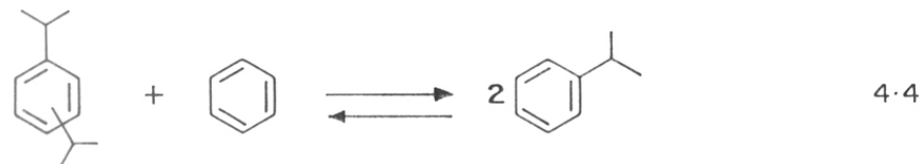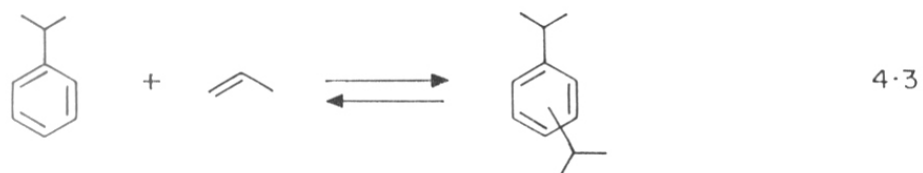
Scheme 4·1

4.2.1 Influence of Si/Al Molar Ratio

The influence of the Si/Al molar ratio of the NCL-1 samples on the activity and product selectivity in the isopropylation of benzene at the same reaction temperature and WHSV is depicted in Figure 4.1(B). As expected, the conversion of benzene (curve a, wt% of theoretical maximum conversion based on benzene/2-propanol molar ratio) decreases with increasing Si/Al molar ratio of the sample. The TOF (turn over frequency, moles of benzene converted per mole of Al in the catalyst per unit time) values for NCL-1 samples with Si/Al = 23, 85, 153 and 257 were found to be 9.7, 25.3, 39.5 and 42.6 h^{-1}, respectively. With increasing Si/Al ratio, the cumene selectivity (curve b) decreases whereas the selectivity towards diisopropylbenzene (DIPB, curve c) increases, probably due to the reasons that: (i) the alkylation of cumene (reaction 4.3) is faster than the alkylation of benzene (reaction 4.2) [9], and (ii) the transalkylation of DIPB with benzene to cumene (reaction 4.4), as well as the cracking of DIPB (reaction 4.3, reverse), need a high density of acid sites [10]. Further, the cracking/dealkylation of the main product of cumene (reaction 4.2, reverse) into benzene may also contribute to the decrease in cumene selectivity. Since no or negligible propene or other gaseous products are obtained, it is also possible that the propene formed due to cumene cracking (reverse of reaction 4.2) alkylates another molecule of cumene to form DIPB, consequently increasing the selectivity towards DIPB. However, the total selectivity of cumene + DIPB remained almost constant at about 94±3 %.

Among the diisopropylbenzene isomers, the 1,3-DIPB isomer is always predominant over the 1,4-isomer (Figure 4.1, A), the 1,2-isomer being absent or formed in small quantities (< 2%). However, 1,3-DIPB decreases sharply with a decrease in Al content (increasing Si/Al ratio) of the zeolite and thus a decrease in benzene conversion. Vapor-phase alkylation of aromatics over the acid form of the zeolites is an electrophilic reaction. Hence, among DIPBs, 1,4 and 1,2 isomers
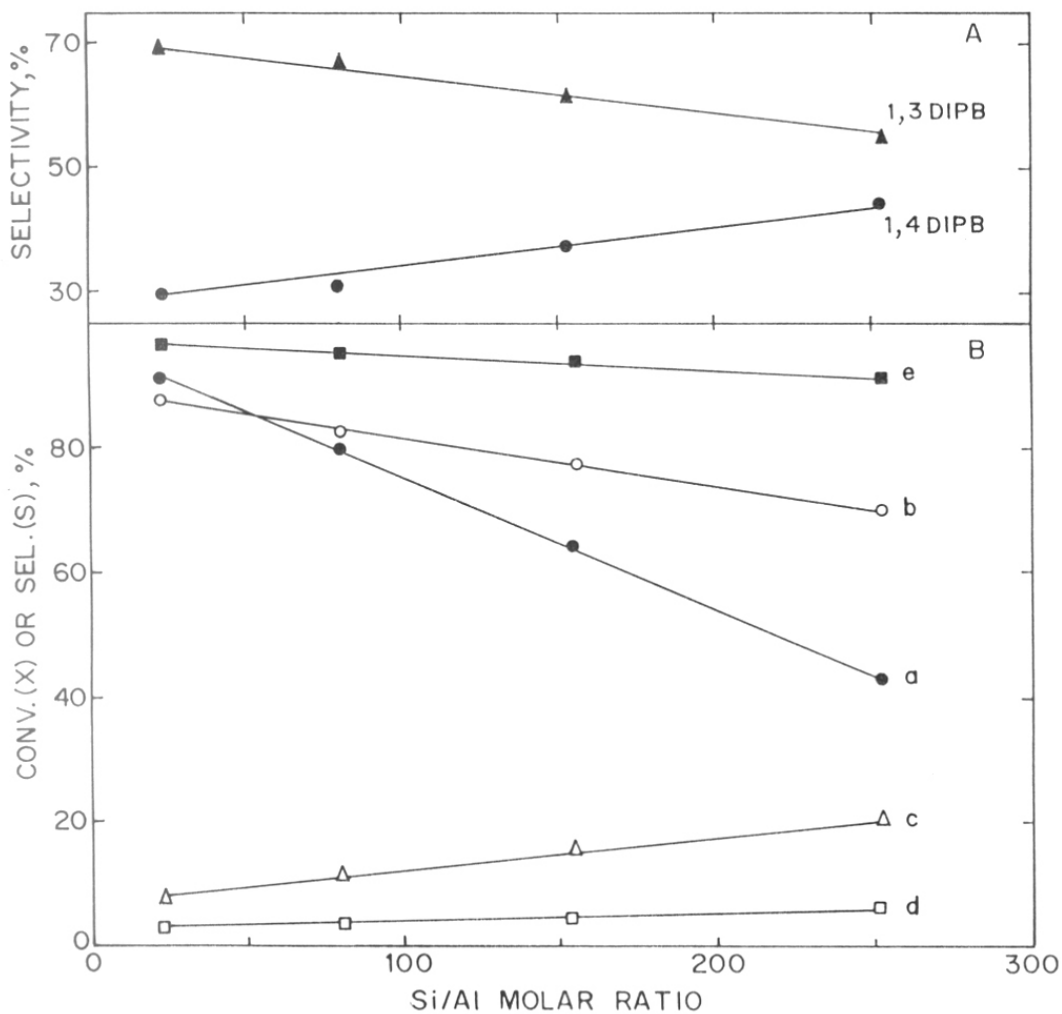
Fig. 4.1   Isopropylation of benzene over zeolite NCL-1. Influence of Si/Al ratio on conversion or product selectivity (lower) and selectivity for 1,3 and 1,4 isomers of diisopropylbenzene (DIPB) (upper). Temperature, 503K; Benzene/ 2-propanol ratio, 6; WHSV, 3.5 h^{-1}. Curve a, conversion; curve b, cumene; curve c, DIPB; curve d, others (aliphatics, n-propylbenzene, C_6-C_8 aromatics, and C_{10} aromatics); and curve e, cumene + DIPB.

can be formed via direct isopropylation of cumene as the primary products. However, during the present studies, the 1,2-isomer was formed only in small quantities (< 2%), the 1,4 and 1,3-isomers being predominant in accordance with the earlier studies [11,12]. It seems that the direct formation of 1,2-DIPB is hindered either sterically or due to overcrowding at the 1,2 positions, the later reason being more probable because even in zeolite beta with 3-dimensional open structure, no or trace amounts of 1,2-DIPB were observed [12]. This argument is further supported by examining the total strain energy of the final energy minimized molecules of 1,2-, 1,3- and 1,4-DIPB, respectively. Since 1,2-DIPB has a very high-strain energy compared to that for 1,3- and 1,4-isomers (4.26, 2.02 and 2.78 k cal mol^{-1} for 1,2-, 1,3-, and 1,4-DIPB respectively), the formation of 1,4-DIPB is highly favored initially, followed by further isomerization to the 1,3-isomer.

The equilibrium geometry of the molecules was obtained by the molecular mechanics method [13,14]. The total strain energy of the molecules is expressed by the equation

$$E_{total\ strain} = E_{bond\ length} + E_{dihedral\ angle} + E_{improper\ torsion} + E_{electronic} + E_{van\ der\ waals}$$

The corresponding equation for the calculation of the individual energy terms are shown below:

$$E_{bond\ length} = K_b\ (r-r_o)^2 \qquad \text{------------------------ (i)}$$

where K_b = stretching force constant

r = bond length in the model

r_o = equilibrium bond length

$$E_{bond\ angle} = K_H\ (H - H_o)^2 \qquad \text{-----------------------(ii)}$$

where K_H = bond bending force constant

H = bond angle in the model

H_o = bond angle in the model

$$E_{dihedral\ angle} = K_\psi \left[H \cos (n\psi_o - \delta) \right] \text{ --------------------(iii)}$$

where ψ_o = equilibrium dihedral angle

δ = deviation of ψ in model from ψ_o

n = periodicity $(360/\psi)$

$$E_{improper\ torsion} = K_t (t - t_o)^2 \text{ ------------------------(iv)}$$

where K_t = torsion force constant

t = proper angle in the model

t_o = equilibrium proper angle

$$E_{electronic} = \sum_{ij > i} q_i\, q_j\, /(4\pi\varepsilon_o r_{ij}) \text{ --------------------------(v)}$$

where $q_i\, q_j$ = atomic partial charges

E_o = dielectric constant

r_{ij} = interatomic distance

$$E_{van\ der\ waals} = \sum_{i>j} [A_{ij}] / (r_{ij})^{12} - [B_{ij}] / (r_{ij})^6 \text{ --------------------(vi)}$$

where A and B are non bonded parameters derived from effective number of outer shell electrons and polarizability of interacting atoms.

Values of various energies contributing to total strain energy for different molecules are given in Table 4.1. The alkylation of aromatic compounds over acid catalysts is an electrophilic (and hence ortho-para directing) reaction, 1,3-DIPB in not expected to be formed as a primary product in the alkylation of cumene, in spite of the low strain energy of the 1,3-isomer. Hence, 1,3-DIPB can be formed either through isomerization of the 1,4-and 1,2 isomers, or via cumene disproportionation into benzene and DIPB (reaction 4.4, reverse). Since 1,3-DIPB decreases with

Table 4.1 Total strain energy (k.cal.mole^{-1}) of various molecules calculated for the equilibrium structure.

$E_{total\ strain} = E_{bond} + E_{angle} + E_{dihedral} + E_{electronic} + E_{van\ der\ waals} + E_{improper\ torsion}$

Molecule	E_{bond}	E_{angle}	$E_{dihedra}$	$E_{electronic}$	$E_{van\ der\ waals}$	$E_{improper}$	$E_{total\ strain}$
Cumene	0.2225	0.6049	0.1275	-1.6204	3.3863	0.0152	2.7360
o-DIPB	0.7851	4.4664	1.9722	-8.3369	5.0583	0.3146	4.2596
m-DIPB	0.2872	1.1496	0.3334	-3.6159	3.8246	0.0416	2.0204
p-DIPB	0.2984	1.2024	0.2606	-2.8792	3.8552	0.0472	2.7845

increasing Si/Al ratio (i.e., decreasing acid site density) and decreasing conversion (at lower conversion–less secondary disproportionation), and the 1,2-isomer is either not observed or formed in small quantities (Figure 4.1), it can be argued that the 1,3-isomer is mainly formed through isomerization of the 1,4-isomer.

4.2.2 Influence of Temperature

The influence of temperature on activity and product distribution is presented in Figure 4.2. The temperature has marked effect on the conversion of benzene and the product distribution. As expected, the benzene conversion increases with temperature. With increased reaction temperature, the selectivity towards: (a) aliphatics decreases very sharply, (b) cumene increases, and (c) DIPB increases initially and then decreases after passing through a maximum. This is probably due to the fact that initially, at lower temperatures, the alkylation of cumene (reaction 4.3) competes favorably with the transalkylation of DIPB with benzene to cumene (reaction 4.4). However, at higher temperatures, the transalkylation of DIPB with benzene (reaction 4.4) predominates over the alkylation of cumene (reaction 4.3). The selectivity towards cumene + DIPB at all temperatures (except 403K) is above 94%. The distribution of 1,3- and 1,4-DIPB is shown in Figure 4.2 (A). At lower temperature, and hence lower benzene conversion, the 1,4-isomer is predominant and the 1,3-DIPB increases at the expense of 1,4- with increasing temperature. The 1,2-isomer is always less than 2%. This suggests that 1,4-DIPB is the primary product on the alkylation of cumene. With increased temperature, the isomerization of 1,4-DIPB into 1,3-DIPB increases and attains a near-equilibrium distribution (1,4 = 32.5%, 1, 3 = 58.5%, and 1,2 = 9.0% at 100°C [9]).
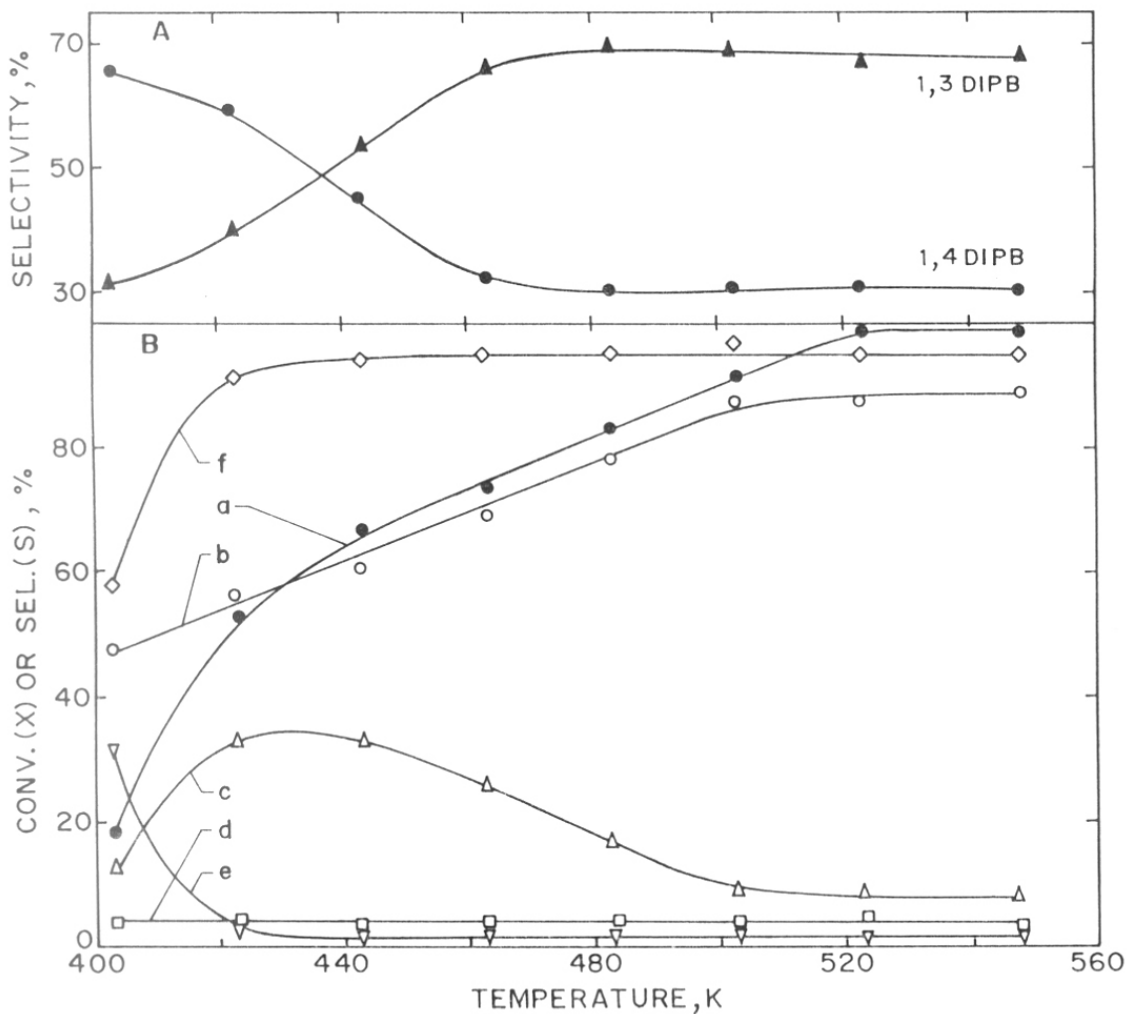
Fig.4.2   Isopropylation of benzene with 2-propanol over NCL-1 (Si/Al = 23). Influence of temperature on conversion or product selectivity (lower) and selectivity for 1,3 and 1,4 isomers of DIPB (upper). WHSV, 3.5 h^{-1}; benzene/2-propanol ratio, 6. Curve a, conversion; curve b, cumene; curve c, DIPB; curve d, others (n-propylbnezene, C_6-C_8 aromatics, and C_{10} aromatics); curve e, aliphatics; and curve f, cumene + DIPB.

4.2.3 Influence of Feed Ratio (Benzene to 2-Propanol)

The influence of the benzene to 2-propanol mole ratio in the feed on the conversion and the product selectivity is shown in Table 4.2. As expected, benzene conversion and TOF (moles of benzene converted per mole of Al atoms present in the catalyst per hour) increased with the benzene/2-propanol ratio. The selectivity towards cumene increases, whereas the selectivity towards DIPB decreases upon increasing the ratio of benzene to 2-propanol. However, the total selectivity for DIPB remained almost constant at about 95%. At a benzene to 2-propanol ratio of 4 the selectivity for DIPB is significantly high (mainly at the cost of cumene) due to increased alkylation of cumene to DIPB (reaction 4.3). At higher benzene to 2-propanol molar ratios, (6, 8, or 15) increased formation of cumene, both via transalkylation of DIPB with benzene (reaction 4.4) as well as through primary reaction of benzene isopropylation may be envisaged. However, among DIPBs, the isomer distribution did not vary significantly with benzene to 2-propanol ratio.

4.2.4 Influence of Weight Hourly Space Velocity

Table 4.3 shows the influence of WHSV on product distribution and activity. As expected, with increased WHSV the conversion of benzene decreased, and the selectivity towards DIPB increased mainly at the cost of cumene. This is because of the increased alkylation of cumene (reaction 4.3) at high WHSV. At higher contact times (lower WHSV) the transalkylation of DIPB with benzene (reaction 4.4) may be significantly contributing, causing an increase in cumene selectivity. However, once again the selectivity for cumene + DIPB did not vary significantly with WHSV. Among DIPBs, the 1,3-isomer decreases, and consequently the 1,4-isomer increases, with increasing WHSV. This further supports that the 1,3-isomer is formed by isomerization rather than cumene disproportionation. This may be due to the fact that at high feed rate (low

Table 4.2 Isopropylation of Benzene with 2-Propanol over H-NCL-1 (23): Effect of Benzene to 2-Propanol Ratio

	Benzene to 2-propanol ratio			
	4	6	8	15
Benzene conversion (wt% of theoretical)	80.0	91.1	97.0	100
TOF $(h^{-1})^a$	42.5	51.7	56.4	61.0
2-Propanol conversion (%)	95.0	100.0	100.0	100.0
Product selectivity (wt%)				
Aliphatics[b]	2.9	0.6	0.3	0.1
Cumene	64.9	88.5	89.6	91.0
DIPB[c]	30.0	8.5	7.8	6.9
n-Propylbenzene	0.5	0.2	0.2	0.1
Others[d]	1.7	2.2	1.9	1.8
DIPB distribution (wt%)				
1,2-DIPB	0.9	1.2	1.3	1.3
1,3-DIPB	62.2	67.5	64.5	65.8
1,4-DIPB	36.9	31.3	34.2	32.9

Note. Temperature, 503K, WHSV, 3.5 h^{-1}; TOS 1h.

[a] Moles of benzene converted per mole of Al present in the catalyst.

[b] Mainly propene

[c] DIPB = diisopropylbenzene

[d] Others include C_6-C_8 aromatics and C_{10} aromatics.

Table 4.3 Isopropylation of Benzene with 2-Propanol over H-NCL-1 (23): Effect of WHSV

	WHSV			
	1.75	3.5	7.0	15
Benzene conversion (wt% of theoretical)	97.8	91.1	77.4	67.6
TOF $(h^{-1})^a$	27.7	51.7	87.8	153.4
2-propanol conversion (%)	100.0	100.0	95.0	90.0
Product selectivity (wt%)				
Aliphatics[b]	0.1	0.6	1.4	2.4
Cumene	90.5	88.5	70.5	66.1
DIPB[c]	6.0	8.5	25.9	29.4
n-propylbenzene	0.2	0.2	0.1	0.2
Others[d]	3.2	2.2	2.0	1.6
DIPB distribution (wt%)				
1,2-DIPB	1.8	1.2	0.8	0.6
1,3-DIPB	69.0	67.5	61.0	55.4
1,4-DIPB	29.2	31.3	38.2	44.0

Note. Temperature, 503K, benzene to 2-propanol , 6; TOS 1h.

[a] Moles of benzene converted per mole of Al present in the catalyst.

[b] Mainly propene

[c] DIPB = diisopropylbenzene

[d] Others include C_6-C_8 aromatics and C_{10} aromatics.

contact times), alkylation reactions are favored over the isomerization of primarily formed 1,4-DIPB into 1,3-DIPB.

4.2.5 Influence of Time on Stream (TOS)

Figure 4.3 exhibits the effect of time-on-stream (TOS) on conversion and the selectivity of the catalyst. At early time-on-stream, the conversion of benzene increased slightly then decreased very slowly. With time, the selectivity to cumene decreases whereas that to DIPB increases, but overall selectivity for cumene + DIPB remains constant. Interestingly, 1,3-DIPB initially decreases with conversion due to deactivation behavior of the catalyst and consequently 1,4-DIPB increases at the cost of 1,3-DIPB. The deactivation may be due to the poisoning of active sites and pore blockage.

4.3 ISOMERIZATION OF 1,3,5-TRIMETHYLBENZENE

The reaction of C_7-C_8 aromatic over acid zeolites have been extensively studied, mainly because of their industrial importance [14-16]. However, not much is known about the isomerization of trimethylbenzenes (TMB). Among trimethylbenzenes, the 1,2,4-trimethylbenzene is an industrially important starting material for plasticisers, polyesterimides, epoxyresins, and high-temperature resistant polyimides [17].

4.3.1 Effect of Si/Al Molar Ratio of Zeolite NCL-1

The influence of the Si/Al ratio on the conversion as well as selectivity for 1,2,4-trimethylbenzene (1,2,4-TMB) and TMB disproportionation is shown in Figure 4.4. Expectedly, as the Si/Al ratio increases the conversion of 1,3,5-TMB decreases due to decrease in the acid site density and conversion. However, the selectivity for 1,2,4-TMB as well as total isomerization products increases slightly with decrease in acid site density. The selectivity for 1,2,3-TMB ranges from 4-5%. With increasing Al content, the disproportionation favors results in lower
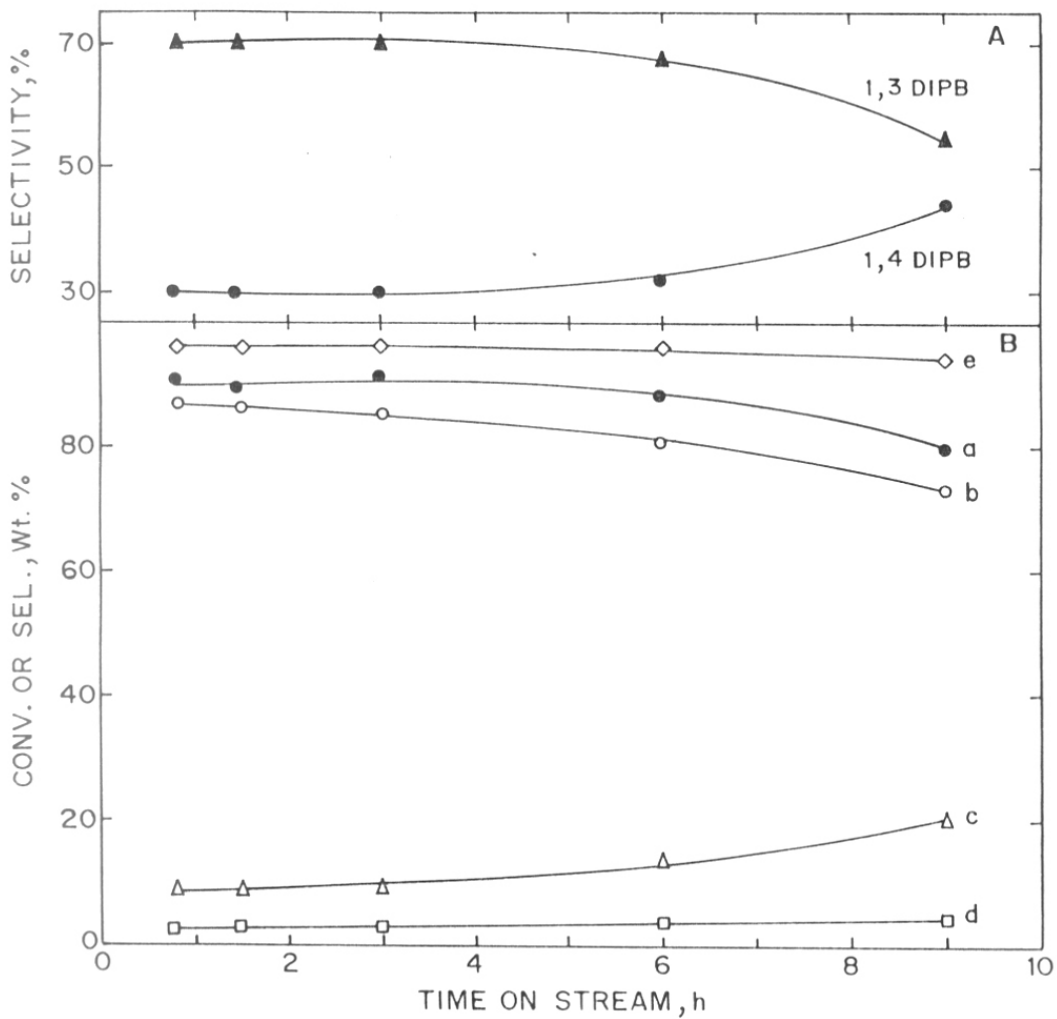
Fig.4.3   Isopropylation of benzene with 2-propanol over NCL-1 (Si/Al = 23).
Influence of time on stream on conversion or product selectivity (lower) and
selectivity for 1,3 and 1,4 isomers of DIPB (upper). Temperature, 503K;
WHSV, 3.5 h^{-1}; benzene/2-propanol ratio, 6. Curve a, conversion; curve b,
cumene; curve c, DIPB; curve d, others (aliphatics, n-propylbenzene, C_6-C_8
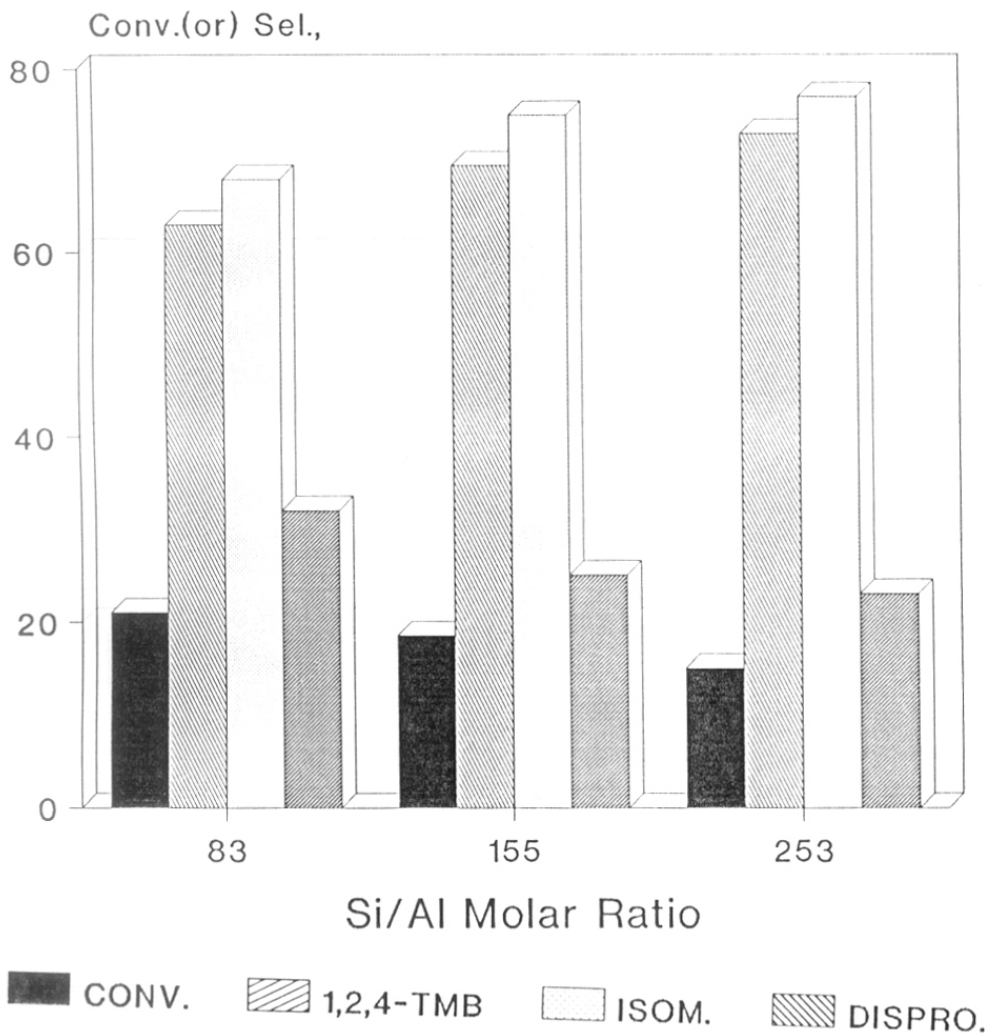aromatics and C_{10} aromatics); and curve e, cumene + DIPB.

Fig.4.4   Isomerization of 1,3,5-trimethylbenzene to 1,2,4-trimethylbenzene over H-NCL-1. Effect of Si/Al ratio on conversion or product selectivity. Temperature, 563K; WHSV, 3.4 h^{-1}.
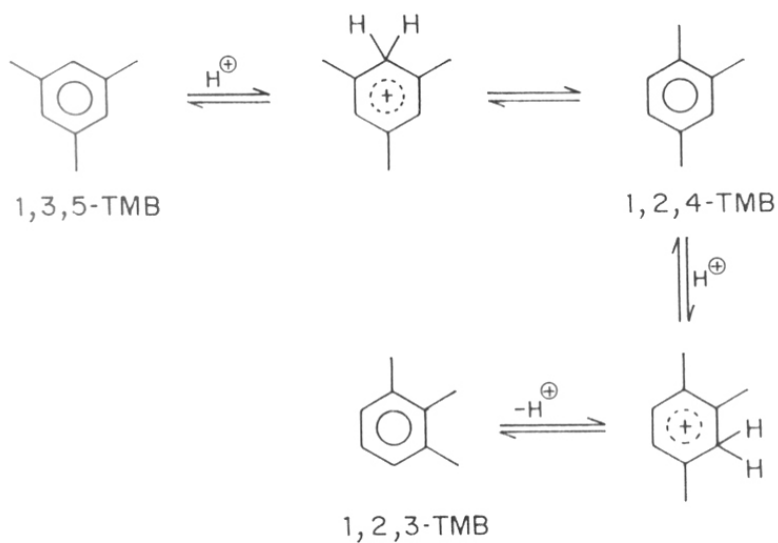
isomerization selectivity. The disproportionation reaction is significant at higher site density as well as conversion. The TOF(h^{-1}) were found to be 33, 55, and 64 for the Si/Al ratios 83, 155 and 252 respectively.

Collins et al.[18], based on kinetic studies on the isomerization and disproportionation of trimethylbenzenes over LaY zeolites, have reported that the isomerization of TMB occurs mainly via a classical 1,2 methyl shift. The disproportionation products (tetramethylbenzene and xylene) may be formed by intermolecular methyl-group transfer via diphenyl methane type intermediate [19] from one TMB molecule to another. Since NCL-1 is also a large-pore zeolite, the 1,2-methyl shift may be predominantly occurring during 1,3,5-TMB isomerization. The plausible reaction paths (both isomerization and disproportionation) are given in scheme 4.2.
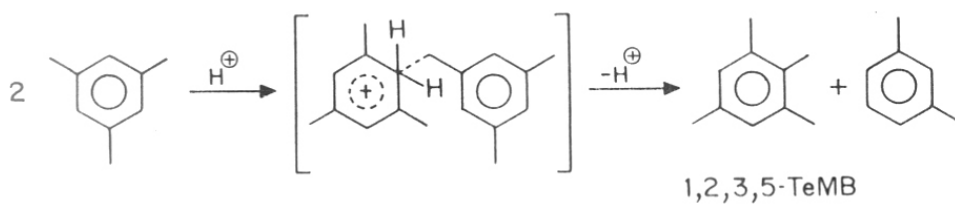
4.3.2 Effect of Temperature

The effect of temperature on the mesitylene conversion over H/Al-NCL-1 (Si/Al = 83) is shown in Figure 4.5. As expected, the conversion increased with reaction temperature (curve a, Figure 4.5). The selectivity for 1,2,4-TMB (curve b), 1,2,3-TMB (curve-c) as well as total isomerized products (1,2,3-TMB + 1,2,4-TMB) decreases slowly with increasing temperature. This is because, at higher temperatures in addition to isomerization reactions, disproportionation (a bimolecular process) takes place at an increased rate which gives rise to products such as xylenes and tetramethylbenzenes. The selectivity for disproportionation ranges between 23-33 mole%. The isomerization to disproportionation ratio decreases (from 3.2 to 2.0) with increasing temperature. The TOF(h^{-1}) values were found to be 4.8, 17.3, 33.0, 35.6 and 86.5 for the temperatures 503, 543, 563, 583 and 613K respectively.

(i) Isomerization for 1,3,5-TMB via 1,2 methyl shift

1,3,5-TMB

1,2,4-TMB

1,2,3-TMB

(ii) Disproportionation for 1,3,5-TMB
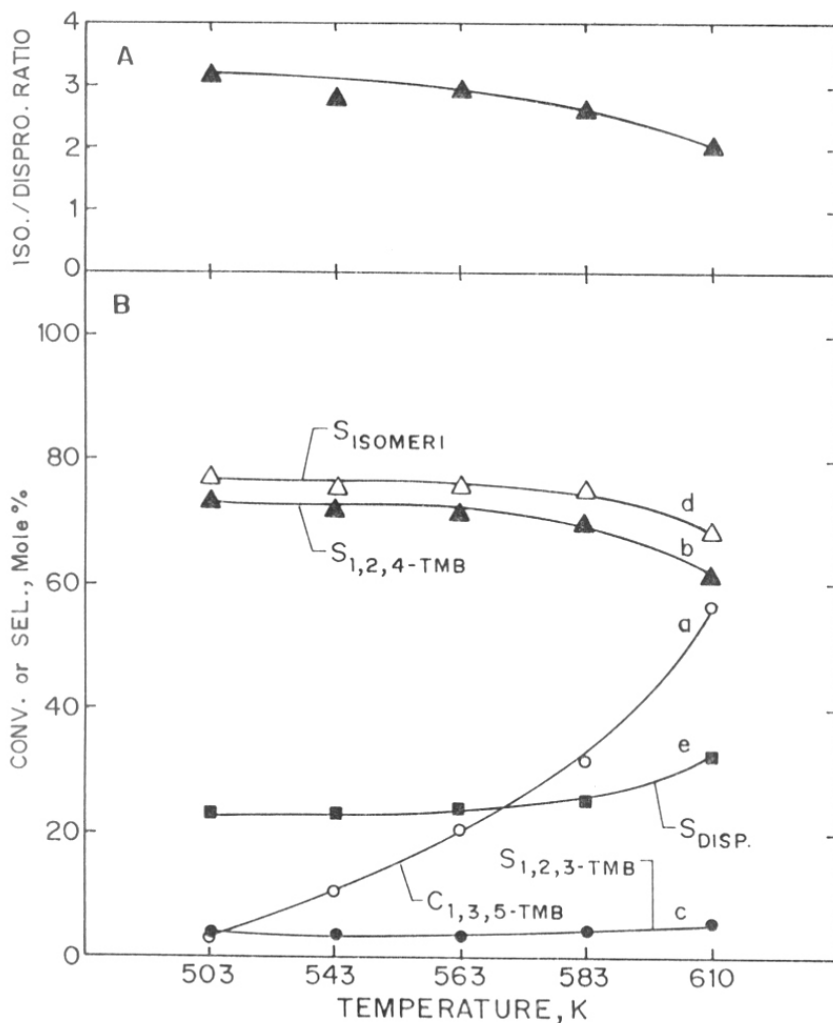

1,2,3,5-TeMB

Scheme-4·2

Fig.4.5   Isomerization of 1,3,5-trimethylbenzene to 1,2,4-trimethylbenzene over H-NCL-1 (Si/Al = 83). Effect of temperature on conversion or product selectivity (lower) and isomerization to disproportionation ratio (upper). WHSV = 3.4 h^{-1}; Curve a, conversion; curve b, 1,2,4-TMB; curve c, 1,2,3-TMB; curve d, total isomerization; and curve e, disproportionation selectivity.

4.3.3 Effect of Weight Hourly Space Velocity (WHSV)

In Table 4.4, the effect of liquid hourly space velocity is given for H/NCL-1 (Si/Al = 83). At higher WHSV (lower contact time) the conversion level decreases. This is due to the reason that at higher feed rate, the contact time decreases and consequently the conversion decreases. The selectivity for 1,2,4-TMB is almost the same and the TOF values decreases with increase of WHSV. (TOF(h^{-1}) values were found to be 120.5, 33.0, 14.5 and 8.2 for WHSV 1.7, 3.4, 5.2, and 6.9, respectively.

4.3.4 Effect of Time-on-Stream (TOS)

Figure 4.6 shows the conversion of 1,3,5-trimethylbenzene with reaction time. With increasing TOS, the conversion decreases steadily, whereas the selectivity for 1,2,4-TMB increases slowly and reaches a maximum of 84% after 5h. However, the selectivity for 1,2,3-TMB was found to be negligible (< 2%) in all the cases. In the beginning, the disproportionation occurs significantly, resulting in the formation of more tetramethylbenzene and xylenes at the expense of 1,2,4-TMB. As the time increases the selectivity for disproportionation also decreases. This may be due to the blocking or narrowing of pores and channels by bulky molecules such as tetramethylbenzenes.

4.4 FRIES REARRANGEMENT OF PHENYLACETATE INTO HYDROXY ACETOPHENONE

Arylesters (eg., phenylacetate) undergo Fries rearrangement over Friedel-Crafts catalysts such as AlCl$_3$, mineral acids like H$_2$SO$_4$, HF etc. Solid acids like zeolites have also been used owing to their heterogeneous, non-polluting nature coupled with reusability. The Fries rearrangement of phenylacetate has been reported using several zeolites and alumina in fixed-bed, continuous gas-phase experiments at atmospheric pressure [20]. Rao et al. [21] have reported that

Table 4.4 Isomerization of 1,3,5-Trimethylbenzene to 1,2,4-Trimethylbenzene over H- NCL-1 (83): Effect of WHSV

	WHSV			
	1.7	3.4	5.2	6.9
Mesitylene conversion (mole %)	39.1	20.1	13.9	10.5
TOF (h^{-1})^a	120.5	33.0	14.5	8.5
Product distribution (mole %)				
Toluene	0.2	0.1	0.1	0.1
Xylene	5.9	2.4	1.8	1.2
1,2,4-trimethylbenzene	25.6	14.2	9.9	7.7
1,2,3-trimethylbenzene	0.9	0.9	0.4	0.2
Tetramethylbenzene	6.2	2.9	1.6	1.2
Others	0.3	0.2	0.1	0.1
Selectivity of 1,2,4-TMB	65.4	71.7	71.3	73.7
log I/D ratio	0.6	0.6	0.7	0.7

a: Moles of trimethylbenzene converted per moles of Al in the catalyst

TMB: Trimethylbenzene

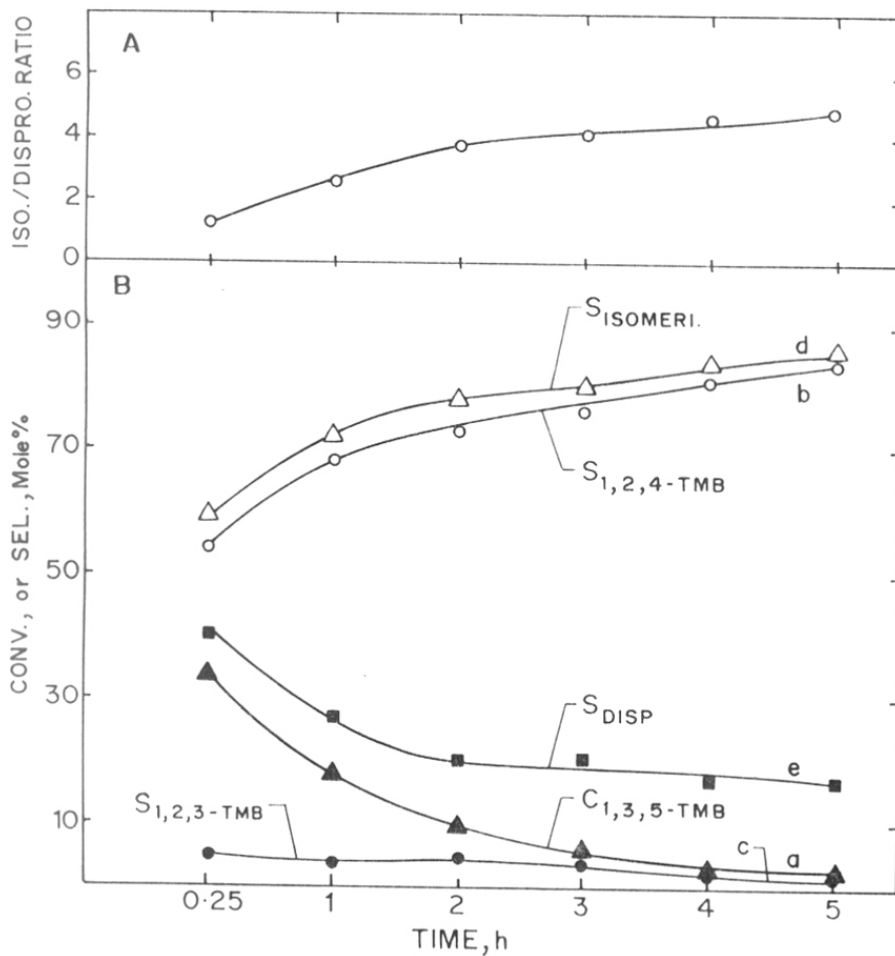I/D: Isomerization/disproportionation.

Fig.4.6   Isomerization of 1,3,5-trimethylbenzene to 1,2,4-trimethylbenzene over H-NCL-1 (Si/Al = 83). Effect of time on stream on conversion or product selectivity (lower) and isomerization to disproportionation ratio (upper). WHSV = 3.4 h⁻¹; temperature, 563K. Curve a, conversion; curve b, 1,2,4-TMB; curve c, 1,2,3-TMB; curve d, total isomerization; curve e, disproportionation selectivity.

phenol and orthohydroxy acetophenone were the major products in the rearrangement of phenylacetate over ZSM-5 type zeolites. However, the selectivity for hydroxyacetophenone was improved by the passivation of the external surface of zeolite catalyst. High-silica, large-pore zeolites have been found to be quite active and selective in Fries rearrangement of phenylacetate [22]. Since zeolite NCL-1 also belongs to the high-silica category, the reaction has been studied using Al-silicates of zeolite NCL-1.

4.4.1 Influence of Si/Al Molar Ratio

Table 4.5 shows the effect of the Si/Al molar ratio on the Fries rearrangement of phenylacetate at 400°C. As the Si/Al molar ratio increases, the conversion of phenylacetate decreases. Since, the conversion of phenylacetate is related to the density of acid sites, the conversion decreases at higher silicon to aluminum ratio. However, the intrinsic activity per Al-atom (TOF) was comparable for all the sample A-C, suggesting that even at high Si/Al ratios, the acid sites present on the catalyst are of adequate strength to promote this reaction. The selectivity for hydroxy acetophenone (vis-à-vis phenol) increased slightly with increasing Si/Al ratio and concurrently decreasing conversion. The p/o ratio was 0.5±0.1 in all the cases. Here it may be pertinent to mention that other zeolite catalysts like Beta, (Si/Al = 14), USY, (Si/Al = 4.7), Mordenite (Si/Al = 5.2), ZSM-12 (Si/Al = 50) and ZSM-5 (Si/Al = 20) produced mainly phenol (65-92%) with low selectivity for hydroxy acetophenone (8-20%) [22]. Since, conversion levels vary considerably, a correlation between zeolite structures and HAP selectivity with zeolite NCL-1 have not attempted.

Table 4.5 Fries Rearrangement of Phenylacetate into Hydroxy Acetophenone: Effect of Silicon to Aluminum Ratio: *Condition;* Temperature = 400°C, WHSV = 4 h^{-1}, TOS =1h^{-1}.

Si/Al ratio	Conversion %	TOF/h	Products distribution, wt%			
			o-HAP	P-HAP	Phenol	Others[a]
83	21.2	37.3	43.1	25.6	23.4	7.9
153	12.9	38.3	47.3	23.4	15.9	7.1
255	8.9	43.2	50.3	30.7	11.5	7.5

[a] Mainly acetoxy acetophenone along with some unidentified high boiling compounds.

Table 4.6 Rearrangement of Phenylacetate over H-NCL-1(83) Under Liquid-Phase condition: Reaction time = 24h, Phenylacetate = 5g, Catalyst = 1.5 g, No solvent was used.

	Temperature	
	140°C	180°C
Conversion	5.5	7.9
Product distribution (wt%)		
o-hydroxy acetophenone	2.2	3.6
p-hydroxy acetophenone	0.90	1.40
Phenol	2.1	2.4
Others[a]	0.3	0.5

[a] Mainly acetoxyacetophenone along with some unidentified high boiling compounds.

4.4.2 Influence of Temperature

Figure 4.7 (A) depicts the conversion of phenylacetate and the product selectivity as a function of temperature. As the temperature increases, the conversion of phenylacetate also increases. The selectivity for HAP (hydroxyacetophenone) remained nearly constant at 67±2. The selectivity for phenol and others (higher boiling products) also did not vary significantly and ranged between 23-27% and 6-9%, respectively. Rearrangements of phenylacetate under liquid-phase conditions are given Table 4.6. In this case p/o ratio as well as HAP, selectivity was slightly less than that observed in the case of vapor-phase, fixed-bed conditions. The p-hydroxy acetophenone is mainly formed via an intramolecular rearrangement mechanism. Scheme 4.3 depicts the mechanism governing this system as proposed by Vogt et al. [22]. Path 'A' leads to the formation of o-hydroxy acetophenone **2** via an intramolecular rearrangement. Path 'B' depicts the decomposition of phenylacetate into phenol **3** and ketene **4**. Ketene **4** can react further by two possible intermolecular pathways: (C) with phenol **3** to produce p-hydroxy acetophenone **5** or (D) with phenylacetate **1** to produce acetoxy acetophenone **6**.

4.4.3 Influence of Weight Hourly Space Velocity (WHSV)

The conversion under fixed-bed, vapor-phase conditions is directly related to WHSV (contact time). For a particular Si/Al ratio, as the weight hourly space velocity increases, the contact time between the catalyst and reactants decreases, which results in less conversion. Figure 4.7 (B) depicts the effect of WHSV on conversion and product selectivity (curve 'a'- 'd'). The conversion of phenylacetate were found to be 25.8, 21.2, 13.6 and 9.4 at WHSV 2, 4, 6 and 8 h^{-1} respectively. However, there was no significant influence of WHSV on selectivity among the distribution of hydroxy acetophenone.
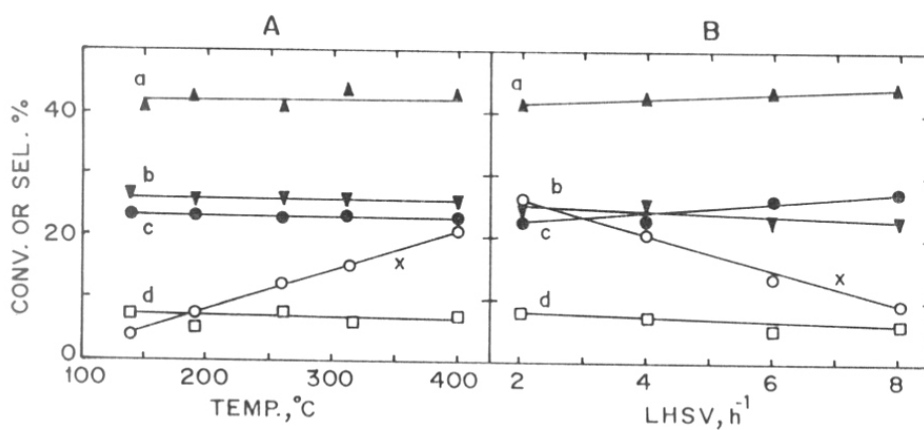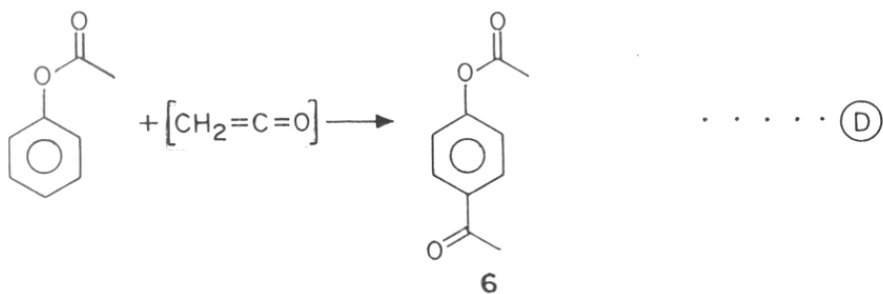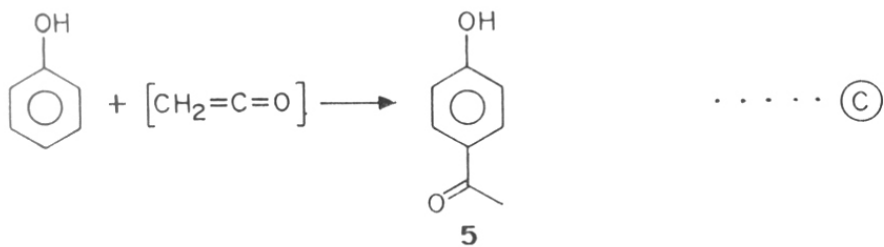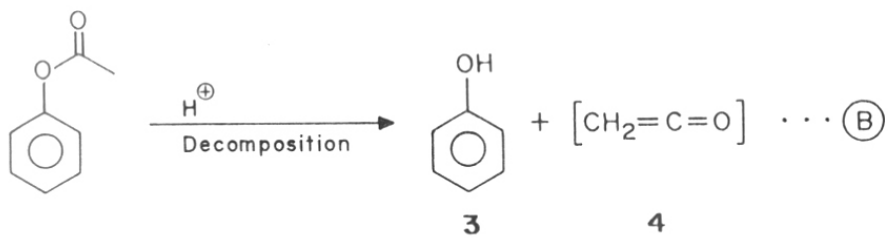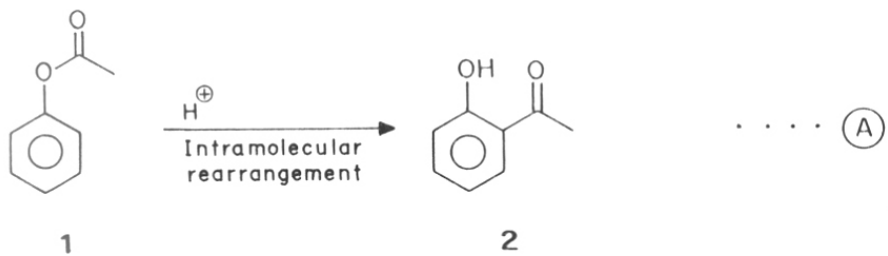
Fig.4.7   Fries rearrangement over zeolite NCL-1 (Si/Al = 83). Phenylacetate conversion (CONV) and product selectivity (SEL) as a function of temperature (A) at WHSV = 4 h^{-1} and WHSV (B) at 400°C; TOS, 1h. Curve x, conversion; curve a, o-hydroxyacetophenone; curve b, p-hydroxyacetophenone; curve c, phenol and curve d, others (unidentified high boiling compounds).

Scheme-4·3

4.4.4 Influence of Time on Stream (TOS)

Figure 4.8 shows the effect of time on stream data of phenylacetate at 400°C. Like other zeolite catalysts, NCL-1 also undergoes faster deactivation. Figure 4.8 'A' and 'B' exhibit the conversion of phenylacetate and selectivity for hydroxy acetophenones with time. Initially the selectivity for HAP increases slightly and then decreases. The rapid deactivation of the catalyst may due to two reasons: (i) deactivation by cocking lay down from the unstable reaction products and intermediates or (ii) the formation of polymeric byproducts in and on the zeolite crystals (due to deposition of degradation products such as acetyl ions, ketenes and the compounds with higher boiling compounds).

Figure 4.9 (A) shows, the selectivities of phenol, total o- + p-hydroxyacetophenone (bottom) and o-, & p-hydroxyacetophenone at different conversion level (Figure 4.9,B) for Si/Al = 83. As expected, the conversion of phenylacetate (curve a) decreases with time. The phenol selectivity increases slowly (curve c) and reaches a maximum of 40 wt%. The total selectivity of o- + p-hydroxyacetophenone slightly increases and then decreases slowly (curve b). Among the hydroxyacetophenone, o-hydroxyacetophenone (curve e) exhibits more selectivity than the p-isomer (curve f). However, the p/o-ratio ranges between 0.5 - 0.6.

4.5 DECOMPOSITION OF CUMENEHYDROPEROXIDE INTO PHENOL AND ACETONE

Phenol is an industrially important chemical generally produced via acid catalyzed decomposition of cumenehydroperoxide [23]. Various Bronsted and Lewis acids in homogeneous systems [24-27] at 0 to 50°C and cation exchange resin in pseudo-heterogeneous systems [28] at 60°C have been reported as catalysts for cumenehydroperoxide decomposition. In this section, efficient use of zeolites and related molecular sieves in catalytic conversion of phenol and acetone.
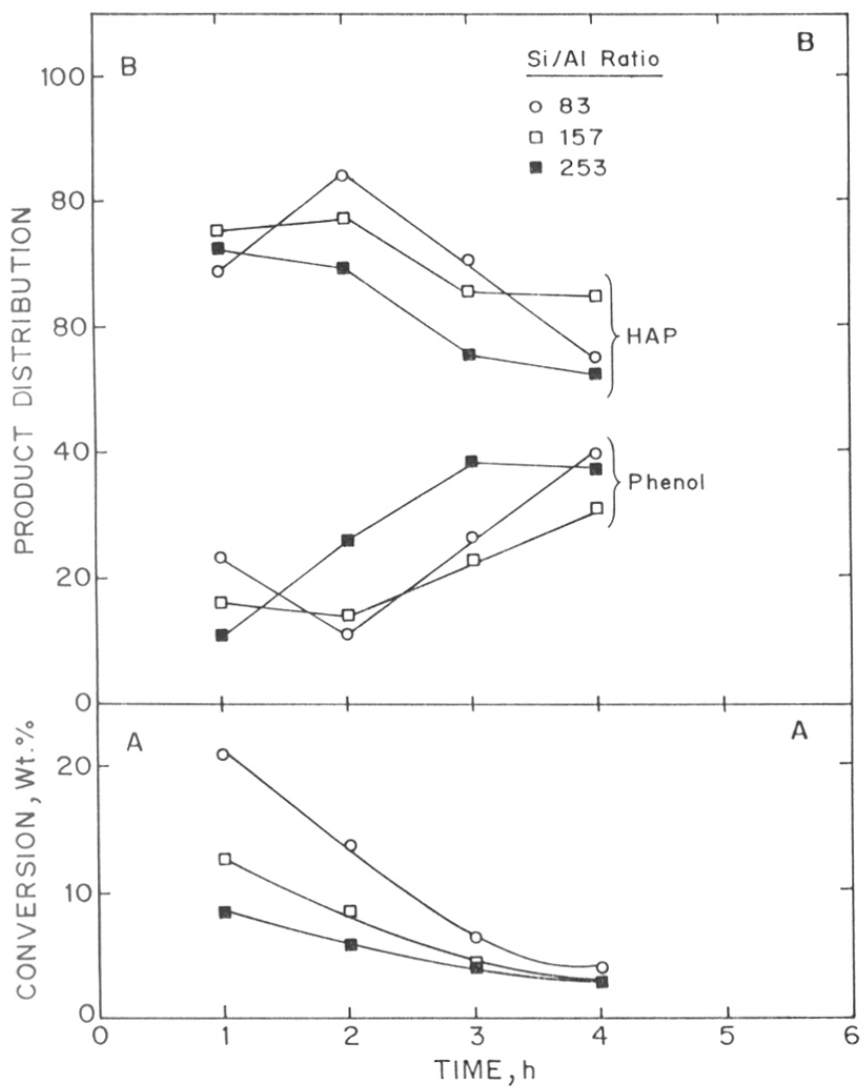
Fig.4.8   Fries rearrangement over zeolite NCL-1. Influence of time on stream on conversion (lower) or product selectivity (upper) for various Si/Al ratios. Temperature, 673K, WHSV, 4 h^{-1}. (A) conversion of phenylacetate, (B) total HAP (hydroxyacetophenone) and phenol selectivity.
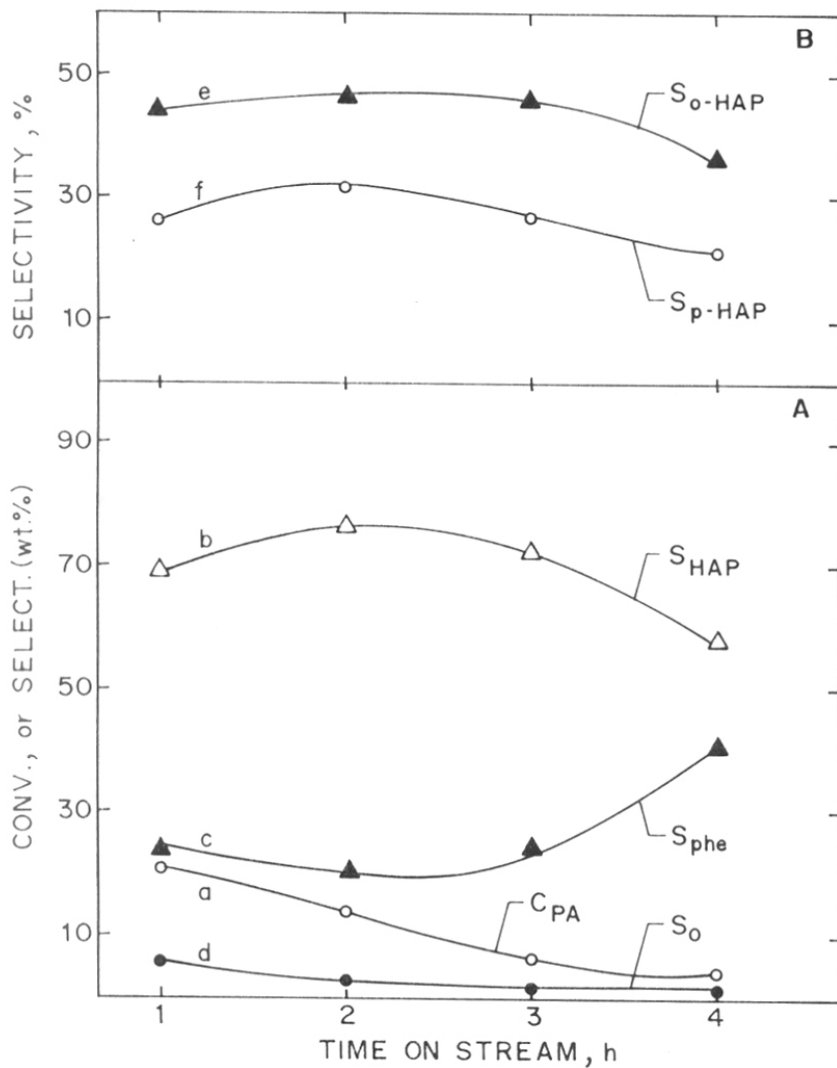
Fig.4.9   Fries rearrangement over zeolite NCL-1 (Si/Al = 83). Influence of time on
stream on selectivity of various products. Temperature, 673K; WHSV, 4 h^{-1};
(A) Curve a, conversion; curve b, total hydroxyacetophenone (HAP), curve c,
phenol; curve d, others (high boiling compounds), (B) curve e, o-hydroxy
acetophenone; curve f, p-hydroxy acetophenone.

is reported. A variety of molecular sieves, including zeolite NCL-1, were studied as catalysts under heterogeneous, liquid-phase conditions both in batch- and fixed-bed reactor system at room temperature to 60°C.

4.5.1 Comparison of Different Catalysts

Table 4.7 (entries **1-9**) indicates that the reaction was completed within 15-20 min at 25°C and the selectivity for the phenol was 90±2% in all the cases. The remaining 10±2% impurity was quinone. Entries **2-4** suggest that not only aluminosilicate zeolites but their Fe-, Ga-, or B-analogues can also be used as catalyst. The phenol selectivity is slightly higher for Ga, Fe, and B-Beta samples. However, over ZSM-12, and NCL-1 (Si/Al = 40 and 23 respectively) slightly lower conversion (entries **10 & 11**) was obtained. Entry **13** exhibits the results obtained in a fixed-bed, down-flow reactor giving 94% phenol selectivity at 99% conversion.

4.5.2 Decomposition under Fixed-Bed Condition

Entry **18** exhibits the results obtained in a fixed-bed, down-flow reactor giving 94% phenol selectivity at 99% conversion. Figure 4.10 shows the effect of time-on-stream on activity and selectivity for the decomposition of cumenehydroperoxide into phenol and acetone under fixed-bed conditions using H/Al-Beta catalyst. The obvious advantages of fixed-bed reaction condition reactions are: (i) no need to separate the solid catalyst from the products and (ii) higher phenol selectivity. However, in fixed bed conditions, the deactivation of the catalyst with time-on-stream is an important parameters. The time on stream data show that during 10 h, the selectivity for phenol and conversion of cumenehydroperoxide decreases slowly.

Table 4.7 Catalytic decomposition of cumenehydroperoxide over various zeolites.

No	Zeolite	Si/Al ratio	Temperature	Reaction time, min	Conversion, wt %	Phenol Sel. mole%
1	H-[Al]-Beta	14	RT	5	100	88.0
2	H-[Ga]-Beta	20	RT	5	100	92.0
3	H-[Fe]-Beta	22	RT	5	100	91.0
4	H-[B]-Beta	30	RT	5	100	92.0
5	H-[Al]-ZSM-5	30	RT	5	100	86.0
6	H-[Ga]-ZSM-5	35	RT	5	100	88.5
7	H-[Fe]-ZSM-5	30	RT	5	100	88.0
8	H-Mordenite	7.0	RT	5	100	86.5
9	H-Y	2.5	40	10	96.0	85.0
10	H-[Al]-ZSM-12	40	40	30	95.0	82.0
11	H-[Al]-NCL-1	40	40	15	85.0	83.5
12	No catalyst	-	-	-	-	-
13	H-[Al]-Beta (fixed-bed results)	14	60	60	99.0	94.0

Note. Fixed bed reaction: Temperature = 333K, Catalyst = H-Beta (1g), WHSV = 2, products were collected after 1h. The zeolite Mordenite and HY were obtained from Degussa. The selectivity of phenol was confirmed by GC-5880 using capillary column. The other products mainly include quinones, catehol and higher boiling products.
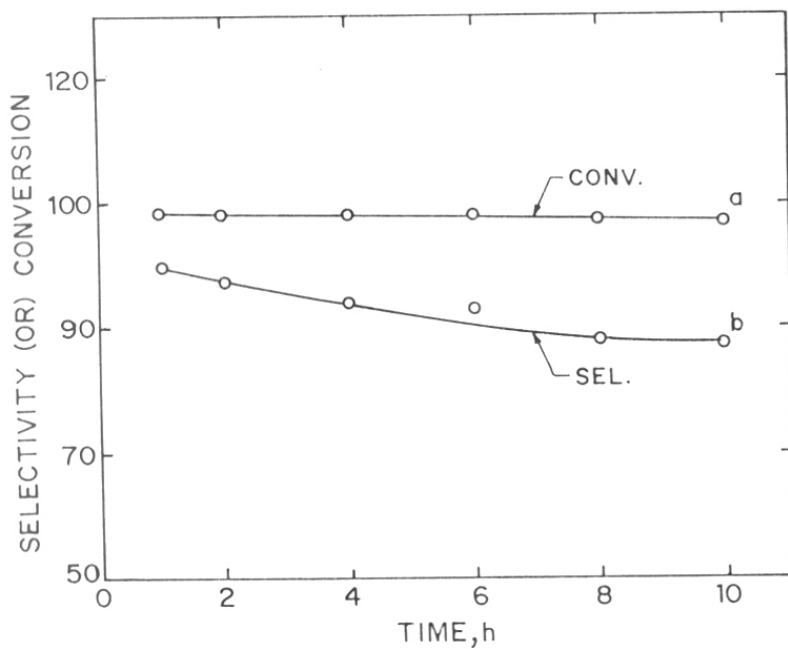
Fig.4.10   Decomposition of cumenehydroperoxide into phenol and acetone over zeolite
Beta (Si/Al = 14). Temperature, 333K, WHSV, 2 h^{-1}. Curve a,
cumenehydroperoxide conversion; curve b, phenol selectivity.

4.6 SUMMARY

Zeolite NCL-1 exhibits high activity and selectivity in the isopropylation of benzene by 2-propanol to form cumene. The cumene selectivity generally ranges between 65 and 90% while cumene + diisopropylbenzene selectivity remains 94±3%. Among DIPBs, while the 1,2-isomer was not formed significantly, 1,4-DIPB was formed as a primary product by the isopropylation of benzene. However, 1,4-DIPB isomerized to give 1,3-DIPB in nearly thermodynamic proportions. The selectivity for cumene and cumene + diisopropylbenzene exhibited by H/NCL-1 are typical of large-pore zeolites.

Zeolite NCL-1 shows both isomerization and disproportionation towards isomerization of 1,3,5-trimethylbenzene to 1,2,4-trimethylbenzene. The selectivity for isomerization is significant at lower conversion vis-a-vis lower acid-site density.

Zeolite NCL-1 exhibits moderate activity in the Fries rearrangement of phenylactate into hydroxyacetophenone. The observed selectivity in the Fries rearrangement of phenylacetate to hydroxy acetophenone is slightly higher than that observed in other large-pore zeolites such as USY, mordenite, beta etc.

Zeolites (particularly beta) can be used as heterogeneous and environmentally safer catalysts for the conversion of cumenehydroperoxide into phenol with high selectivity.

4.7 REFERENCES

1.	E.k. Jones, and D.D. Dettener, US Pat. 2 860 173 (1958).

2.	H. Miki, US Pat. 4 347 393 (1982).

3.	K.H. Chandavar. S.G. Hegde, S.B. Kulkarni and P. Ratnasamy, *J. Chem. Technol. Biotechnol.* **34A**, 165 (1984).

4.	W.W. Keading and R. Holland , *J. Catal.* **109**, 212 (1988).

5.	A.R. Pradhan, A.N. Kotasthane and B.S. Rao, *Appl. Catal.,* **72**, 311 (1991).

6.	B.S. Rao, I. Balakrishnan, V.R. Chumbhale, A.R. Pradhan and P. Ratnasamy, in " *Procedings, First Tokyo Conference on Advanced Catalytic Science and Technology,* (TOCAT-1), July 1-5, p69 (1990).

7.	K.S.N. Reddy, B.S. Rao and V.P. Shiralkar, *Appl. Catal. A,* **95**, 53 (1993).

8.	A.R. Pradhan and B.S. Rao, *J. Catal.,* **132**, 79 (1991).

9.	E.F. Harper, D.Y. Ko, H.K. Lee, E.T. Sabourin and R.C. Williamson, in *"Industrial and Laboratory Alkylations"* (L.F. Albright and A.R. Goldsby, eds.), ACS Symposium series 55, p371. Am. Chem. Soc., Washington, DC, 1977.

10.	N.R. Meshram, S.B. Kulkarni and P. Ratnasamy, *J. Chem. Technol. Biotechnol.* **34A,** 119 (1984).

11.	A. Corma, J.L.G. Fierro, R. Montanana and F.Thomas, *J. Mol. Catal.,* **30**, 361 (1985).

12.	B.W. Wojciechowski, *Rev. Chem. Intermed.,***8**, 21 (1987). [CA 107: 235644e).

13.	B.R. Gelin and M. Karplus, *Biochemistry,* **18**, 1256 (1979).

14.	B.M. Bhawal, R. Vetrivel, T.I. Reddy, A.R.A.S. Deshmukh and S. Rajappa, *J. Phys. Org. Chem.,* **7**, 377 (1994).

15.	G.N. Rao, R. Kumar and P. Ratnasamy, *Appl. Catal.,* **49**, 307 (1989).

16.	Anuj Raj, J.S.Reddy and R. Kumar, *J. Catal.,* **138**, 518 (1992).

17. E. Sastre, A. Corma, F. Fajula, F. Figueras and J. Perez-Pariente, *J. Catal.*, **126**, 457 (1990).

18. D.J. Collins, C.B. Quirey, E.J. Fertig and B.H. Davis, *Appl. catal.*, **28**, 35 (1986).

19. J.A. Martins, J. Perez-Parientte, E. Sastre and P.A. Jacobs, *Appl. Catal.*, **45**, 85 (1988).

20. (a) Y. Pouilloux, N.S. Gnep, P. Magnoux and G.J. Perot, *J. Mol. Catal.*, **40**, 231 (1987).

    (b) Y. Pouilloux, J.P. Bobido, I. Neves, M. Gubelmann and G.J. Perot, *Stud. Surf. Sci. Catal.*, **59**, 513 (1990).

21. Y.V.S. Rao, J. Kulkarni, M. Subramanyam and A.V.Rama Rao, *Tet. Lett.*, 7799 (1993).

22. A. Vogt, H.W. Kouwenhoven, R. Prins, *Appl. Catal. A*, **123**, 37 (1995).

23. H. Hock, S. Loung, *Ber. Dttsch. Chem. Gen.*77, 257 (1944).

24. H. Hock, *Rev. Angew. Chem.* **69**, 313 (1957).

25. R.A. Sheldon and J.A. Van Doorn, *Tet. Lett.*, 1021 (1973).

26. N.C. Deno, W.E. Bllups, K.E. Kramer and R.R. Lastomirsky, *J. Org. Chem.*, **35**, 3080 (1970).

27. J.O. Turner, *Tet. Lett.*, 887 (1971).

28. J. Vodnar, P. Fejes, K. Varga and F. Berrger, *Appl. Catal.*, **122**, 33 (1995).

LIQUID-PHASE CARBON-CARBON BOND FORMATION REACTIONS

5.1 INTRODUCTION

Zeolites are well known catalysts for the carbon-carbon bond formation reactions such as alkylation and acylation of arenes via an electrophilic attack, both under vapor as well as liquid-phase conditions [1]. Zeolites, particularly MFI and Faujasite type, have also been used to catalyse the nucleophilic C-N (reaction of alcohols with amine and addition of ammonia and amines to olefins [2-14]), C-O (addition of H_2O, alcohol and carboxylic acids to alkenes [15-25]), C-S (reaction of H_2S to olefins to give thiol and thioethers [26-28]) bond formation reactions. Further, nucleophilic C-C bond formation catalyzed by other solid acids such as clays (Montmorillonite), Nafion-117 and CaY [34] zeolites is well studied. It is interesting to note that zeolites can play their role by activating the "leaving group" through protonation or metal ion coordination and by limiting consecutive side reactions resulting in high selectivity. In this chapter, following nucleophilic C-C bond formation reactions between silylenol ethers (enolic form of ketones) and various reactants catalyzed by TS-1 and other zeolites are described. The reactions are (i) Mukaiyama aldol condensation (ii) Michael addition (iii) acylation and (iv) tert. butylation. The catalyst used in this works are tabulated in Table 5.1 along with their some physico-chemical characterization as well as the corresponding reference for their preparation.

5.2 MUKAIYAMA ALDOL CONDENSATION REACTION

The Mukaiyama aldol condensation [35] between silylenol ethers and aldehyde/ketal, a facile method for C-C bond formation, is catalyzed by Lewis acids both under homogeneous and heterogeneous reaction conditions at subambient temperatures [34, 36-39]. Kawai et.al. [34] have reviewed the catalytic activity and selectivity of various conventional solid acids such as SiO_2-Al_2O_3, clays (Montmorillonite), Nafion-117, CaY zeolite etc. in Mukaiyama aldol condensation

Table 5.1 Physico-Chemical Characterization of Zeolites Used in this Section

Sample	Si/M ratio[a]	Particle size, μm	Surface area, m^2g^{-1}	C_6H_{12} ads. (wt%)[b]	Reference
TS-1(Ti-MFI)	36	0.2-0.3	405	6.5	29
TS-1	52	0.2-0.3	398	6.1	29
TS-2(Ti-MEL)	64	0.5-1.0	375	5.9	30
VS-1(V-MFI)	86	0.4-0.6	460	8.6	31
RE-Y[c]	2.5-3.0	0.5-0.7	712	21.7	-
La-Y[c]	2.5-3.0	0.5-0.7	725	21.5	-
Na-Y	2.5-3.0	0.5-0.7	720	21.8	-
SnS-1(Sn-MFI)	70	0.4-0.6	518	12.8	32
Zn/ZSM-5[d]	40	0.8-1.0	460	6.7	-
ZSM-5	40	0.8-1.0	474	6.9	33

[a] M= Ti (TS-1 & TS-2), V(VS-1), Al(REY, LaY, NaY, Zn/ZSM-5 & ZSM-5) or Sn(SnS-1).

[b] Gravimetric adsorption of cyclohexane (Cahn balance), temperature = 298K, $p/p_o = 0.5$.

[c] Na-Y was obtained from United Catalyst India Ltd and converted onto RE-Y & La-Y by ion exchange with respective rare earth solutions.

[d] Na-ZSM-5 was treated with $Zn(CH_3COO)_2$ (1M solution) at 80°C. The process was repeated thrice in order to get 70% exchange.

reactions. However, like homogeneous systems [36-39], these heterogeneously catalyzed reactions were also carried out at low temperatures between 0°C to -95°C.

Here, the use of titanium-silicate molecular sieve, TS-1 as an efficient heterogeneous catalyst in Mukaiyama aldol condensation involving silylenol ethers and aldehydes to produce β-hydroxyesters in good yields at room temperature or at 60°C is described. This is the first example where titanium-silicate zeolites (TS-1) is used as non-oxidative, Lewis acid catalyst. The preparation of TS-1 is described in chapter 2.

5.2.1 Typical Reaction and Scheme

In a typical reaction, the catalyst (300 mg) was added to a mixture of silylenol ether (Aldrich 96%) (10 mmol) and an aldehyde (10 mmol) in dry THF (10 ml), taken in a glass, round bottom flask (batch reactor), which was stirred magnetically. The reactions were carried out under nitrogen atmosphere at room temperature unless stated otherwise. The progress of the reaction, was monitored by TLC (thin layer chromatography), and after completion of the reaction, the catalyst was filtered off and the products were separated by column chromatography and characterized by ^{1}H and ^{13}C NMR, IR and mass spectral techniques. The reaction scheme is depicted in scheme 5.1.

5.2.2 Results and Discussion

Table 5.2 shows that the TS-1 (entries 1-11) is a quite efficient catalyst (vis-a-vis other solid catalysts) for the condensation of silylenol ether with various aldehydes (**1-8**) to produce the corresponding β-hydroxy esters in good yields with 100% selectivity (scheme 5.1). Both, cyclic and aromatic aldehydes exhibited good reactivity. Although, propanal (**6**) was also quite reactive, octanal (**7**) (with long chain) and isobutanal (**8**) (with branched chain) gave relatively lower yields (67-70%) compared to other aldehyde **1-5**. Entry 10 shows that as-synthesized TS-1 (with pores
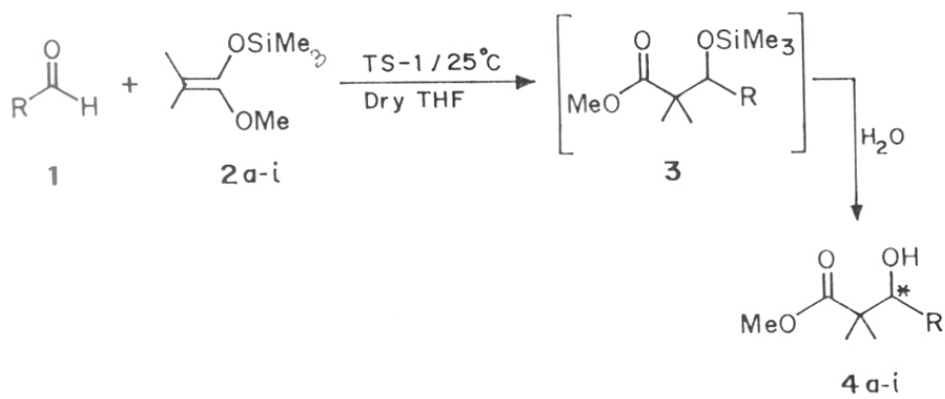
Scheme-5·1

Table 5.2 Reaction of methyl trimethylsilyl dimethylketene acetal **1** with various aldehydes (RCHO) catalyzed by TS-1 molecular sieves

Entry	RCHO	R	Catalyst	Temp. °C	Product, **4a-i** conv./yield[a] (%)
1	Benzaldehyde **2a**	C_6H_5-	TS-1	RT	85
2	4-nitrobenzaldehyde **2b**	$4-NO_2 C_6H_4$-	TS-1	RT	90
3	4-cyanobenzaldehyde **2c**	$4-CN C_6H_4$-	TS-1	60	82
4	4-methoxybenzaldehyde **2d**	$4-CH_3O C_6H_4$-	TS-1	RT	85
5	furfuraldehyde **2e**	C_4H_7O-	TS-1	60	85
6	propionaldehyde **2f**	C_2H_5-	TS-1	RT	70
7	octylaldehyde **2g**	C_7H_{15}-	TS-1	60	85
8	isobutyraldehyde **2h**	C_4H_9-	TS-1	RT	67
9	2-nitrobenzaldehyde **2i**	$2-NO_2 C_6H_4$-	TS-1	RT	70
10[b]	**2b**	$4-NO_2C_6H_4$-	TS-1	RT	40
11[c]	"	"	TS-1	RT	90
12[d]	"	"	TS-1	RT	75
13[e]	"	"	RE-Y	60	50
14[e]	"	"	La-Y	60	37
15[f]	"	"	SnS-1	60	25
16[e]	"	"	Beta	60	20
17[e]	"	"	H-ZSM-5	60	10

[a] Isolated yield of the product.
[b] As synthesised, uncalcined TS-1.
[c] Solvent dichloromethane
[d] Solvent nitromethane.
[e] Si/Al ratios: Beta = 60; LaY and RE-Y = 2.4 and H-ZSM-5 = 33.
[f] Si/Sn = 60.

filled with organic template) was considerably less active compared to its organic free calcined form (with free pores, entry 2). Further, 2-nitro benzaldehyde (entry 9) gave 70% yield indicating that the external surface may also be active in this reaction. Entries (2,11 and 12) show that while tetrahydrofuran (THF) and dichloromethane (DCM) are good solvents for this reaction using TS-1 catalyst, nitro methane (NM) seems to lower the yields.

As a result of condensation between silylenol ethers of ketone and aldehydes, an asymmetric center (the carbon atom attached to four different substituents) is created in the product β-hydroxy esters (scheme 5.1). The product was analyzed by polarimeter to find out the presence of optical rotation by dissolving it in an inert solvent. The absence of any significant optical rotation in the product suggests the formation of racemic mixture.

5.3 MICHAEL REACTION OF SILYLENOL ETHERS WITH α,β-UNSAT – URATED CARBONYL COMPOUNDS

The Michael addition reaction between silylenol ethers and α,β-unsaturated carbonyl compounds is usually carried out using several homogeneous Lewis acids such as $TiCl_4$, $SnCl_4$, $Ti(O^i\text{-}Pr)_4$, in stoichometric amounts and at lower temperatures [40]. The utility of bifluorides such as $(Me_2N)_3S + Me_3SiF_2^-$ [41], $(Me_2N)_3S + Me_3SiF_3^{2-}$ and the perchlorate Ph_3CClO_4 [42], have also been reported in homogeneous medium. However, only a few heterogeneous catalyst like CsF, $ZnCl_2$, and Al-clay (montmorillonite) [43,44] in the temperature range of -20 to -78°C have been reported. In this dissertation, the Michael addition reactions between silylenol ethers and various α,β-unsaturated carbonyl compounds at 40°C in presence of dry solvents over titanium-silicate as the Lewis-acid catalyst are described.

120

5.3.1 Typical Reaction and Scheme

The reaction was carried out using a batch reactor under N_2 atmosphere in dry condition. In a typical reaction 10 mmol of silylenol ether in **dry** dichloromethane was added to pre-activated catalyst (0.5g), then 10 mmol of methyl methacrylate was added to the reaction vessel. Then this reaction mixture was magnetically stirred at 40°C for 12h in perfect dry conditions. The progress of the reaction was monitored by TLC using 10% ethylacetate in pet ether as solvent system. Once the reaction was completed, the catalyst was separated, the product was extracted with 25 ml of dichloromethane. The extraction was repeated thrice. Then the combined extract was dried over anhydrous Na_2SO_4 and the solvent was removed in vacuum. The products were identified by NMR, IR and mass spectral analyses. The reaction between various α,β-carbonyl compounds and silylenol ether is shown in the scheme 5.2.

5.3.2 Results and Discussion

Table 5.3 shows the effect of various zeolites over the 1,4-addition of methylmethacrylate with silylenol ether. Among various catalysts scanned for this reaction, TS-1 shows better activity (yield = 62%) than that exhibited by other zeolites. For example RE-Y and La-Y exhibit moderate yields (ca. 40%). However, in the case of isomorphously substituted Sn-ZSM-5, cation exchanged Zn/ZSM-5 and steamed-Y, the yields are very low (20%). Na-Y and VS-1 (vanadium silicate) exhibit almost no activity in this reaction. Eventhough, RE-Y and La-Y, quite strong Lewis acids and efficient catalysts for electrophilic acylation and alkylation, are less reactive in this nucleophilic C-C bond formation reaction. However, the product selectivity was 100% (no other product) in all the cases.

Table 5.4 shows the result of 1,4-addition of various α,β-unsaturated carbonyl compounds with silylenol ether producing corresponding products in moderate to good yield. Entries 2, 3 and

Table 5.3: Addition of methylmethacrylate, **2a** to silylenol ether **1** over various zeolites to give the addition product **3a**.

Entry	Catalyst	Temperature °C	Reaction Time, hour	Conv./yield[a] %
1	TS-1	40	12	62
2	TS-1	40	12	55
3	TS-2	40	12	45
4	VS-1	40	12	nil
5	RE-Y	40	12	45
6	La-Y	40	12	40
7	Na-Y	40	12	nil
8	SnS-1	40	12	20
9	Zn/ZSM-5	40	12	20
10	ZSM-5	40	12	nil

[a] isolated yield by column chromatography, product selectivity was 100%, the remaining was unreacted starting materials.

Table 5.4: Addition of α,β-unsaturated carbonyl compounds to silylenol ether **1** over TS-1.

Condition: 10 mmol silylenol ether; 10 mmol α,β-unsaturated carbonyl compounds; 10 ml dry solvent (dichloromethane); 20 wt% activated TS-1; Temperature = 40°C; Reaction time = 12 h.

Entry	α,β-unsaturated carbonyl compounds	Formula		Product	Conv./ yield[a], %
		R_1	R_2		
1	Methylmethacrylate, **2a**	CH_3	CH_3	**3a**	62
2	Methylethacrylate, **2b**	CH_3	C_2H_5	**3b**	35
3	2-ethyl hexylacrylate, **2c**	C_2H_5	C_6H_{13}	**3c**	30
4	2-hydroxyethylmethacrylate, **2d**	$-C_2H_4-OH$	CH_3	**3d**	20
5	2-methyl cyclohexenone **2e**	-	-	**3e**	40
6	Cyclohexenone **2f**	-	-	**3f**	55
7	Methylvinylketone **2g**	-	-	**3g**	40
8[b]	Methylmethacrylate **2a**	CH_3	CH_3	**3a**	35
9[c]	Metylmethacrylate **2a**	CH_3	CH_3	**3a**	40
10[d]	Methylmethacrylate **2a**	CH_3	CH_3	**3a**	55

[a] Isolated yield by column chromatography, product selectivity was 100%, the remaining was unreacted starting material.

[b] Dry tetrahydrofuran

[c] nitromethane as solvent

[d] The reaction was carried out using acetonitrile at 70°C.

Scheme-5·2

Reaction 1 (top):

2a-d → 3a-d, TS-1, dry DCM, 40°C, 12h

a : $R_1 = R_2 = CH_3$; b : $R_1 = CH_3$, $R_2 = C_2H_5$

c : $R_1 = C_2H_5$, $R_2 = C_6H_{13}$; d : $R_1 = HO-C_2H_4$, $R_2 = CH_3$

Reaction 2 (bottom):

2e : $R_3 = CH_3$ 2g
2f : $R_3 = H$

TS-1, dry DCM, 40°C, 12h

3e : $R_3 = CH_3$
3f : $R_3 = H$

3g

1 : Me_3SiO , MeO

124
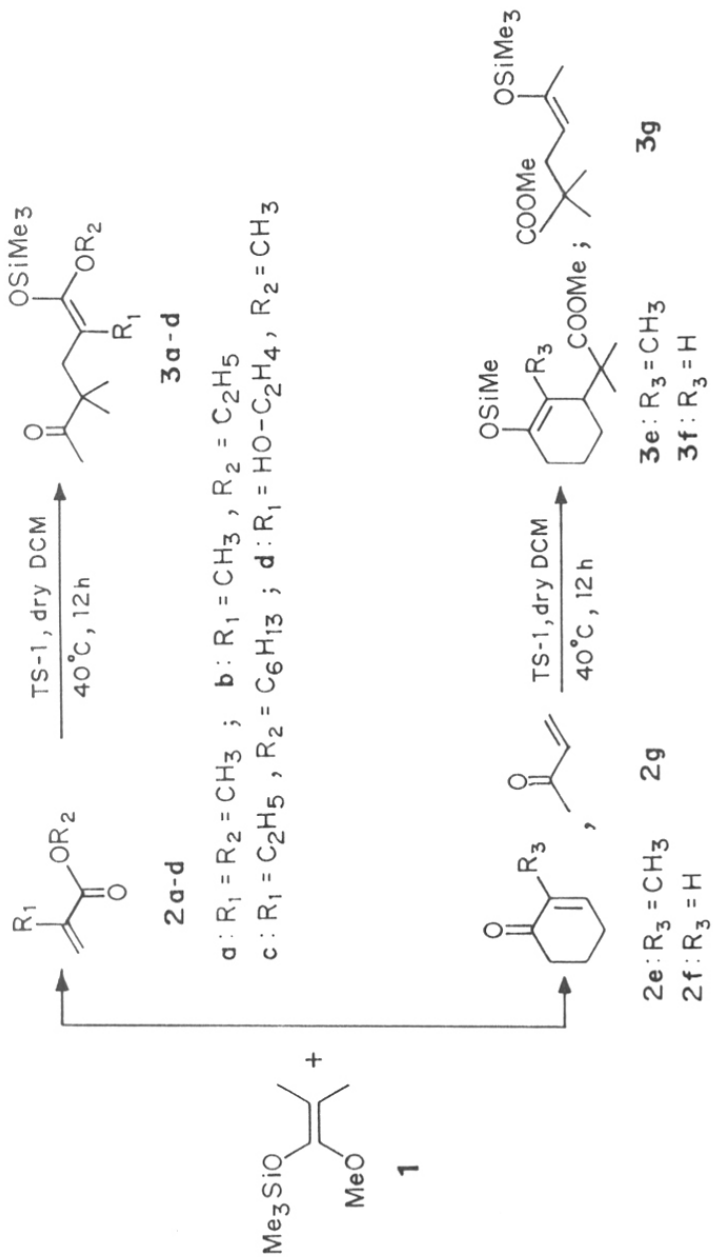
4 clearly indicate that as the bulkiness of the carbonyl group increases, the reaction proceeds slowly resulting in less conversion. This may be partly due to electronic effects and diffusional limitation in the pores and channels as observed in the other oxidation reactions. However, the use of different solvents (entries 1, 8-10) reveals that dichloromethane is a good solvent for this carbon-carbon bond formation reaction. Figure 5.1 shows the reaction progress with reaction time exhibiting that the conversion reaches maximum in 12h after that no further increase in the conversion was observed.

5.4 ACYLATION OF SILYLENOL ETHERS OF KETONE WITH ACID-CHLORIDE (PREPARATION OF 1,3-DIKETONE)

The acylation of silylenol ethers of ketones with acid chloride is known to yield the corresponding diketones [45-47]. Here, the titanium-silicate catalyzed acylation of silylenol ethers of ketone with acid chloride at 40°C with moderate yield is described.

5.4.1 Typical Reaction and Scheme

In a typical reaction procedure for acylation, 10mmol of silylenol ether (trimethlsilyloxy cyclohexene, an enolic form of cyclohexanone) was added to dry dichloromethane (15ml) containing 20 wt% of activated TS-1 followed by the addition of 10 mmol of acetylchloride under dry condition. The reaction temperature was raised to 40°C and magnetically stirred for 5h. After the completion of reaction, the catalyst was filtered and the excess acid-chloride was removed by washing with water. The organic layer was thoroughly washed with water, dried over anhydrous Na_2SO_4 and evaporated under vacuum. The products were further purified by column chromatography and identified by ^1H, ^{13}C, IR and mass spectra. The reaction between various silylenol ethers and acylchlorides is shown in the scheme 5.3
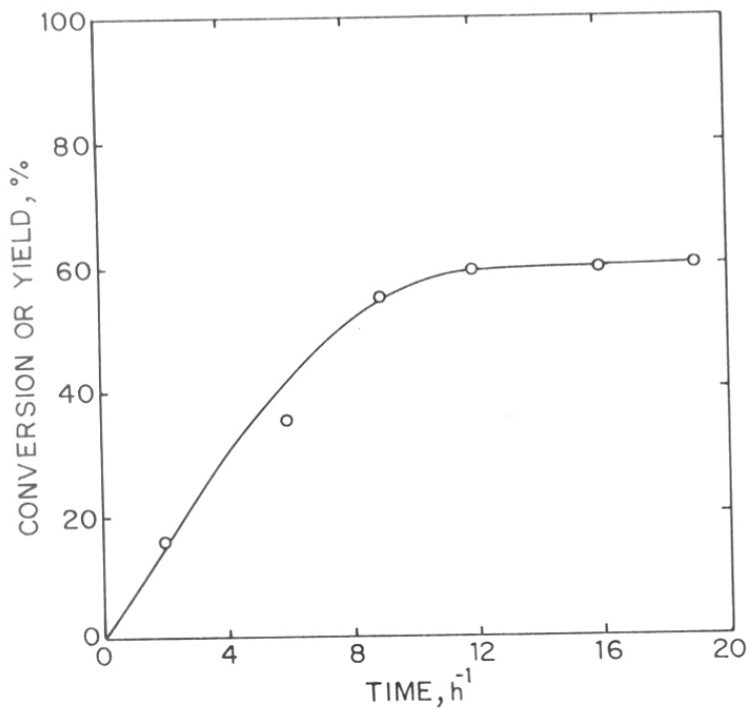
Fig.5.1　　1,4-addition of methylmethacrylate with silylenol ethers catalysed by titanium-silicate (TS-1). Effect of reaction time on conversion.
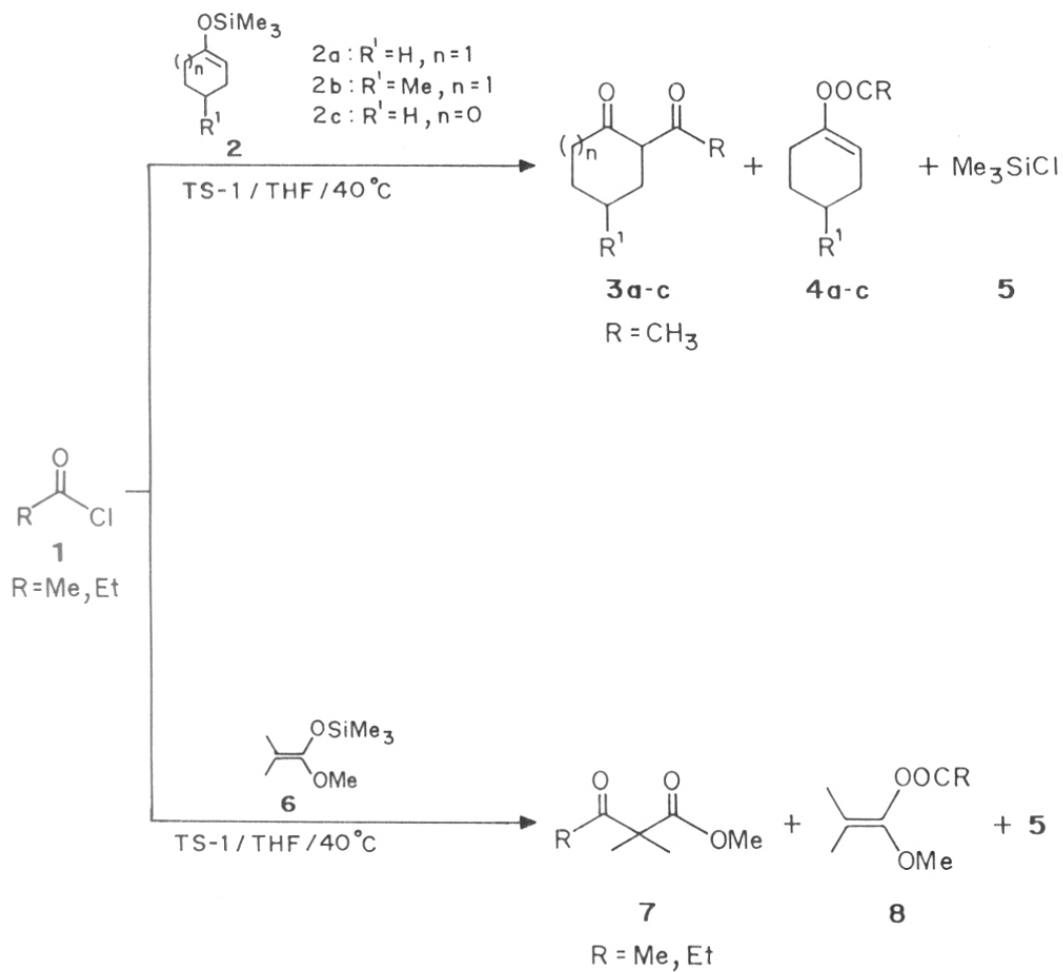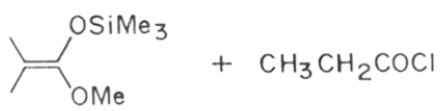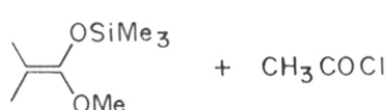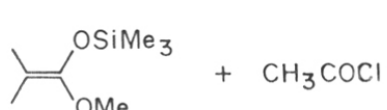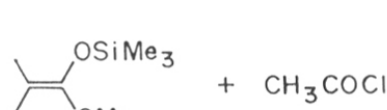
Scheme-5·3
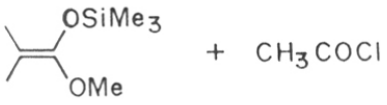
5.4.2 Results and Discussion

Table 5.5 shows the results of acylation of silylenol ethers with acetyl as well as propionyl chlorides in the presence of catalytic amount (20wt% with respect to substrate) of TS-1 catalyst. The acylation of silylenol ethers occurs at both, the carbon-center (C-atom) as well as the oxygen-center (O-atom) in silyloxy group of silylenol ethers leading to the formation of 1,3-diketone and ketene esters, respectively. While the open chain silylenol ethers exhibit more selectivity for C-acylation giving 1,3-diketones, the cyclic silylenol ethers predominantly undergo O-acylation giving ketene esters. This is quite expected, because the CH_3O- group favors the migration of double bond giving rise to more C-acylated product[45]. The acylation reaction has also been carried out using other zeolites like RE-Y, La-Y, TS-2 and all the modified catalysts lead to complete conversion in 5h with similar C-acylated products. Thus the product distribution in acylation reaction shows that there is a dual attack at both carbon-atom as well as oxygen-atom of the silylenol ether leading to diketone and ketene ester, respectively.

5.5 SN$_1$ ALKYLATION (Tert. BUTYLATION) OF SILYLENOL ETHERS OF KETONES

The α-alkylation of silylenol ethers of ketones using SN$_1$ active tert-alkyl halide is one of the most important and selective alkylation reactions [48-50]. Using SN$_2$ active (primary and secondary) alkyl halides as alkylating agents, enolates are commonly used for α-alkylation. However, when SN$_1$ active tert-alkylating agents are used, silylenol ethers of ketones are needed. The nucleophilic alkylation (SN$_1$) of silylenol ethers is mediated by Lewis-acids such as $TiCl_4$, $ZnCl_2$, $FeCl_3$, $SnCl_4$, etc. [50,51] in equimolar (substrate to catalyst ratio) quantities at -40°C to -70°C. Here, the nucleophilic tert-butylation of silylenol ethers with tert-butyl chloride over titanium-silicates at 60°C is described.

Table 5.5 Acylation of Silylenol ethers of ketones; **Condition:** Silylenol ether = 10mmol, Acylchloride = 10mmol, Catalyst = 20wt%, Temperature = 40°C.

Entry	Reaction	Product distribution[a]	
		Ketone ester (O-acylation)	Diketone (C-acylation)
1	$OSiMe_3$ / OMe structure + CH_3COCl	35·0	65·0
2	$OSiMe_3$ cyclohexene structure + CH_3COCl	78·0	22·0
3	$OSiMe_3$ methylcyclohexene structure + CH_3COCl	71·0	29·0
4	$OSiMe_3$ cyclopentene structure + CH_3COCl	70·0	30·0
5	$OSiMe_3$ / OMe structure + CH_3CH_2COCl	40·0	60·0
6[b]	$OSiMe_3$ / OMe structure + CH_3COCl	42·0	58·0
7[c]	$OSiMe_3$ / OMe structure + CH_3COCl	48·0	52·0
8[d]	$OSiMe_3$ / OMe structure + CH_3COCl	37·0	63·0

[a] Conversion = 100 %
[b] RE-Y   [c] La-Y   [d] TS-2

5.5.1 Typical Reaction and Scheme

In a typical reaction for alkylation, 10 mmol of silylenol ether (trimethyl silyloxy cyclohexene) was added to dry THF (15ml) containing 20wt% of activated TS-1. To the above mixture, 15 mmol of tert-butyl chloride was added and the reaction temperature was raised to 60°C. The reaction mixture was magnetically stirred for 16h and the progress of the reaction was monitored by TLC using 10% ethylacetate in pet ether as solvent system. Using the above solvent system, the consumption of reactants and formation of products were analyzed from thin layer chromatography. After 16h, the catalyst was filtered through celite, the organic layer was washed with water and extracted with 25 ml of dichloromethane. The extraction was repeated thrice and the combined extracts were evaporated under vacuum and dried over anhydrous Na_2SO_4. The products were purified through chromatography and identified by ^1H, ^{13}C NMR, IR, and mass spectral techniques. The typical reaction scheme is shown in the scheme5.4.
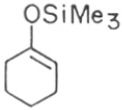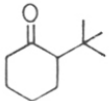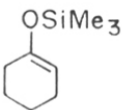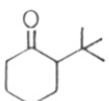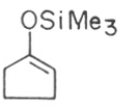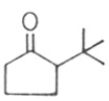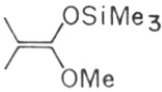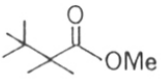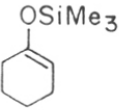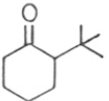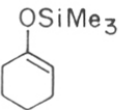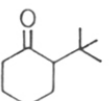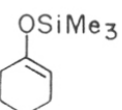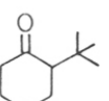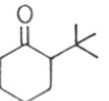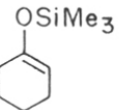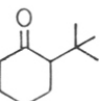
5.5.2 Results and Discussion

Table 5.6 shows the tert-butylation of various silylenol ethers of ketones over titanium-silicates. The SN_1 reaction involves the attack of nucleophile on either side of stable planar electrophilic-carbon moiety leading to the formation of substitution products. The interaction of Lewis acid oxo-philic sites of titanium-silicates with silylenol ether leads to the formation of a nucleophilic species. The nucleophilic species then attacks the carbocation (tert-butyl chloride) in SN_1 fashion as observed under homogeneous condition. Eventhough, the product, tert-butyl cyclohexanone is bulky for medium-pore TS-1 (Ti-MFI), the conformational flexibility (c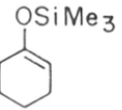hair form $\longleftrightarrow$ boat form [52]) may favor the substitution product (the free energy of chair form is less than that of boat form). Since, the chair-form of cyclohexanone with axial $\longleftrightarrow$ equitorial substituent is less sterically hindered than the other counterpart (boat form), the reaction may.
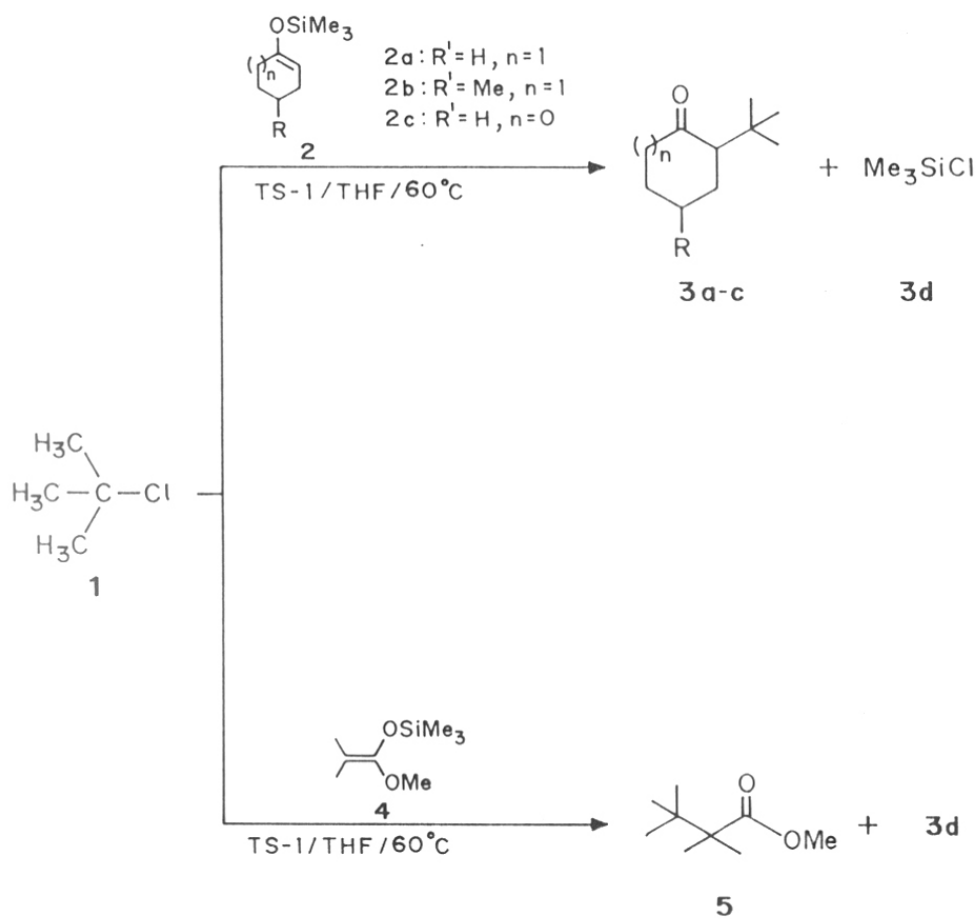
Scheme·5·4

Table 5.6 Tert.butylation of silylenol ethers of ketones; **Condition:** Silylenol ether = 10mmol, tert-butylchloride = 10mmol, Catalyst = 20wt%, Solvent = dry THF(20ml), Temperature = 60°

Entry	Silylenol ether	Product	Yield,%[a]
1	$OSiMe_3$		55
2	$OSiMe_3$		40
3	$OSiMe_3$		40
4	$OSiMe_3$, OMe	OMe	46
5[b]	$OSiMe_3$		30
6[c]	$OSiMe_3$		40
7[d]	$OSiMe_3$		45
8[e]	$OSiMe_3$		50
9[f]	$OSiMe_3$		35

[a] Conversion ; [b] Dichloromethane ; [c] Acetonitrile ; [d] TS-2 ; [e] RE-Y ; [f] La-Y

occur smoothly like other oxidation reactions over titanium-silicates. Further, the Ti-species present on the external surface may also activate the enolic oxygen of silylenol ether. The conversion of silylenol ether is more for cyclohexanone analogue than the open chain analogue. The conversion ranges between 30-55% for tert-butylation. As observed in other nucleophilic reactions, the tert-butylation also reacts selectively (no consecutive reactions) to tert-butyl substituted ketones. The rest was unreacted starting materials. The reaction has also been carried out over TS-2, RE-Y, and La-Y with moderate yield (45, 40 and 45% respectively). Among the solvents studied, THF was found to be better than dichloromethane or acetonitrile.

5.6 REACTION MECHANISM FOR NUCLEOPHILIC C-C BOND FORMATION OVER TS-1

In the complete absence of water TS-1, exhibits "oxophilic Lewis acid" sites [53], while the presence of Brönsted acid sites has been suggested [54] in the presence of aqueous H_2O_2. However, our experimental results, where no H_2O_2 or H_2O has been used, indicate the role of TS-1 as oxo-philic Lewis acid in this reaction. The key step in these reactions involving silylenol ethers is the activation of enolic oxygen followed by the migration of double bond thus facilitating the formation of nucleophilic-moiety at β-carbon position leading to the condensation. Apparently, the Ti^{4+} in TS-1 with its d_o configuration offers oxophilic sites to the enolic oxygen of the reacting species, probably giving rise to a favorable six-membered transition state similar to the one proposed by Mukaiyama [35] leading to the aldol. The probable species are given in the

scheme 5.5. The formation of nucleophile, while lead to carbon-carbon bond formation is similar

for all the reactions described in this section 5.1 - 5.4.
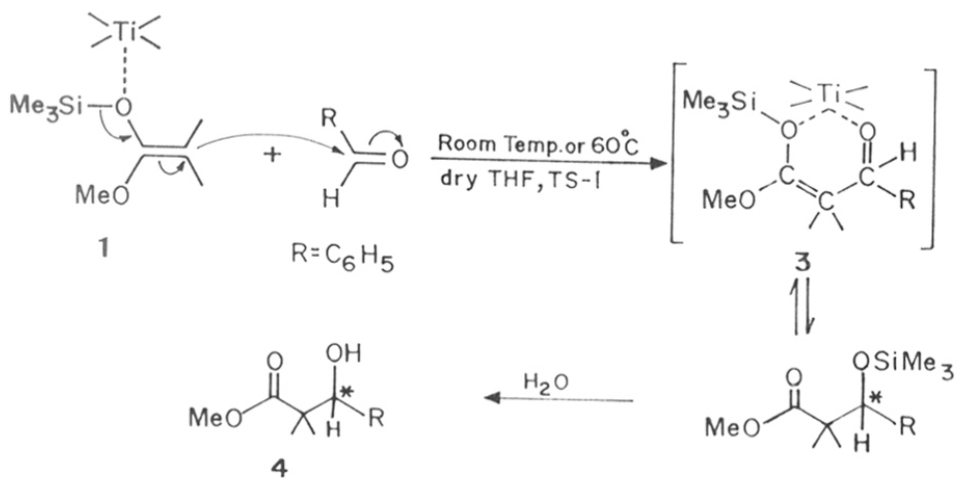
Scheme·5·5

5.7 SUMMARY

A novel use of TS-1 in non-oxidative carbon-carbon bond formation reactions namely; (i) Mukaiyama aldol condensation between silylenol ether and various aldehydes, (ii) Michael addition between silylenol ether with various α,β-unsaturated carbonyl compounds to give 1,4-adduct, (iii) acylation of silylenol ethers of ketone with acid-chloride to 1,3-diketone and ketene ester, and (iv) nucleophilic tert-butylation of silylenol ethers of ketone (SN_1 reaction) with tert-butylchloride is presented for the first time. The "oxophilic Lewis-acidity" of titanium-silicates in the absence of H_2O_2 and H_2O is responsible for the feasibility of these reactions. The modified zeolites such as RE-Y, La-Y, Sn/ZSM-5, VS-1, cation exchanged Zn-ZSM-5 exhibit low to moderate activity than that exhibited by titanium-silicate zeolites.

5.8 REFERENCES

1. "Introduction to Zeolite Science and Practice": (eds. H. Van Bekkum, E.M. Flanigen, J.C. Jansen) in *Studies in Surface Science and Catalysis*, **58**, 649 (1991).

2. F.J. Weigert, *J. Catal.,* **130**, 20 (1987).

3. Y. Ashina, T. Fujita, M. Fukatsu, K. Niwa and Y. Yagi, *Proc. 7th Int. Zeol. Conf.,* Tokyo, 1986, p.779.

4. R.D. Shannon, M. Keane, L. Abrams, R.H. Staley, T.E. Gier and G.C. Sonnichsen, *J. Catal.,* **113**, 367 (1988); **114**, 8 (1988); **115**, 79 (1989).

5. H.E. Bergna, M. Keane, D.H. Ralston, G.C. Sonnichsen, L. Abrams and R.D. Shannon, *J. Catal.,* **115**, 148 (1989).

6. H.E. Bergna, D.R. Corbin and G.C. Sonnichsen, US Pat. 4 683 334 (1987) and 4 752 586 (1988), Dupont.

7. M. Deeba, M.E. Ford and T.A. Johnson, Eur.Pat. 252 424 (1988), Air Prod. Chem. Inc.

8. T.A. Johnson, M.E. Ford and M. Deeba, DEOS, 3 543 228 (1986), Air. Prod.Chem. Inc.

9. M. Deeba, M.E. Ford and T.A. Johnson, *Stud. Surf. Sci. Catal.,* **38**, 221 (1987).

10. M. Deeba and M.E. Ford, *J. Org. Chem.,* **53**, 4594 (1988).

11. M. Deeba, M.E. Ford and T.A. Jhonson, *J. Chem. Soc., Chem. Commun.,* 562 (1987).

12. J. Peterson and H.S. Fales, US Pat. 4 307 250 (1981); Eur.Pat. 39 918 (1984), Air Prod. Chem. Inc.

13. J. Peterson and H.S. Fales, US Pat. 4 375 002 (1983), Air. Prod. Chem. Inc.

14. C.D. Chang and W.H. Lang, US Pat. 4 434 299 (1984), Mobil Oil Corp.

15. W.F. Hölderich, M. Hesse and F. Näumann, *Angew. Chemie.* **100**, 232 (1988).

16. M. Onaka, M. Kawai and Y. Izumi, *Chem. Lett.*, 779 (1985).

17. E. Kikuchi, T. Matsuda, K. Shimomura, K. Kawahara and Y. Morita, *Stud. Surf.Sci. Catal.*, **28**, 771 (1986).

18. M. Iwamoto, M. Tajima and S. Kagawa, *J. Catal.*, **101**, 195 (1986).

19. K. Eguchi, T. Tokiai and H. Arai, *Appl. Catal.*, **34**, 275 (1987).

20. P. Chu and G.H. Kuehl, US Pat. 4 605 787 (1986), Mobil Oil Corp.

21. J.A. Daniels and A. Stewart, Eur. Pat. 055. 045 (1986), ICI.

22. M.R. Klotz, US Pat. 4 584 415 (1986), Amoco.

23. L.B. Young, US Pat 4 365 084 (1982), Mobil Oil Corp.

24. Jap. Pat. 56 092 833 (1979), Mitsubishi Gas Chem. Ind.

25. S. Haruhito, DBP 3 249 979 (1982), Idemitsu Kosan Co.

26. H.E. Fried, Eur.Pat. 122 654 (1984), Shell Int. Res.

27. D. Kallo, G. Onyestyak and J. Papp, in *Proc. 6th Int. Zeol. Conf.*, Reno, Butterworth, 1984, p.444.

28. G. Onyestyak, D. Kallo, J. Papp and J.E. Detrekoy, Hung. Pat. 29 972 (1984).

29. M. Tarramasso, G. Perego and B. Notari, US Pat. 4 410 501 (1983).

30. J.S. Reddy, R. Kumar and P. Ratnasamy, *Appl. Catal.*,**58**, L1 (1990).

31. M.S. Rigutto and H. Van Bekkum, *Appl. Catal.*, **68**, L1 (1991).

32. N.K. Mal, V. Ramaswamy, S. Ganapathy and A.V. Ramaswamy, *J. Chem. Soc., Chem. Commun.*, 1933 (1994).

33. P. Ratnasamy, R.B. Borade, S. Sivasanker and V.P. Shiralker, *Acta. Phys. Chem.*, **31**, 137 (1985).

34. M. Kawai, M. Onaka and Y. Izumi, *Bull. Chem. Soc. Jpn.*, **61**, 1237 (1988).

35. T. Mukaiyama, K. Banno and K. Narasaka, *J. Am. Chem. Soc.*, **96**, 7503 (1974); Y. Yamamoto, K. Maruyama, K. Matsumoto, *J. Am. Chem. Soc.* **105**, 6963 (1983).

36. E. Nakamura, M. Shimizu, I. Kuwajima, J. Sakata, K. yokoyama and R. Noyori, *J. Org. Chem.* **48**, 932 (1983).

37. R. Noyori, I. Nishida and J. Saakata, *J. Am. Chem. Soc.*, **105**, 1598 (1983).

38. T. Mukaiyama, S. Kobayashi and M. Murakami, *Chem. Lett.*, 447 (1985); S. Kobayashi, M. Murakami and T. Mukayama, *Chem. Lett.*, 1535 (1985); Y. Naruse, J. Ukai, N. Ikeda and H. Yamamoto, *Chem. Lett.*, 1451 (1985).

39. P.G. Cozzi, C. Floriani, A. Chiesi-Villa and C. Rizzoli, *Synlett.*, 857 (1994).

40. K. Narasaka, K. Soai, Y. Aikawa and T. Mukaiyama, *Bull. Chem. Soc. Jpn.*, **49**, 779 (1976).

41. C.H. Heathock, M.H. Norman and D.E. Uehling, *J. Am. Chem. Soc.*, **107**, 2797 (1985).

42. O.W. Webster, W.R. Hertler, D.Y. Sogah, W.B. Farnham and T.V. Rajan Babu, *J. Am. Chem. Soc.*, **105**, 5706 (1983).

43. S. Kibayashi, M. Murakami and T. Mukaiyama, *Chem. Lett.*, 953 (1985).

44. J. boyer, R.J.P. Corriu, R. Perez and C. Reye, *Tetrahedron*, **39**, 117 (1983).

45. I. Kopka, M.W. Rathke, *J. Org. Chem.*, **46**, 3771 (1981).

46. M.W. Rathke and D.F. Sullivan, *Tetrahedron Lett.*, 1297 (1973).

47. T.H. Chan and P. Brownbridge, *J. Chem. Soc., Chem. Commun.*, 578 (1979).

48. E. Nakamura, T. Murofushi, M. Shimizu and I. Kuwajima, *J. Am. Chem. Soc.*, **98**, 2346 (1976).

49. E. Nkamura and I. Kuwajima, *J. Am. Chem. Soc.,* **99**, 961 (1977).

50. M.T. Reetz and W.F. Naier, *Angew. Chem. Int. Ed. Engl.,* **17**, 48 (1978).

51. M.T. Reetz, *Angew. Chem. Int. Ed. Engl.* **21,** 96 (1982).

52. "Stereochemistry of Carbon Compound" by Ernest L Eliel, 124, (1962).

53. G. Bellussi and M.S. Rigutto, *Stud. Surf. Sci. Catal.,* **85,** 177 (1994); M. Muscas, V. Solinas, S. Gontier, A. Tuel and A. Auroux, *Stud. Surf. Sci. Catal.,* **94**, 101, (1995).

54. G. Bellussi and V. Fattore, *Stud. Surf. Sci. Catal.,* **69**, 79 (1991).

CHAPTER 6

SUMMARY AND CONCLUSIONS

SUMMARY

High-silica, large pore zeolites are of great importance in the areas of adsorption and catalysis. The addition of organic additives (templates) leads to high- silica zeolites. High silica, large pore zeolite NCL-1 as well as its Al-free silica ... polymorph were synthesized by using hexamethylene bis (tri ethylammonium bromide) as organic additive. NCL-1 can be prepared from wide range of Si/Al ratio (23-α). This zeolite was modified through isomorphous substitution of iron and gallium by hydrothermal synthesis. The effect of various inorganic cations as well as the influence of various silica sources on the synthesis of Si-NCL-1 has been studied. These zeolites have been characterized by x-ray diffraction, framework IR, electron spin resonance spectroscopy, solid state MAS NMR, scanning electron microscopy, chemical analysis, adsorption and catalytic methods.

The results obtained through various spectroscopic techniques given below suggest that the metals Al, Ga and Fe are in the tetrahedral sites.

(I) Preliminary studies indicate that NCL-1 possesses orthorhombic symmetry with a =1.195 ±0.03, b =0.836±0.003 and c =2.870±0.004nm. The 'd' values calculated on the basis of the above unit cell dimension compare reasonably well with those observed experimentally.

(ii) FT IR study of hydroxyl groups for metallosilicate analogues of zeolite NCL-1 exhibits two peaks at 3632 and 3598 cm^{-1} corresponding to acidic Al-OH-Si- groups apart from silanol groups at 3730 cm^{-1}.

(iii) FT IR spectra of chemisorbed pyridine of isomorphously substituted zeolites show the presence of both, the Brönsted and the Lewis acid sites.

(iv) ESR spectra of Fe-NCL-1 samples exhibit two peaks with g values g = 2 and 4.3, typical of ferrisilicate molecular sieves.

(v) ^{29}Si MAS NMR spectra of Si-NCL-1 exhibited only one signal at -112 ppm, attributed to Si(0Al). In ^{27}Al MAS NMR spectra, only one signal was observed at 52 ppm, attributed to tetrahedral Al^{3+} ions and no signal was observed due to octahedral Al^{3+} ions. ^{71}Ga NMR spectra of Ga-NCL-1 exhibited only one signal at 148 ppm suggesting the presence of Ga in tetrahedral environment.

(vi)   Scanning electron microscope shows that the crystallites are like needles or bundles of needles.

(vii)   The adsorption capacities of isomorphously substituted zeolites are comparable with those of Al-NCL-1.

Zeolite NCL-1 exhibits high activity and selectivity in the isopropylation of benzene to form cumene. The selectivity generally ranges between 65 and 90% while cumene + diisopropylbenzenes selectivity remains 94±3%. In the isomerization of 1,3,5- trimethylbenzene, zeolite NCL-1 shows both isomerization and disproportionation. Both, the lower acid-site density as well as lower conversion favor the selectivity for isomerization product. Zeolite NCL-1 exhibits moderate selectivity in the Fries rearrangement of phenylacetate into hydroxy acetophenone. Zeolites (particularly Beta) can be used as heterogeneous and environmentally safer catalysts for the conversion of cumenehydroperoxide into phenol with high selectivity.

TS-1 has been efficiently used in the carbon-carbon bond formation reactions such as (i) Mukaiyama aldol condensation using silylenol ether and aldehydes, (ii) Michael addition between silylenol ether and various α,β-unsaturated carbonyl compounds, (iii) acylation of silylenol ethers of ketone with acid chlorides to form 1,3-diketone, and (iv) nucleophilic tert-butylation of silylenol ethers of ketone (SN$_1$ reaction) with tert-butylchloride. The "oxophilic Lewis-acidity" of titanium-silicates in the absence of H_2O_2 and H_2O is responsible for the feasibility of reaction.

Publications

1   Isopropylation of Benzene with 2-Propanol over High-Silica, Large-Pore Zeolite: NCL-1; **M.Sasidharan**, K.R. Reddy and R. Kumar, J.Catal.,**154** (1995) p216

2   Catalytic Oxidation of Ethers with H_2O_2 over Zeolites, **M. Sasidharan**, S. Suresh and A. Sudalai, Tetrahedron Letters., **36** (1995) 9071.

3   Titanium-Silicate Molecular Sieves TS-1, Catalyzed C-C Bond Formation in Mikaiyama Type Aldol Reactions, **M. Sasidharan**, S.V.N. Raju, K.V. Srinivasan, V. Paul and R. Kumar, JCS.,Chem.Commun, (1996) 126.

4   Synthesis, Characterization and Catalytic Properties of Ferri- and Gallo-Silicate Analogues of Zeolite NCL-1, **M. Sasidharan** and R. Kumar, Catalysis Letters, **38 (3),** (1995) 245.

5   Titanium Silicate Molecular Sieves (TS-1 & TS-2) Catalyzed Micheal Reaction of Silylenol Ethers with α,β- Unsaturated Carbonyl Compounds, **M.Sasidharan** and R. Kumar, Catalysis Letters, **38 (4),** (1996) 251.

6   Selective Fries Rearrangement of Phenylacetate to Hydroxyacetophenone Catalyzed by High-Silica Zeolite NCL-1, **M. Sasidharan** and R. Kumar, Studies in Surface Science and Catalysis, in 11th International zeolite Conference, Seoul, (1996) in press.

7   Chromium Silicalite-2 (CrS-2): an Efficient Catalyst for the Chemoselective Epoxidation of Alkenes with TBHP, Reni Joseph, **M. Sasidharan**, R. Kumar A. Sudalai and T. Ravindranathan, JCS., Chem.Commun. (1995) 1341.

8   Chromium Silicalite-2 (CrS-2): an Efficient Catalyst for the Direct Oxidation of Primary Amines to Nitro Compounds with TBHP, B. Jayachandran, **M. Sasidharan**, A. Sudalai and T. Ravindranathan, JCS., Chem.Commun., (1995) 1523.

9   Selective Oxidation of Benzylic Alcohols into the Corresponding Carbonyl Compounds with TBHP Over CrS-2, N.V. Barhate, **M. Sasidharan**, A. Sudalai and R.D. Wakharkar, Tetrahedron Letters, **37,** (1996) 2067.

10   A Facile and Selective Method for the Synthesis of β-Keto Esters via Trans-Erification Catalyzed by Zeolites, B.S. Balaji, **M.Sasidharan**, R. Kumar and B. Chanda, JCS., Chem.Commun, (1996) 707.

11   High-Silica, Large Pore Zeolites in the Selective Removal of Dialkylphenols from Aqueous Effluents, **M. Sasidharan** and R. Kumar, 11th National Symposium on Catalysis, Modern Trends, eds (N.M. Gupta & D.K. Chakrabarthy) p175, December 1994.

12   Effect of Various Inorganic Cations (Li, Na, K and Cs) and Silica Sources on the Synthesis of Silica Analogue of Zeolite NCL-1, **M. Sasidharan** and R. Kumar, Microporous Materials, (1996) in press.

13   Regioselective Chlorination of Aromatics with Cl_2 Catalyzed by Kaolinitic Clay, B. Jayachandran, **M. Sasidharan**, A. Sudalai, T. Ravindranathan and M. Lalithambika, JCS.,Chem.Commun, (1996) accepted.

14   CrS-2: an Efficient Catalyst for Chemoselective Oxidation of Thioethers to Sulfoxide with H_2O_2, T.T. Upadhaya, T. Daniel, **M. Sasidharan**, A. Sudalai and T. Ravindranathan, <u>JCS., Chem.Commun</u>, (1996) submitted.

15   Isopropylation of Cumene to Diisopropylbenzene over High-Silica, Large Pore Zeolite NCL-1, **M. Sasidharan** and R. Kumar, <u>12th National workshop on Catalysis,</u> Poster Presentation, December 1995.

16   Removal and Recovery of Dissolved Phenolic Impurities in Aqueous Effluents Using High-Silica, Large Pore Molecular Sieve Adsorbents, **M. Sasidharan** and R. Kumar, <u>Applied Catalysis B: Environmental</u>, (1995) submitted.

17   Catalytic Oxidation of Amino Acids to the Corresponding Keto Acids with H_2O_2 Over TS-1, M. Anbazhagan, **M. Sasidharan** and A. Sudalai, <u>Synlett,</u> (1996) submitted.

18   Remarkable Selectivity Shown by CrS-2 Towards Oxidation of Phenols to P-Benzoquinoes, R. Ramani, **M. Sasidharan**, S. Suresh, A. Sudalai and B. Chanda, <u>J.Chem. Research</u>, (1996) submitted.

19   Selective Decomposition of Cumenehydroperoxide to Phenol and Acetone Over High-Silica Zeolites, **M. Sasidharan** and R. Kumar, <u>JCS., Chem.Commun.</u>, submitted.

20   Selective Liquid Phase Alkylation and Acylation Cyclic Ketones Over Titanium Silicates, **M. Sasidharan** and R. Kumar, <u>Angew.Chem.Int.eds.</u> to be communicated.

21   Isomerization of 1,3,5-Trimethylbenzene to 1,2,4-Trimethylbenzene Over High-Silica, Large Pore Zeolite NCL-1, **M. Sasidharan** and R. Kumar, <u>J.Catal.</u>,to be Communicated.

22   Synthesis of Zeolite NCL-1 using TEA-OH as a New Templating Agent, **M. Sasidharan** and R. Kumar, <u>Microporous Materials</u>, to be communicated.

23   Bayer-Villiger Oxidation of Cyclic Ketones to Lactones Using the Combination of Molecular Oxygen-benzaldehyde Over Copper Complex Encapsulated Y-Zeolites, Robert Raja, **M. Sasidharan** and P. Ratnasamy, <u>J.Catal</u>, to be communicated.

Patents

1   An Improved Process for the Selective Decomposition of Cumenehydroperoxide into Phenol and Acetone Over Various High-Silica Zeolites, **M. Sasidharan** and R Kumar, Indian Patent, applied.

2   A Process for various C-C bond formation reactions using Titanium Silicate as Lewis acid Catalyst, **M. Sasidharan** and R. Kumar, Indian Patent, applied.

3   A Process for the Synthesis of Various β-Ketoesters via Transesterification Methods using Various Zeolite Catalysts, B. S. Balaji, **M. Sasidharan**, R. Kumar and B. Chanda, Indian Patent, applied.